Coordination Chemistry Reviews 470 (2022) 214702

Contents lists available at ScienceDirect

Coordination Chemistry Reviews

journal homepage: www.elsevier.com/locate/ccr

Review

Folate-based radiotracers for nuclear imaging and radionuclide therapy

Laurène Wagner [a,b], Bibigul Kenzhebayeva [a,c], Batoul Dhaini [d,e], Samir Boukhlef [f], Albert Moussaron [a,d], Serge Mordon [f], Céline Frochot [d], Charlotte Collet [b,g,*], Samir Acherar [a,*]

[a] Université de Lorraine, CNRS, LCPM, Nancy F-54000, France
[b] NancycloTEP, Plateforme d'imagerie moléculaire, Vandœuvre-lès-Nancy F-54511, France
[c] Institute of Chemical and biological technologies, Satbayev University, Almaty 050013, Republic of Kazakhstan
[d] Université de Lorraine, CNRS, LRGP, Nancy F-54000, France
[e] Laboratory of Materials, Catalysis, Environment and Analytical Methods Faculty of Sciences, Section I, Lebanese University Campus Rafic Hariri, Hadath, Lebanon
[f] University of Lille, INSERM, CHU-Lille, U1189-ONCO-THAI, Assisted Laser Therapy and Immunotherapy for Oncology, France
[g] Université de Lorraine, INSERM, U1254 IADI, Nancy F-54000, France

ARTICLE INFO

Article history:
Received 14 January 2022
Accepted 26 June 2022
Available online 8 July 2022

Keywords:
Folic acid
Ovarian cancer
Radiopharmaceutical
Nuclear imaging
Targeted radionuclide therapy
Theranostic

ABSTRACT

Folate receptor α (FRα) is overexpressed on numerous tumorous cell types such as ovarian or endometrial cancer cells. Moreover, FRα is absent from most healthy tissues as it is normally expressed only on the surface of proximal tubules cells of kidneys and choroid plexus. Thus, folate-based radiopharmaceuticals have emerged this last two decades as FRα is a target of choice to diagnose and treat numerous cancers. Nuclear imaging is a performing diagnostic technology using highly sensitive detectors and specific radiopharmaceuticals used to detect tumors at an earlier stage. Herein, an overview of the development of folate-based radiopharmaceuticals to detect FRα-positive tumors by nuclear imaging using positron emission tomography (PET) and single photon emission computed tomography (SPECT) is exposed. Strategies developed to improve precursor synthesis, bioavailability, clearance, and affinity to FRα will be detailed. Advances made to decrease kidney uptake open the gate to targeted radionuclide therapy (TRT) using folate-based radiopharmaceuticals to treat FRα-positive tumors. Thus, radiofolates used in TRT and more precisely in a theranostic approach will be depicted in this review.

© 2022 Elsevier B.V. All rights reserved.

Abbreviations: %IA/g, Percentage of the injected activity per gram of tissue weight; 5-Me-THF, 5-Methyl-tetrahydrofolate; AB, Albumin binder entity; Bz, Benzyl; CT, Computed tomography scan; Cys, Cysteine (C); CuAAC, Copper-catalyzed azide-alkyne cycloaddition; DAV, δ-Aminovaleric acid; dc, Decay corrected; DFO, Deferoxamine; DNA, Deoxyribonucleic acid; DOTA, 1,4,7,10-tetraazacyclododecane-1,4,7,10-tetraacetic acid; DO3A-EA, 1,4,7-tris (carboxymethyl)-10-(4-aminoethyl)-1,4,7,10-tetraazacy clododecane; DOTAGA, 2,2′,2″-(10-(2,6-Dioxotetrahydro-2*H*-pyran-3-yl)-1,4,7,10-tetraazacyclododecane-1,4,7-triyl)triacetic acid; DOTATOC, DOTA-octreotide; DTPA, Diethylenetriaminepentaacetic acid; EC, Electron capture; ECG, Glutamic acid-cysteine-glycine; EDA, Ethylenediamine; EDBE, 2,2′-ethylenedioxy-bis-ethylamine; EDDA, Ethylenediamine-*N*,*N*'-diacetic acid; FA, Folic acid; FBA, 4-fluorobenzylamine; FDG, 2-deoxy-2-fluoro-D-glucose; FR, Folate receptor; Glu, Glutamic acid or glutamate (E); Gly, Glycine (G); HBED, *N*,*N*'-Bis(2-hydroxybenzyl) ethylenediamine-*N*,*N*'-diacetic acid; His, Histidine (H); HYNIC, Hydrazino-nicotinamide or 6-[2-(4-dimethylamino)benzalde hydehydrazono]nicotinate; IAC_{50}, Half maximal inhibitory activity concentration; IC_{50}, Half maximal inhibitory concentration; i.p., Intraperitoneally; i.v., Intravenous; K_d, Dissociation constant; Log $D_{7.4}$, Logarithm of the distribution coefficient at pH 7.4; Log P, Logarithm of the partition coefficient; Lys, Lysine (K); MRI, Magnetic resonance imaging; MTT, 3-(4,5-Dimethylthiazol-2-yl)-2,5-diphenyltetrazolium bromide; NC, Not communicated; NODAGA, 1,4,7-Triazacyclononane,1-glutaric acid-4,7-acetic acid; NOTA, 1,4,7-Triazacyclononane-1,4,7-trisacetic acid; OEG, Oligoethylene glycol; PAMA, Picolylamine monoacetic acid; PBS, Phosphate-buffered saline; PCFT, Proton-coupled folate transporter; PDT, Photodynamic therapy; PDX, Patient derived xenograft; PEG, Polyethylene glycol; PEG_2, 2,2′-(Ethylenedioxy)-bis-ethylamine; PET, Positron emission tomography; p.i., Post-injection; PMX, Pemetrexed; PSMA, Prostate specific membrane antigen; RFC, Reduced folate carrier; RGD, Arginine-glycine-aspartic acid peptide; ROIs, Region of interests; RCY, Radiochemical yield; SPECT, Single-photon emission computed tomography; TEPA, Tetraethylenepentamine; THF, Tetrahydrofolate; TPPMS, Diphenylphosphinobenzene-3-sulfonic acid sodium; TPPTS, Trisodium triphenylphosphine-3,3′,3″-trisulfonate; TRT, Targeted radionuclide therapy; TS, Thymidylate synthase.

* Corresponding authors at: NancycloTEP, Plateforme d'imagerie moléculaire, Vandœuvre-lès-Nancy F-54511, France (C. Collet); Université de Lorraine, CNRS, LCPM, Nancy F-54000, France (S. Acherar).

E-mail addresses: charlotte.collet@univ-lorraine.fr (C. Collet), samir.acherar@univ-lorraine.fr (S. Acherar).

https://doi.org/10.1016/j.ccr.2022.214702
0010-8545/© 2022 Elsevier B.V. All rights reserved.

1. Introduction

Folate receptor α (FRα) shows promising prospects in targeting ovarian, endometrial, colorectal, non-small cell lung and renal cancers and has a highly limited expression in normal tissues except for kidneys [1,2]. In fact, FRα is overexpressed in 72–100% of ovarian carcinomas [3–6]. Various studies have been initiated to develop folic acid (FA)-conjugated agents for diagnosis by molecular imaging or for the treatment of such diseases [7]. For example, the interest of FA as targeting agent for peritoneal metastasis treatment thanks to photodynamic therapy (PDT) has been largely proved by Frochot and co-workers [8–15]. FA can also be an ideal molecule for selective nuclear imaging using FR-targeted radiopharmaceuticals. In fact, radiofolates have been developed to diagnose rheumatoid arthritis [16,17], osteoarthritis [18,19] and atherosclerosis plaque [20,21] by detection of activated macrophages in concerned tissues which overexpressed FRβ and tumorous cells overexpressing FRα. Moreover, radiopharmaceuticals using alternatives to FA as monoclonal antibodies like MOv-18 [22,23] and M9346A [24,25], and peptides like C7 [26] have been developed to target FRα. It is also worth noting that within the last decade, researchers have taken an interest in the use of small-molecule radiotherapeutics targeting receptors for a targeted radionuclide therapy (TRT) of cancers [27]. The development of folate-based radiopharmaceuticals for nuclear imaging or radionuclide therapy consists of similar strategies using α- or β^--emitters radionuclides for therapy and β^+ or γ-emitters radionuclides for nuclear imaging (*i.e.*, β^+ for positron emission tomography (PET) and γ for single-photon emission computed tomography (SPECT)).

1.1. Folic acid receptors and carriers

Different high affinity receptors to folates are reported in the literature: reduced folate carrier (RFC) [28], proton-coupled folate transporter (PCFT) [29] and folate receptor (FR) are receptors having good affinity to folate and/or reduced folates. RFC is involved in the transport and internalization of reduce folates used in the *de novo* synthesis of DNA. At it is also able to transport antifolates, it plays a major role in chemotherapeutic drugs transport such as pemetrexed or methotrexate [30]. PCFT is involved in carrier-mediated intestinal folate transport system and is expressed in normal cell but also in the majority of tumor cell lines. As it is an acidic pH-responsive carrier, the low pH of cancerous cells improves its transport function. Thus, it is a target of choice for therapeutic agents such as antifolates [31]. FR exists in four isomers: FRα, FRβ, FRγ and FRδ. These isomers differ from about 30% in sequence homology [32]. FRα and FRβ are 38 kDa glycosylphosphatidylinositol anchored glycoproteins mediating the internalization of FA *via* endocytosis route [33]. FRα is absent from the majority of healthy tissues [34] as it is normally expressed only on the surface of proximal tubules cells of kidneys (for folate resorption) [35], lungs and choroid plexus [36]. Salivary glands are also able to release a soluble form of FRα in the saliva [37]. FRα is a folate-binding protein overexpressed in 40% of solid tumors including epithelial cancerous cells (serous and endometrioid epithelial ovarian, endometrial, breast, cervical, colorectal, non-small cell lung and renal cancers). FRβ is overexpressed on placenta [38,39] but also on activated (but not resting or quiescent) macrophages which are recognized either to cause or to contribute to inflammatory and auto-immune diseases like rheumatoid- and osteo-arthritis [40], lupus [41], Crohn's disease or atherosclerosis [42]. FRγ is a secreted protein as the signaling sequence for membrane anchoring is missing in this isomer form. FRγ is secreted by lymphoid cells in the thymus, spleen and bone marrow and is related to malignancies with hematopoietic origins [43]. FRδ, also known as FOLR4 or Juno protein is also a member of the FR family but is not able to bind FA compared to FRα, FRβ and FRγ. It is involved in fertilization as this receptor is anchored on egg surface and recognized by Izumo1 on sperm surface [44].

1.2. Targeting agent of folic acid receptors

FA is a water-soluble molecule (441 Da), also known as the synthetic and oxidized form of folate (vitamin B9) which has a strong affinity to FRα (1 nM). Its structure is divided in three distinct parts: pterin, aminobenzoate and glutamate entities (Fig. 1, left). Pterin and aminobenzoate entities form the pteroate moiety. In 2013, crystal structure of FA bound to FRα was successfully determined and gave tangible information on the recognition area of FA which is the pteroate moiety [45]. FA is crucial to ensure normal functions of the human body in various metabolic (amino acids, nucleic acids) and biochemical processes. The human body does not store FA, thus, a FA deficiency can lead to several defects, such as spina bifida or anencephaly [46]. FA deficiency has also been associated with certain types of congenital defects (heart and neural tube defects) or malformations (cleft lip) or pregnancy complications [47].

5-methyl-tetrahydrofolate (5-Me-THF) is the reduced form of folate. It differs from this latter by the presence of a methyl group on 5-N of the pterin entity and the presence of an asymmetrical carbon (6-C). Thus, 5-Me-THF is found under two forms: (6*S*)- and (6*R*)-diastereomers (Fig. 1, right). It is the cofactor of thymidylate synthase (TS) involved in the *de novo* synthesis of DNA building block 2′-deoxy-thymidylate (dTMP) [48].

1.3. Nuclear medicine

Nuclear medicine is a medical domain where i) diagnosis are determined thanks to nuclear molecular imaging exams (PET and SPECT) and ii) treatments are performed thanks to radiopharmaceuticals administered to patients, which can target tumor cells and damage their DNA (TRT).

Molecular imaging is defined as the *in vivo* targeted imaging of biological process and takes an important place to establish diagnosis of many diseases. PET and SPECT are two nuclear imaging techniques which had numerous impacts of access to health care [49–52]. These techniques consist in injecting molecular imaging agents named radiotracers or radiopharmaceuticals to detect interactions with specific cellular target.

Radionuclides can be directly integrated in the targeting agent or be coupled with it thanks to a radiolabelled prosthetic group or inserted into a chelating agent *via* coordination chemistry for metal radionuclides [53]. Most widespread radionuclides are radiometals labelled with chelating agent. Depending on their nature, they do not form the same number of coordination bonds with chelating agent and do not have the same oxidation level. There is a wide variety of chelating agents which can be cyclic (*i.e.*, 1,4,7,10-tetraazacyclododecane-1,4,7,10-tetraacetic acid (DOTA), 1,4,7-tria zacyclononane-1,4,7-trisacetic acid (NOTA)), or linear (*i.e.*, *N*,*N*'-Bi s(2-hydroxybenzyl)ethylenediamine-*N*,*N*'-diacetic acid (HBED), deferoxamine (DFO), diethylene-triaminepentaacetic acid (DTPA), 6-hydrazinonicotinic acid (HYNIC)) [54]. Most representative chelating agents of folate-based radiopharmaceuticals are presented in Fig. 2.

Radionuclides used for **PET imaging** are positrons (β^+) emitting. The PET scanner detects the pair of 511 keV photons produced by

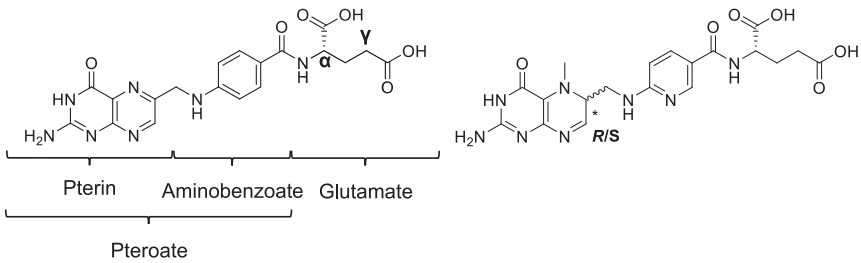

Fig. 1. Chemical structures of folic acid (FA) (left) and 5-Me-THF (right).

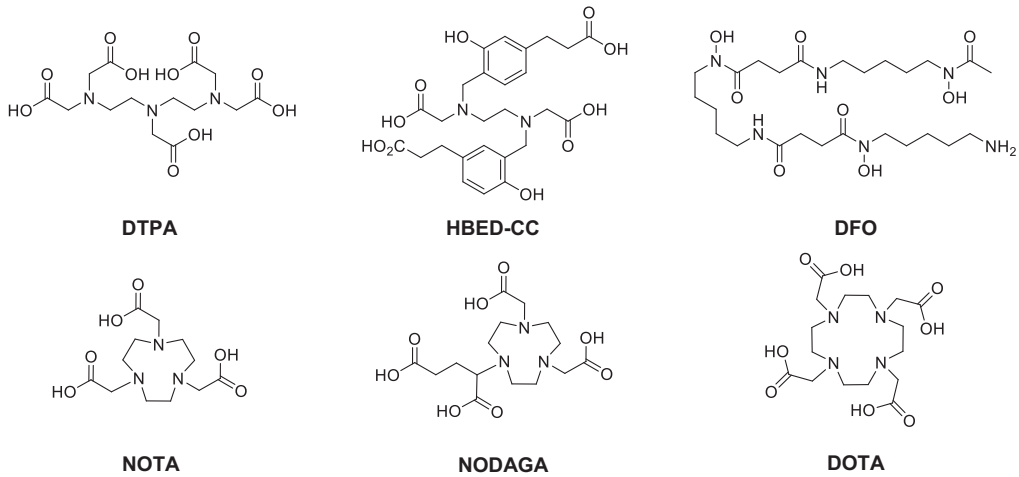

Fig. 2. Chemical structures of linear and cyclic chelating agents.

Table 1
Chemical properties of PET radionuclides used to radiolabel folate-based probes.

Isotope	Half-life	Decay mode	Mean β^+ energy (keV)	Production	Oxidation number	Number of coordination	References
^{18}F	109.8 min	β^+ (95%)	β^+,250	^{18}O(p,n)^{18}F	1-	NA	[66,77]
^{18}F-Al		EC (3%)			3+	6	
^{44}Sc	4.04 h	β^+ (94%)	β^+, 632	^{44}Ti/^{44}Sc generator	3+	8–9	[73,78]
		EC (6%)		^{44}Ca(p,xn)^{44}Sc			
				^{44}Ca(p,n)^{44}Sc			
^{55}Co	17.5 h	β^+ (76%)	β^+, 570	^{55}Ni(p,α)^{55}Co	2+	6	[79]
				^{56}Fe(p,n)^{55}Co			
				^{54}Fe(d,n)^{55}Co			
^{64}Cu	12.7 h	β^+ (19%)	β^+, 653	^{64}Ni(p,n)^{64}Cu	2+	6	[74]
		EC (41%)					
		β^- (40%)					
^{68}Ga	67.7 min	β^+ (89%)	β^+, 836	^{68}Ge/^{68}Ga generator	3+	6	[73,80]
		EC (11%)		^{68}Zn(p,n)^{68}Ga			
^{152}Tb	17.5 h	β^+ (17%)	β^+, 1140	Spallation of tantalum target	3+	6–9	[81]
				^{155}Gb(p,n)^{155}Tb			
				^{159}Tb(p,5n)^{155}Dy$\rightarrow^{155}$Tb			

EC: Electron capture; n: neutron; p: proton; d: deuteron; α: alpha particle; xn: one or more neutron; NA: Not applicable.

annihilation of β^+ with an electron (Table 1) [55–59]. An image is reconstructed to locate exactly the production site of the pair of photons. As this technique is very sensitive, radiopharmaceuticals are injected in pico- or nanomolar chemical concentrations depending of the radiofolate with activity range from 0.37 to 600 MBq for preclinical studies and from 300 to 600 MBq for clinical trials [60,61].

Fluorine-18 (^{18}F) is the most widespread radionuclide for PET imaging. Its radiochemistry is essentially performed by nucleophilic substitution. Fluorine-18 fixation on biomolecules is a big issue as fluorination reactions need harsh conditions. As biomolecules are quite sensitive, the development of conjugation approach has emerged. It consists in fixing fluorine-18 to a small molecule (a prosthetic group) which can react with biomolecules in soft conditions *via* amino, thiol or click chemistry [62–65]. In 2009, a novel radiochemistry strategy as emerged in which fluorine-18 is used as co-ligand in the coordination of aluminum [66,67].

PET metal radionuclides like gallium-68 (^{68}Ga) are incorporated into macrocyclic compounds (DOTA [68], NOTA [69,70], NODAGA [71] or acyclic chelators (HBED) [72] by coordination chemistry in aqueous phase. The use of gallium-68 is growing to radiolabelled biomolecules for clinical applications. New PET metal radionu-

clides like scandium-44 (^{44}Sc) [73], copper-64 (^{64}Cu) [74,75] and cobalt-55 (^{55}Co) [76] can be coordinated to the same chelating agents as gallium-68 and are currently under study to evaluate their capability to be good diagnostic radionuclides.

Radionuclides used for **SPECT imaging** are γ-emitting with an energy range of 25 to 300 keV (Table 2) [55,56,59,82]. γ Radiation can be detected by small animal or clinical SPECT devices in a range of 25–250 keV or 60–300 keV, respectively. However, since the development of whole-body SPECT apparatus [60,61], the development of SPECT imaging agents to have access to quantifiable information for therapy purpose became interesting [83,84].

The most used SPECT radionuclide is technetium-99 m (^{99m}Tc). Its radiochemistry is well-known, and it is one of the cheapest radionuclides available for nuclear imaging. Technetium-99 m can be used under different oxidation state with a large variety of chelators [85]. Gallium-67 (^{67}Ga) is incorporated by coordination chemistry into macrocyclic compound such as NOTA and DOTA and acyclic chelating agents like DFO or HBED. Indium-111 (^{111}In) is also incorporated by complexation into macrocyclic compounds like DOTA and acyclic chelating agents like CHX-A"-DTPA [54].

Radionuclides used for **therapeutic application** (Table 3) are α or β^- emitting and could directly treat tumors thanks to the TRT approach. Most widespread radionuclides are radiometals coordinated with chelating agents like DOTA [87] or DOTAGA [88].

The most used therapeutic radionuclide is lutetium-177 (^{177}Lu). Scandium-47 (^{47}Sc), yttrium-90 (^{90}Y), terbium-161 (^{161}Tb) and rhenium-188 (^{188}Re) are radionuclides used in β^--therapy, but they also could be used to performed SPECT imaging due to their γ radiation to evaluate biodistribution and tumor uptake, and to give dosimetry information for example. Terbium-149 (^{149}Tb) is a radionuclide used in α-therapy and the choice of the therapeutic radionuclide will depend on the nature of tumors.

The research of **new radiopharmaceuticals** is mostly based on the development of targeting specific agents for tumor-associated receptor. Recent radiopharmaceuticals are now used in clinical routine diagnosis and for a personalized medicine approach [92]. It is the case for two well-known ^{68}Ga-radiopharmaceuticals: [^{68}Ga]Ga-DOTATOC (DOTA-Tyr^3-octreotide) and [^{68}Ga]Ga-PSMA-11. This type of biological targeting specific agent is often a biomolecule such as peptide, protein or antibody able to bind a membrane receptor overexpressed on cancer cells. They allow to establish diagnosis and staging of diseases, treatment selection, guidance or for PET-guided radiotherapy as theranostic probes [93,94].

Theranostic is composed of the term diagnostic and therapy. It aims at developing radiopharmaceuticals usable both in nuclear imaging to perform diagnostic and TRT. It is a novel approach associated to personalized medicine. This approach has the advantage to give the good treatment to the good patient. Radionuclides used in this approach must emit rays detected by diagnostic tools (β^+ for PET and γ for SPECT) and rays with high energy (α and β^-) for therapy. Thus, radionuclides like lutetium-177 and terbium-161 are a perfect choice for the development of theranostic agents [73,95–97]. In this theranostic approach, radionuclides used could be different (gallium-68/lutetium-177 for example) [97] or used as matched pairs (copper-64/copper-67, scandium-44/scandium-47) or matched quadruplet (terbium-152/terbium-155/terbium-149/terbium-161) [81,98,99]. Four promising terbium radioisotopes (terbium-149, terbium-152, terbium-155 and terbium-161) were identified for applications in theranostic [81]. Thanks to identical chemical characteristics and complementary physical decay characteristics, these terbium radioisotopes could be used to compare the effectiveness of PET (terbium-152 or terbium-149) *vs.* SPECT (terbium-155) imaging and α *vs.* β^- therapy (terbium-149 and terbium-161, respectively). Thus, it also has the advantage to combine preclinical study of imaging and therapy for the same radioconjugate.

Table 2
Chemical properties of SPECT radionuclides used to radiolabel folate-based probes.

Isotope	Half-life	γ-energy (keV)	Production	Oxidation number	Number of coordination	References
^{67}Ga	3.26 d	93 (39%), 185 (21%), 300 (17%), 394 (5%)	^{67}Zn(p,n)^{67}Ga	3+	6	[54]
^{99m}Tc	6.02 h	141 (89%)	^{99}Mo/^{99m}Tc generator	5+	6–8	[86]
^{111}In	2.80 d	171 (91%), 245 (94%)	^{111}Cd(p,n)^{111}In	3+	7–8	[54]
^{155}Tb	5.32 d	43 (86%), 49 (20%), 87 (52%), 105 (25%)	Spallation of tantalum target ^{155}Gb(p,n)^{155}Tb	3+	6–9	[81]

EC: Electron capture; n: neutron; p: proton.

Table 3
Chemical properties of therapeutic radionuclides (α and β^-) used to radiolabel folate-based probes.

Isotope	Half-life	Decay mode	Energy (keV)	Production	Oxidation number	Number of coordination	References
^{47}Sc	3.35 d	β^- (100%)	β^-, 162*	^{47}Ti(n,p)^{47}Sc	3+	8–9	[73,78]
		γ	γ, 159 (68.3%)	^{46}Ca(n,γ)^{47}Ca→^{47}Sc			
^{90}Y	2.67 d	β^- (100%)	β^-, 926*	^{90}Zr(n,p)^{90}Y	3+	8–9	[54,89]
^{149}Tb	4.12 h	α (17%)	α, 3967	Spallation of tantalum target	3+	6–9	[81,90]
		β^+ (7%)	β^+, 730*	^{152}Gd(p,4n)^{149}Tb			
		EC (76%)		^{142}Nb(^{12}C,5n)^{149}Dy→^{149}Tb			
^{161}Tb	6.89 d	β^- (100%)	β^-, 154*	^{160}Gb(n,γ)^{161}Gd → ^{161}Tb	3+	6–9	[73,81]
		γ	γ, 25 (23%), 49 (17%), 74 (10%)				
^{177}Lu	6.65 d	β^- (100%)	β^-, 134*	^{176}Lu(n,γ)^{177}Lu	3+	6–9	[73,89]
		γ	γ, 113 (6.4%), 208 (11%)	^{176}Yb(n,γ)^{177}Yb → ^{177}Lu			
^{188}Re	16.9 h	β^-	β^-, 784*	^{188}W/^{188}Re generator	4+	6–8	[86,91]
		γ	γ, 155 (15%)	^{187}Re(n,γ)^{188}Re			

EC: Electron capture; n: neutron; p: proton; γ: gamma, *: mean energy.

1.4. Structure of folate-based radiopharmaceuticals

Folate-based radiopharmaceuticals are composed of FA that has been modified by nucleophilic substitution with fluorine-18 or functionalized with a chelating agent (metal radionuclide) or a prosthetic group possessing fluorine-18. Hence, as the recognition part of FA is the pteroate moiety, the main challenge is to fix selectively the chelating agent/prosthetic group on the glutamic acid unit. Some studies demonstrated the necessity to preserve the α-carboxylic acid of glutamic residue to keep a good FRα-affinity [100,101]. One the other side, other scientists like Müller and co-workers demonstrated that both α- and γ-analogs present similar *in vivo* properties [102,103]. Wedeking *et al.* confirmed these results after description of good *in vivo* properties of α-analog [104]. Hence, α-carboxylic acid of glutamic residue was included to this recognition part for most research teams. Consequently, Boss *et al.* decided to confirm previous results by studying 3 pairs of α- and γ-^{18}F-radiofolates [105].The necessity to fix chelating agent on γ-carboxylic acid of glutamic acid residue led to develop regioselective synthesis strategies. These syntheses need lots of steps and overall yields are consequently low. However, some teams decided to circumvent this problem by fixing chelating agent to γ-carboxylate of glutamic acid and then, fixed this compound onto pteroate [106]. Others made the choice to develop folate-like radiopharmaceuticals by removing or replacing glutamic acid [107]. In this way, recognition part is maintained but cannot be considered as FA anymore.

1.5. Focus and content of the review

Targeting FRα in diagnosis and therapy has attracted a lot of attention from researchers and various studies have already shown the frequent high-level expression of FRα in ovarian cancer, in a broad cross-section of non-small cell lung cancer patients, as well as in other cancers [6,108–110].

Herein, this review will be focused on folate-based radiopharmaceuticals used to diagnose FRα-overexpressing tumors using nuclear imaging (PET and SPECT), and to treat them more effectively by TRT. FRβ-targeted radiopharmaceuticals, non-folate-based radiopharmaceuticals targeted FRα and nanoparticles-based radiofolates will not be depicted in this review but are reviewed by other researchers [111–119]. The different FA(α)- and/or FA(γ)-conjugates (*i.e.*, functionalization of FA at the α- and/or γ-position of the glutamate moiety) that have been developed to be radiolabelled with SPECT isotopes (technetium-99 m, indium-111, gallium-67) and/or PET isotopes (fluorine-18, gallium-68, copper-64, scandium-44) or for therapeutic application (lutetium-177, terbium-161) will be described and compared. Improvement of radiofolate synthesis and *in vivo* properties using folate-derivatives will be presented. Albumin-binding (AB) folate radiopharmaceutical, an innovative class of radiofolate allowing the improvement of diagnostic (*i.e.*, improvement of the tumor-to-kidney ratio by reducing kidney uptake) will be described. Finally, TRT studies inscribe or not in a theranostic approach will be exposed.

In vitro studies as well as *in vivo* tests (biodistribution and imaging) in tumor-bearing mice will be reported. FA and folates are essential nutrients for organism. Thus, the development of stable radiofolates is essential regarding radiometabolite. Stability tests were performed for all described radiopharmaceuticals in phosphate-buffered saline (PBS) or serum and no significant degradation was observed within two half-life times showing the interest of radiofolates for diagnosis or therapeutic applications. *In vitro* studies were performed using FRα-positive cells such as HeLa (human cervical carcinoma cell line), KB and KB-V1 (subclone and muti-resistant subclone of Hela cells, respectively), IGROV-1 (human ovarian carcinoma), SKOV-3ip (human ovarian adenocarcinoma), HT29 and LoVo (colorectal carcinoma), 24JK-FBP (mice sarcoma),CT-26 (mouse colon cancer cell), MA104 (embryonic monkey cell), M109 (murine lung carcinoma) and MT-1 (human breast carcinoma) and FRα-negative cells such as WI38 (human lung fibroblast primary cell), A549 (human lung carcinoma), HT1080 (human fibrosarcoma) and PC-3 (human prostate cancer).

2. Radiofolates developed for SPECT imaging application

2.1. Gallium-67 radiofolates

2.1.1. [^{67}Ga]Ga-deferoxamine-folate

The first radiofolate was described in 1996 by Wang *et al.* [100]. They designed the radioconjugate **[^{67}Ga]Ga-1** ([^{67}Ga]Ga-DFO-(γ)-folate) (Fig. 3) composed of a DFO chelating agent linked to FA *via* an amine bond on the γ-carboxylate function of the glutamic acid entity. Results showed that **[^{67}Ga]Ga-1** was internalized into KB cells but not in WI38 cells (32.3 ± 2.4% and 0.22 ± 0.04%, respectively) highlighting the selective uptake of **[^{67}Ga]Ga-1** by FRα. Biodistribution and imaging tests were performed in a second study [120]. For biodistribution tests, KB cells were subcutaneously inoculated in male athymic nude mice to induce tumor formation and **[^{67}Ga]Ga-1** was i.v. injected. Significant tumor and kidney uptakes were respectively 5.2 ± 1.5 %IA/g and 2.02 ± 0.32 %IA/g. No significant uptake was observed for other organs leading to an excellent tumor-to-background contrast. Tumor-to-kidney ratio was of 2.6. KB cells were subcutaneously injected in abdomen of mice for imaging study. γ-Scintigraphy images were obtained 46 h after i.v. injection of **[^{67}Ga]Ga-1** (6.66 MBq). Only kidneys and tumor were clearly visible on images and the contrast was of a good quality. To conclude, **[^{67}Ga]Ga-1** was suitable for further investigations as it was fast cleared from mice body *via* renal way. Moreover, uptake was observed only for tumor and kidneys with one of the best tumor-to-kidney ratios for FRα-positive tumor-bearing mice and images managed to clearly reveal tumor.

2.1.2. [^{67}Ga]Ga-DOTA-folates

Mindt *et al.* developed in 2009 another ^{67}Ga-radiofolate: **[^{67}Ga]Ga-2** ([^{67}Ga]Ga-DOTA-click-(γ)-folate) [101]. DOTA chelator was regio-specifically coupled to γ-carboxylic acid of FA *via* copper-catalyzed azide-alkyne cycloaddition (CuAAC) click chemistry reaction to obtain compound **2** (Fig. 4A). IC_{50} of **[^{67}Ga]Ga-2** was determined on KB cells and revealed a high affinity of 1.6 nM for FRα. KB cells were subcutaneously inoculated in female BALB/c mice to prepare small animal SPECT/CT imaging. Images were recorded 18 h after i.v. injection of 15 MBq of **[^{67}Ga]Ga-2** in this mice model. Only tumors and kidney were visible and activity intensity was more important for tumors than kidneys (Fig. 4A). Imaging test results were quite promising, but further investigations, notably the achievement of biodistribution tests were required to confirm promising results and to hope the fulfilment of clinical trials.

Müller *et al.* worked on the DOTA radiofolate **[^{67}Ga]Ga-3** ([^{67}Ga]Ga-DOTA-Bz-EDA-(γ)-folate) also called [^{67}Ga]Ga-EC0800 (*i.e.*, gallium-67-labelled version of EC0800, Endocyte Inc.) [121]. DOTA chelator was fixed to γ-carboxylic acid of folate by the ethylenediamine (EDA) linker (Fig. 4B). *In vitro* uptake tests were performed in KB cells. Good results were obtained as at 4 h, 30% of radioconjugate was internalized. **[^{67}Ga]Ga-3** were injected in female athymic nude mice bearing KB tumor for biodistribution and SPECT/CT imaging (1 and 20 MBq, respectively). Uptake in tumor and kidneys were of 6.08 ± 0.89 %IA/g and 84.53 ± 14.10 %IA/g, respectively. This led to a low tumor-to-kidney ratio of 0.07 ± 0.01. Significant uptake was also observed in salivary glands as the

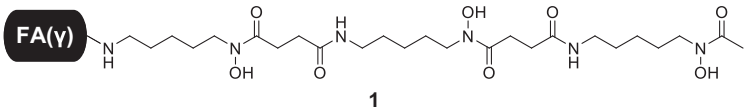

Fig. 3. Chemical structure of **1** [100].

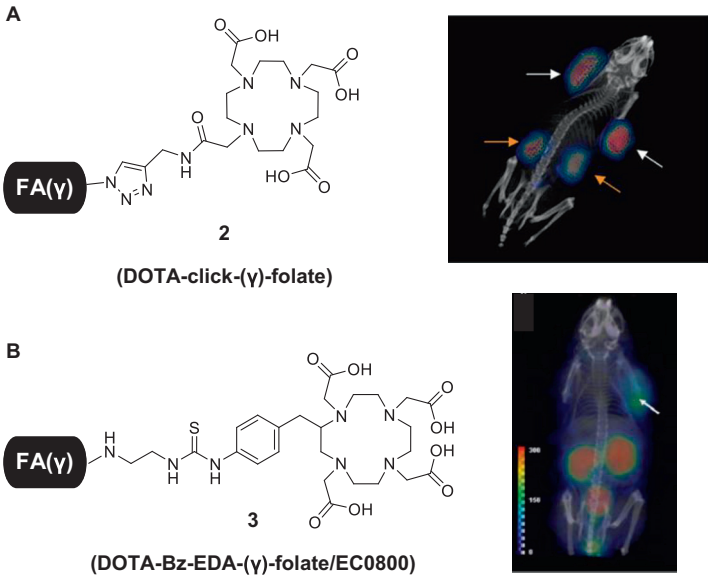

Fig. 4. (A) Chemical structure of **2** and SPECT image of KB tumor-bearing mice at 18 h p.i. of **[^{67}Ga]Ga-2** (15 MBq). Reprinted with permission from [101] Copyright 2022 American Chemical Society. (B) Chemical structure of **3** and SPECT image of KB tumor-bearing mice at 4 h p.i. of **[^{67}Ga]Ga-3** (20 MBq). Reprinted with permission from [121]. Copyright 2022 Elsevier.

uptake was of 6.93 ± 1.67 %IA/g. Nevertheless, radioconjugate uptake in salivary glands significatively decreased in time whereas tumor and kidney uptake stayed stable. This indicated a fast-renal clearance, and that salivary gland uptake is not due to the presence of FRα. SPECT/CT images (Fig. 4B) showed a moderate activity intensity in tumor and kidneys. High uptake in bladder confirmed a fast renal clearance. To conclude, this radioconjugate was well internalized by tumors but also in non-targeting organ which can be problematic for ovarian cancer diagnostic.

2.2. Indium-111 radiofolates

2.2.1. [^{111}In]In-DTPA-folate

The first folate-based radioconjugate using indium-111 was described by Wang *et al.* in 1997 [122,123]. Compound **4** is composed of a DTPA chelating agent linked to γ-carboxylic acid of FA *via* an EDA linker (Fig. 5). Evaluation of the affinity of **[^{111}In]In-4** ([^{111}In]In-DTPA-(γ)-folate) using KB cells showed significative fixation of the derivative on FRα. Biodistribution study in KB tumor-bearing athymic nude mice was realized with **[^{111}In]In-4**. It was demonstrated that this radioconjugate was significantly uptake in kidneys and tumors. The tumor-to-kidney ratio was of 1.00 which appears to be an excellent value knowing the important presence of FRα in kidneys. Tumor uptake was 3.1 ± 0.6 %IA/g for **[^{111}In]In-4**. However, uptake in lungs, liver, spleen and kidneys was also important and resulted in a very poor tumor-to-background contrast. KB tumor-bearing mice were i.v. injected with **[^{111}In]In-4** 1 h before imaging. γ-Scintigraphy of KB tumor-bearing mice at 5 and 24 h p.i. of **[^{111}In]In-4** revealed a significant accumulation of the radioconjugate only in the tumor and kidneys. **[^{111}In]In-4** is also rapidly excreted primarily in the urine. These suggest that imaging tests of FRα-positive tumors on humans using **[^{111}In]In-4** could be explored to develop a non-invasive imaging method to diagnose FRα-positive tumors (section 2.4.1.).

In 2008, Müller *et al.* published further investigations on the suitability of **[^{111}In]In-4** for SPECT imaging [124]. Biodistribution experiments were performed on three types of mice model: IGROV-1 tumor-bearing mice, SKOV-3ip tumor-bearing mice and SKOV-3ip metastasis bearing mice. At 4 h p.i. of **[^{111}In]In-4** in IGROV-1 or SKOV-3ip tumor-bearing mice, radioconjugate uptake in the IGROV-1 tumor was of 9.79 ± 3.21 %IA/g and 7.57 ± 0.61 % IA/g for SKOV-3ip tumor. Kidney uptake was also observed in both IGROV-1 and SKOV-3ip tumor-bearing mice with 85.61 ± 11.90 and 103.38 ± 18.79 %IA/g, respectively. Salivary gland uptake was also observed in both model with 12.18 ± 1.23 and 12.12 ± 1.62 %IA/g, respectively. Thus, a low tumor-to-kidney ratio was observed for both IGROV-1 or SKOV-3ip tumor-bearing mice, with 0.11 ± 0.04 and 0.08 ± 0.01, respectively. These low ratios are unfavorable for imaging and diagnostic quality as an important kidney uptake could hide metastasis in the intraperitoneal region for example. SPECT/CT imaging was performed on the three mice models at 4 h p.i. of **[^{111}In]In-4** (Fig. 5). Images showed that tumor and kidneys fix **[^{111}In]In-4**. Tumor-to-background contrast was excellent, but metastases were not clearly visible on SPECT/CT images as kidney uptake was too important. This article concluded that results were quite promising and showed that **[^{111}In]In-4** is suitable to detect ovarian carcinoma or ovarian adenocarcinoma. Nevertheless, this radiofolate is not suitable to detect SKOV-3ip metastasis using microPET imaging.

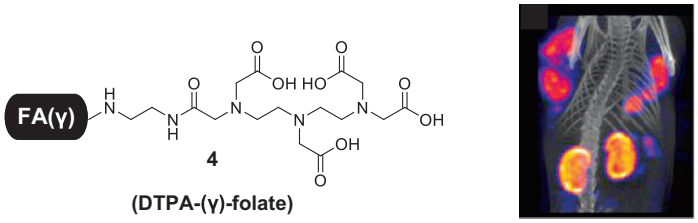

Fig. 5. Chemical structure of **4** and SPECT image of IGROV-1 tumor-bearing mice at 4 h p.i. of **[^{111}In]In-4** (30–50 MBq). Reprinted with permission from [124]. Copyright 2022 SNMMI.

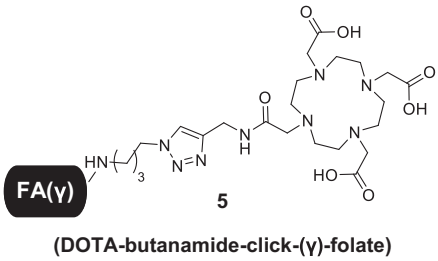

Fig. 6. Chemical structure of **5** [125].

2.2.2. [^{111}In]In-DOTA-folate

Müller *et al.* developed new ^{111}In-radiofolate tracer by designing a radioconjugate called **[^{111}In]In-5** ([^{111}In]In-DOTA-butanamide-click-(γ)-folate) (Fig. 6). FA was coupled to a DOTA chelating agent using CuAAC click chemistry [125]. The advantage of this chelating agent over DTPA is its capacity to coordinate with a wide range of diagnostic (*e.g.*, indium-111, gallium-67, gallium-68, copper-64) and therapeutic (*e.g.*, lutetium-177, copper-47, yttrium-90) radionuclides. Tissue distribution of **[^{111}In]In-5** was performed on KB tumor-bearing female athymic nude mice. Tumor uptake was of 5.80 ± 0.55 %IA/g whereas kidney uptake was ten times superior with 55.88 ± 3.91 %IA/g. In addition, liver and salivary glands uptake were also observed with 5.20 ± 2.00 and 6.13 ± 1.84 %IA/g, respectively. The tumor and kidney uptake values stayed stable 24 h after injection whereas liver and salivary glands uptake significatively decreased after 4 h. Tumor-to-kidney ratio was insufficient but stayed stable for 24 h (0.11 ± 0.02). SPECT/CT imaging was performed on KB tumor-bearing mice at 24 h p.i. of **[^{111}In]In-5**. Tumors and kidneys were clearly visible on images and no liver or salivary glands fixation were visible at 24 h. Rapid renal clearance of the radioconjugate contributes to its safety and the high quality of images. To conclude, compared to **[^{111}In]In-5, [^{111}In]In-4** is more suitable for clinical trials.

2.3. Technetium-99 m radiolofates

2.3.1. [^{99m}Tc]Tc-HYNIC-folates

In 1999, Guo *et al.* developed the first ^{99m}Tc-radiofolate named **[^{99m}Tc]Tc-6** ([^{99m}Tc]Tc-HYNIC-(γ)-folate)(tricine/TPPTS) [126]. FA was coupled to HYNIC chelator *via* an amide bond (Fig. 7). HYNIC conjugate was used because, unlike DTPA, its radiolabelling with ^{99m}Tc was effective even at low concentration. The authors decided to perform *in vivo* experiments with 24JK-FBP tumor-bearing C57BL/6 female mice because 24JK-FBP was more representative of tumors in humans than KB cells. The biodistribution results showed an important tracer uptake in the kidneys and tumors. Tumor-to-kidney ratio at 4 h was quite low (0.26 ± 0.03). 24JK-FBP tumor-bearing mice expressed less FRα on tumor cell surfaces explaining a tumor-to-blood ratio seven times lower than in KB tumor-bearing mice. On γ-scintigraphy images, kidneys appeared with a significant brilliance. Tumors were quite visible even if their radiation intensities were lower than kidneys one.

Lu *et al.* synthesized HYNIC-NHHN-FA which was formed of a hexane-1–6-diamine (NHHN) linker between HYNIC chelator and FA [127]. HYNIC-NHHN-FA was radiolabelled with technetium-99 m in presence of tricine/diphenylphosphinobenzene-3-sulfonic acid sodium (TPPMS) or tricine/trisodium triphenylphosphine-3,3′,3″-trisulfonate (TPPTS) to form **[^{99m}Tc]Tc-7** ([^{99m}Tc]Tc-(HYNIC-NHHN-(γ)-folate)(tricine/(TPPMS)) and **[^{99m}Tc]Tc-8** ([^{99m}Tc]Tc-(HYNIC-NHHN-(γ)-folate)(tricine/(TPPTS)), respectively (Fig. 7). These co-ligands played an important role in improving pharmacokinetic properties and increasing the stability of folate-based radioconjugate. Biodistribution of the two radioconjugates in KB tumor-bearing athymic nude mice revealed tumor and kidney uptake of 0.19 ± 0.05 and 3.62 ± 1.43 %IA/g for **[^{99m}Tc]Tc-7** and 9.79 ± 1.66 and 114.88 ± 8.12 %IA/g for **[^{99m}Tc]Tc-8**, respectively. Thus, no significant tumor uptake was observed for **[^{99m}Tc]Tc-7** whereas TPPTS analog exhibited good FRα-positive cell uptake and retention and a good tumor-to-background contrast. These results highlighted the important of the choice of co-ligands to chelate ^{99m}Tc as they play an important role on biological properties. They concluded that the TPPMS analog was quickly excreted due to its high hydrophobicity (log P of −2.34 ± 0.01) which conferred it different pharmacokinetic properties. Tumor-to-kidney ratio was low with 0.085 for **[^{99m}Tc]Tc-8**. This study demonstrated that only **[^{99m}Tc]Tc-8** presented favorable biological characteristics and could lead to promising results for small animal imaging experiments.

To pursue their work, the same team synthesized HYNIC-PEG$_2$-FA which was composed of HYNIC chelator linked to FA thanks to 2,2′-(ethylenedioxy)-bis-ethylamine (PEG$_2$). Tricine/TPPTS, tricine/TPPMS and ethylenediamine-*N*,*N*′-diacetic acid (EDDA) were co-ligands used to coordinate technetium-99 m [128]. The three complexes formed were respectively **[^{99m}Tc]Tc-9** ([^{99m}Tc]-Tc-(HYNIC-PEG$_2$-(γ)-folate)(tricine/TPPTS)), **[^{99m}Tc]Tc-10** ([^{99m}Tc]-Tc-(HYNIC-PEG$_2$-(γ)-folate)(tricine/TPPMS)) and **[^{99m}Tc]Tc-11** ([^{99m}Tc]Tc-(HYNIC-PEG$_2$-(γ)-folate)(EDDA)) (Fig. 7). Biodistribution was performed on KB tumor-bearing mice and a major accumulation in kidneys for **[^{99m}Tc]Tc-9**, **[^{99m}Tc]Tc-10** and **[^{99m}Tc]Tc-11** with 149.70 ± 19.57, 24.38 ± 3.25 and 121.41 ± 11.5 %IA/g, respectively, was observed. Tumor uptakes of **[^{99m}Tc]Tc-9**, **[^{99m}Tc]Tc-10** and **[^{99m}Tc]Tc-11** were respectively of 11.35 ± 0.67, 0.67, 1.24 ± 0.01 and 5.52 ± 0.58 %IA/g leading to tumor-to-kidney ratios of 0.075, 0.05, 0.045, respectively. The tumor-to-kidney ratios of **[^{99m}Tc]Tc-10** and **[^{99m}Tc]Tc-11** were the lowest never observed in radiofolate studies. These results clearly demonstrated that **[^{99m}Tc]Tc-9** was the best of the three developed complexes. The linker used here was more hydrophilic than NHHN previously described (log P of −3.40 ± 0.12 for **[^{99m}Tc]Tc-9** *vs.* −3.26 ± 0.08 for **[^{99m}Tc]Tc-8**) and enhanced the hydrophilicity of the tracer and so its renal clearance. Through this, the team wanted to improve SPECT imaging quality. **[^{99m}Tc]Tc-9** was selected for SPECT imaging studies on KB tumor-bearing mice. Only tumor and kidneys were visible on images which confers to

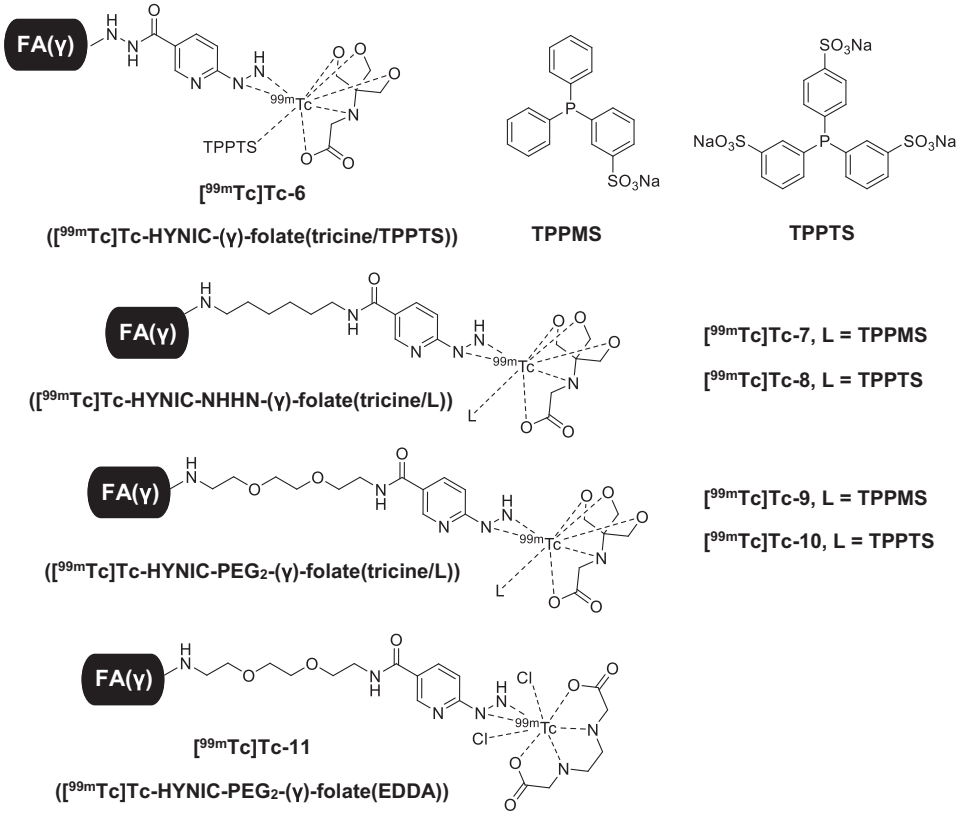

Fig. 7. Chemical structures of **[^{99m}Tc]Tc-6**, co-ligands TPPMS and TPPTS, **[^{99m}Tc]Tc-7**, **[^{99m}Tc]Tc-8**, **[^{99m}Tc]Tc-9**, **[^{99m}Tc]Tc-10** and **[^{99m}Tc]Tc-11** [126,127].

[^{99m}Tc]Tc-9 a good tumor-to-background contrast ability. Moreover, high activity found in bladder confirmed the renal clearance way. To conclude, **[^{99m}Tc]Tc-9** was the most suitable compound developed in this study for nuclear imaging.

Guo *et al.* studied **[^{99m}Tc]Tc-12** ([^{99m}Tc]Tc-HYNIC-T-(γ)-folate-(tricine/TPPTS)) [129]. HYNIC-T-(γ)-folate was composed of HYNIC chelator linked to the γ-carboxylate group of glutamate residue of FA using CuAAC click chemistry reaction (Fig. 8). Biodistribution study in KB tumor-bearing athymic nude mice revealed accumulation in tumor with a concentration in radiofolate of 8.14 ± 0.45 %IA/g at 4 h and especially in kidneys with 57.72 ± 4.50 %IA/g. This induced a low but correct tumor-to-kidney ratio equal to 0.14. SPECT imaging was performed 4 h after radioconjugate injection and brought forward tumor and kidneys but also bladder (Fig. 8). Guo *et al.* came to the conclusion that **[^{99m}Tc]Tc-12** has a strong tumor uptake, a low uptake in non-specific organs such as in the liver and muscles and a fast renal clearance way. In short, this study shows that **[^{99m}Tc]Tc-12** was a good candidate to track the evolution of therapies by SPECT imaging.

Guo *et al.* coupled HYNIC to the ε-amine of lysine-pteroate *via* an amide bond to give the HYNIC-Lys-pteroate compound. Tricine and TPPTS were used as co-ligands to coordinate technetium-99 m, affording **[^{99m}Tc]Tc-13** ([^{99m}Tc]Tc-(HYNIC-lys-pteroate)(tricine/TPPTS)) (Fig. 9) [130]. Biodistribution in KB tumor-bearing BALB/c nude male mice showed that the largest accumulation of **[^{99m}Tc]Tc-13** was found in kidneys with 89.60 ± 5.06 %IA/g whereas tumor uptake was only of 9.60 ± 1.46 %IA/g at 2 h. Tumor-to-kidneys ratio was equal to 0.11 and tumor-to-liver ratio was low (3.89) leading to a massive hepatobiliary excretion of the radiofolate which was not optimal for a good diagnostic as renal excretion way is more suitable. SPECT imaging was performed on KB tumor-bearing mice at 2 h p.i. of **[^{99m}Tc]Tc-13** (Fig. 9) and a major activity was found in tumor, kidney, liver and bladder. This confirmed hepatobiliary excretion of the radiofolate that is not an optimal way of clearance. Moreover, the intense activity found in the abdomen area could mask a potential tumor or metastasis in this area. Thus, this radiofolate was not suitable for FRα-overexpressing tumor diagnosis.

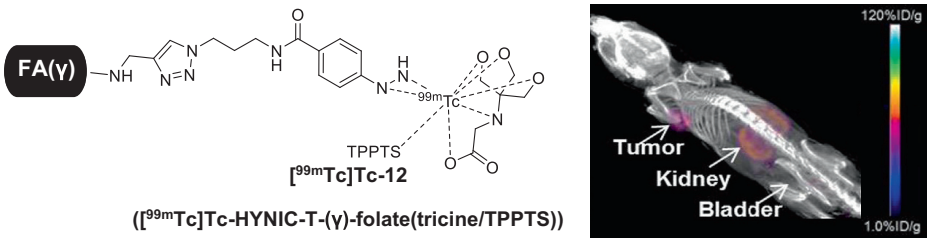

Fig. 8. Chemical structure of **[^{99m}Tc]Tc-12** and SPECT image of KB tumor-bearing mice at 4 h p.i. of **[^{99m}Tc]Tc-12** (18 MBq). Reprinted with permission from [129]. Copyright 2022 Elsevier.

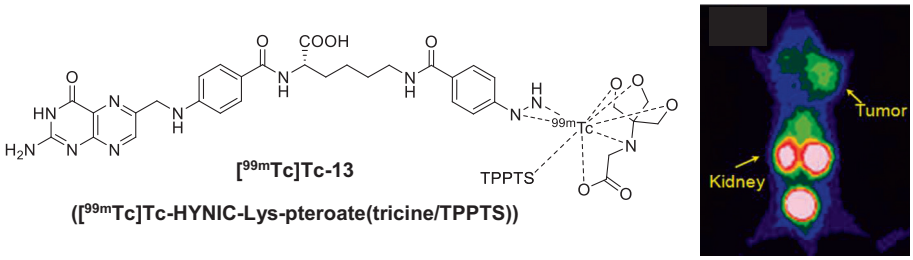

Fig. 9. Chemical structure of **[^{99m}Tc]Tc-13** and SPECT image of KB tumor-bearing mice at 2 h p.i. of **[^{99m}Tc]Tc-13** (7.4 MBq). Reprinted with permission from [130]. Copyright 2022 Elsevier.

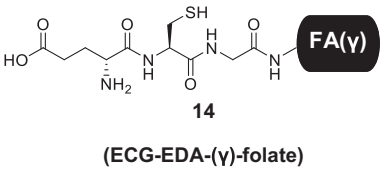

Fig. 10. Chemical structure of **14** [131].

2.3.2. [^{99m}Tc]Tc-peptide-folate

Kim *et al.* synthesized **[^{99m}Tc]Tc-14** ([^{99m}Tc]Tc-ECG-EDA-(γ)-folate) by coupling the peptide H-Gly-Cys-Glu-OH to FA thanks to an EDA linker(Fig. 10) [131]. The peptide moiety played the role of the chelating agent. Biodistribution in KB tumor-bearing BALB/c athymic nude mice showed significant accumulation of **[^{99m}Tc]Tc-14** in the tumor, kidney, liver, intestines and gallbladder. These non-specific accumulations hepatobiliary clearance way might be due to the hydrophobic nature of **[^{99m}Tc]Tc-14**. Scintigraphy imaging was performed at 4 h p.i. of radioconjugate and revealed KB tumor, kidneys, liver, intestines and bladder with a huge activity intensity. SPECT/CT imaging allowed to well visualize KB tumor, intestines and kidneys even 22 h p.i. of radioconjugate. **[^{99m}Tc]Tc-14** showed good tumor absorption but further studies have to be performed to overcome the problem of non-specific organ uptake which conduct to a poor tumor-to-background contrast.

2.3.3. [^{99m}Tc]Tc-ethylenedicysteine-folate

Ligan *et al.* developed **[^{99m}Tc]Tc-15** ([^{99m}Tc]Tc-ethylenedicysteine-(γ)-folate) which was formed of the ethylenedicysteine chelator linked to FA on its γ-carboxylate function *via* an EDA linker (Fig. 11) [132]. Biodistribution in female Fischer 344 rats inoculated with mammary tumor cells of the cell line 13762 revealed a significant uptake of **[^{99m}Tc]Tc-15** in kidneys with 5.102 ± 0.276 % IA/g at 2 h whereas tumor uptake was low and of the same order than other tested organs. This led to the lowest tumor-to-kidney ratio (0.04) observed for a ^{99m}Tc-radiofolate. These let to think that tumor cells selected for this study did not express enough FRα on cell surface. SPECT images were recorded at 4 h p.i. of radioconjugate and exhibited intense activity in the tumor and kidneys. Furthermore, a renal excretion way as intense activity in bladder was also observed. These results suggested that **[^{99m}Tc]Tc-15** might not be a good candidate for imaging of FRα-positive tumors.

2.3.4. [^{99m}Tc]Tc-TEPA-folate

The radiodiagnostic agent **[^{99m}Tc]Tc–16** ([^{99m}Tc]Tc–TEPA-(γ)-folate) was developed by Panwar *et al.* [133]. It was composed of the TEPA chelating agent coupled to FA on the γ-carboxylic acid of the glutamic entity *via* an amide bond (Fig. 11). Affinity binding assay was performed on KB cells and revealed that **[^{99m}Tc]Tc-16** had a K_d of 5 ± 0.06 μM meaning an affinity 5000 times lower for FRα than FA (1 nM). Biodistribution in KB tumor xenografted nude mice revealed a major uptake of **[^{99m}Tc]Tc-16** at 4 h in the kidneys following by liver, intestines and tumor (*i.e.*, 16.0 ± 1.2, 16.1 ± 2.0, 4.56 ± 0.3 and 4.26 ± 1.3 %IA/g, respectively). Important non-specific uptakes were not a good result for the suitability of this radioconjugate in diagnostic imaging. Scintigraphy was performed with the same mice model at 1 h p.i. of radioconjugate and displayed intense activity in kidneys, liver, intestines and tumors leading to a real poor image quality. These non-specific targeting may be explained by the hydrophobicity of the molecule, the chelating agent having any electronegative groups expected for the 5 amine functions. This increased the hepatobiliary clearance and so accumulation in liver and intestines. In summary, modifications on the compound structure are required to increase the tumor specificity.

2.3.5. [^{99m}Tc]Tc-DO3A-EA-folate

[^{99m}Tc]Tc-17 ([^{99m}Tc]Tc-DO3A-EA-(γ)-folate) has been developed by Mishra *et al.* [134]. DO3A chelator and FA composed this tracer (Fig. 11). The affinity coefficient of 4.2 ± 0.8 μM indicated that **[^{99m}Tc]Tc-17** was not as specific as FA and could lead to non-specific binding. Biodistribution on KB tumor-bearing nude mice showed a major accumulation of **[^{99m}Tc]Tc-17** at 4 h in liver and kidneys, less but significant uptake was also observed for tumors and intestines with respectively 12.2 ± 1.5, 13.2 ± 1.1,

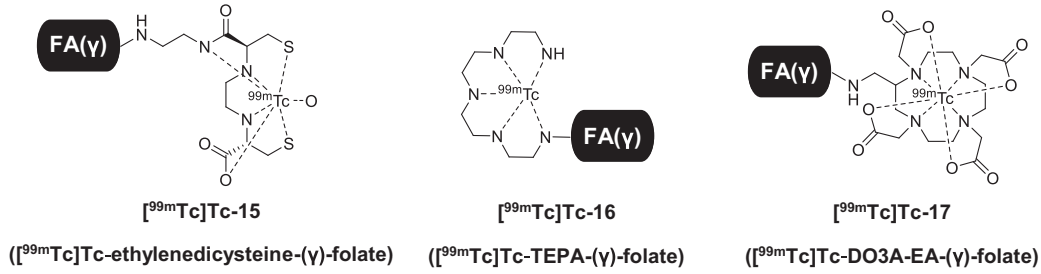

Fig. 11. Chemical structures of **[^{99m}Tc]Tc-15**, **[^{99m}Tc]Tc-16** and **[^{99m}Tc]Tc-17** [132–134].

6.26 ± 0.8 and 4.1 ± 0.8 %IA/g. SPECT scintigraphy images were recorded at 4 h p.i. of radioconjugate and tumor was well visualized. Massive activity was detected in the whole abdomen of mice leading to poor quality images. High uptake in intestines presumes hepatobiliary clearance that is not recommended for good pharmacokinetic properties of radioconjugate and could prevent to see tumor in abdomen area. Too important non-specific uptake and poor images quality were problematic and jeopardize further investigations.

2.3.6. [^{99m}Tc]Tc(CO)$_3$-folates

Müller *et al.* also worked on [^{99m}Tc]Tc(CO)$_3$-radiofolates by developing three radioconjugates: **[^{99m}Tc]Tc-18** ([^{99m}Tc]Tc(CO)$_3$-PAMA-(α)-folate), **[^{99m}Tc]Tc-19** ([^{99m}Tc]Tc(CO)$_3$-PAMA-(γ)-folate) and **[^{99m}Tc]Tc-20** ([^{99m}Tc]Tc(CO)$_3$-PAMA-pteroate) [102,135]. The chelating agent picolylamine monoacetic acid (PAMA) was developed to chelate technetium-99 m using three carbon monoxide co-ligands. Compounds **18** and **19** were composed of PAMA entity linked to the α- and γ-carboxylic acids of FA, respectively. Compound **20** was composed of PAMA entity coupled *via* an amide bond to the pteroate entity (Fig. 12). For these three radioconjugates, binding assay on KB cells showed excellent and similar cell binding (48% for **[^{99m}Tc]Tc-20**, 57% for **[^{99m}Tc]Tc-19** and 60% for **[^{99m}Tc]Tc-18**). Excellent K_d constant was obtained compared to free FA (2.51, 2.09, 14.52 and 7.22 nM for **[^{99m}Tc]Tc-18**, **[^{99m}Tc]Tc-19**, **[^{99m}Tc]Tc-20** and FA, respectively). Biodistribution in KB tumor-bearing athymic nude mice indicated no significant uptake of **[^{99m}Tc]Tc-20** in tumor and kidneys at 4 h p.i. and was rejected from the further studies. Significant uptake was observed only for **[^{99m}Tc]Tc-19** and **[^{99m}Tc]Tc-18** in tumor (2.33 ± 0.36 and 1.24 ± 0.19 %IA/g, respectively) and kidneys (18.48 ± 0.72 %IA/g and 12.36 ± 1.86 %IA/g, respectively) leading to tumor-to-kidney ratios of 0.13 and 0.10, respectively. Indeed, **[^{99m}Tc]Tc-19** expressed slightly better biodistribution results than **[^{99m}Tc]Tc-19** and was chosen for SPECT imaging study performed on KB tumor-bearing mice. At 24 h**,** tumors, kidneys and intestines were highly visible on images. This could be explained by the high radioconjugate concentrations in the content of intestines due to a hepatobiliary excretion way. To conclude, **[^{99m}Tc]Tc-19** successfully assessed *in vitro* and *in vivo* tests compared to **[^{99m}Tc]Tc-20**. **[^{99m}Tc]Tc-19** and **[^{99m}Tc]Tc-18** showed similar properties and are both suitable for further investigations notably to improve their bioavailability. Müller *et al.* pursued their investigations with **[^{99m}Tc]Tc-19** by exploring its targeting behavior for eight FRα-positive cancer cell lines (*i.e.*, KB, IGROV-1,SKOV-3ip, HT29, LoVo, 24JK-FBP, KB-V1 and HeLa cells) [136]. *In vitro* cell uptake study and *in vivo* biodistribution of **[^{99m}Tc]Tc-19** on the 8 different FRα-positive tumor-bearing mice models using revealed that **[^{99m}Tc]Tc-19** is suitable to detect all tested FRα-positive cell lines and so different cancerous cell types.

Müller and co-workers designed **[^{99m}Tc]Tc-21** ([^{99m}Tc]Tc(CO)$_3$-triazole-(γ)-folate) through an innovative strategy called click-to-chelate [137,138]. This strategy consisted in conjugating a small molecule to FA by CuAAc click chemistry reaction and using the small molecule and the formed triazole ring as chelator moieties (Fig. 13). The team also synthesized an analog of **[^{99m}Tc]Tc-21** by replacing the triazole entity by a histidine to give **[^{99m}Tc]Tc-22** ([^{99m}Tc]Tc(CO)$_3$-N(τ)His-(γ)-folate). *In vitro* cell uptake assay of **[^{99m}Tc]Tc-21** and **[^{99m}Tc]Tc-22** was performed on KB cells and showed a similar uptake of 50%. Biodistribution on KB tumor-bearing mice revealed similar profile for both radiofolates as the only significant different was a high liver uptake for **[^{99m}Tc]Tc-22** than for **[^{99m}Tc]Tc-21** (3.83 ± 1.49 *vs*. 0.89 ± 0.42 %IA/g at 4 h p.i., respectively). Significant uptake was observed in kidneys and tumors in the same level. A second biodistribution study was performed on KB tumor-bearing mice using **[^{99m}Tc]Tc-22** and similar results were obtained, excepted for salivary glands showing a significant non-specific uptake of 5.72 ± 0.63 %IA/g [138]. *Ex vivo* autoradiography confirmed biodistribution results as uptake in tumor, kidneys and salivary glands was significant. SPECT/CT images were recorded at 24 h p.i. of **[^{99m}Tc]Tc-22**. High activity was measured in KB tumors, kidneys and salivary glands. These results confirm the suitability of **[^{99m}Tc]Tc-22** for SPECT/CT diagnostic as no non-specific uptake in the abdominal area was observed (Fig. 13).

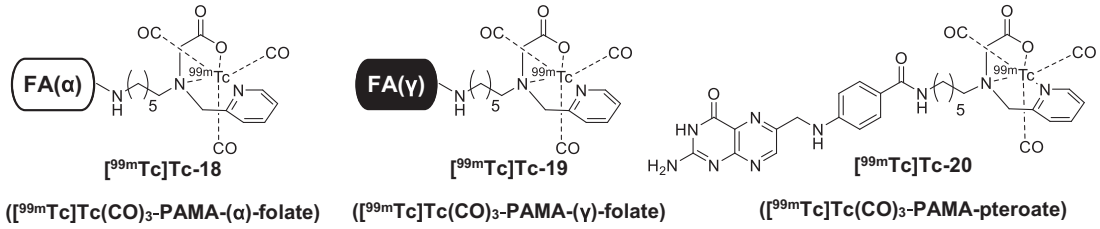

Fig. 12. Chemical structures of **[^{99m}Tc]Tc-18**, **[^{99m}Tc]Tc-19** and **[^{99m}Tc]Tc-20** [102,135].

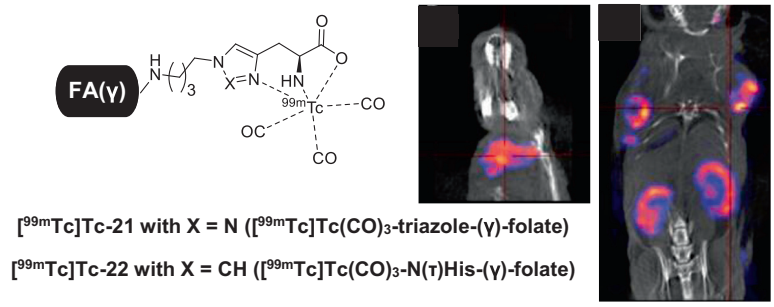

Fig. 13. Chemical structures of **[^{99m}Tc]Tc-21** and **[^{99m}Tc]Tc-22**, and SPECT images of KB tumor-bearing mice at 24 h p.i. of **[^{99m}Tc]Tc-22** (500 MBq). Reprinted with permission from [138]. Copyright 2022 SNMMI.

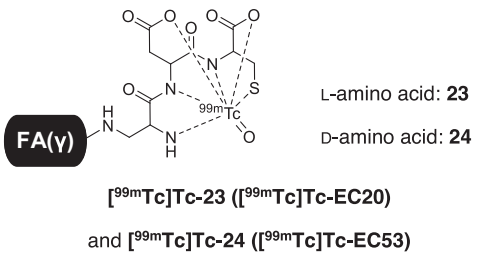

Fig. 14. Chemical structures of **[^{99m}Tc]Tc-23** and **[^{99m}Tc]Tc-24** [139].

2.3.7. [^{99m}Tc]Tc-EC20

Leamon *et al.* used the innovative folate-based radioconjugate for SPECT imaging **[^{99m}Tc]Tc-23** ([^{99m}Tc]Tc-EC20 also called [^{99m}Tc]Tc-etarfolatide^{TM}, Endocyte Inc.) (Fig. 14) [139]. Technetium-99 m formed 4 coordination bonds with the chelating agent and 2 with an oxygen atom as co-ligand. The IC_{50} of 128 nM obtained was closed to those of FA and **[^{111}In]In-4** meaning that **[^{99m}Tc]Tc-23** is as specific for FRα as a successful clinical trial radioconjugate. Biodistribution profile was achieved on M109 tumor-bearing BALB/c mice. Significant uptake was observed 4 h p.i. in tumor and kidneys (17.2 ± 1.02 and 138 ± 12.4 %IA/g, respectively) and no significant uptake was observed in non-specific organs. Tumor-to-kidney ratio was of 0.12 for **[^{99m}Tc]Tc-23** consolidating the promising of the observed results. Metabolism study revealed that **[^{99m}Tc]Tc-23** is predominantly eliminated from the body *via* the renal way. SPECT imaging was performed on the same mice model at 4 h p.i. of radioconjugate. Tumor and kidneys were clearly visible on images and other organs did not express activity intensity. To conclude, these preliminary results are very encouraging to push further tests with clinical trials.

The study of **[^{99m}Tc]Tc-23** was continued, and comparative experiments were made with its D-amino acid analog **[^{99m}Tc]Tc-24** ([^{99m}Tc]Tc-EC53) (Fig. 14) [140]. Affinity tests was performed on KB cells. **[^{99m}Tc]Tc-23** and **[^{99m}Tc]Tc-24** afforded K_d of 0.92 and 0.23 nM, respectively, meaning that **[^{99m}Tc]Tc-24** had a highest specificity to FRα. Biodistribution study was performed in M109 and 4 T1 tumor-bearing BALB/c mice, and revealed a significant uptake in KB tumor and kidneys for both radioconjugates. The uptake in almost all organs was lower of 33% for **[^{99m}Tc]Tc-24** compared to **[^{99m}Tc]Tc-23**, leading to the same tumor-to-kidney radio of 0.15. Additional biodistribution tests were done in KB tumors-bearing mice after i.v. and i.p. injections of **[^{99m}Tc]Tc-23**, respectively. Biodistribution profiles were quite similar and led to conclusion that uptake is independent of tumor and injection localization. With the objective of enhancing the tumor-to-kidney ratio, KB tumor-bearing mice were pre- or co-injected with free FA without success. Despite a general decrease of organs uptake in a dose-dependently manner that led to the same tumor-to-kidney ratio, injection of 1 equivalent of free FA improved the tumor-to-background contrast. As **[^{99m}Tc]Tc-24** gave no better results than **[^{99m}Tc]Tc-23**, they focused their research on the first developed radioconjugate.

2.4. Clinical evaluation of SPECT radiofolate

Two radiofolates were evaluated in clinical trials for SPECT imaging diagnosis of FRα-overexpressing tumors: **[^{111}In]In-4** and **[^{99m}Tc]Tc-23.** The first-in-human application was performed with **[^{111}In]In-4**. **[^{99m}Tc]Tc-23** is the only SPECT folate radioconjugate that was used clinically and in official studies. It is currently used in clinical routine. This following section resumed both clinical trials of **[^{111}In]In-4** and **[^{99m}Tc]Tc-23.**

2.4.1. [^{111}In]In-DTPA-folate

Regarding promising preclinical results, Phase I and II clinical trials were pursued using **[^{111}In]In-4** as a diagnostic imaging agent for ovarian cancer [141]. These trials were performed to study its safety, biodistribution and efficacy. 33 women from 31 to 82-years-old participated in this study, out of which 14 with malignant tumors (7 ovarian tumors, 2 recurrent endometrial tumors and 5 recurrent ovarian tumors), 18 with benign pelvic masses and 1 with a borderline malignancy. After SPECT imaging at 4 h p.i. (Fig. 15A), a biopsy was performed on patients to clearly define the malignant nature or not of masses. Only 5 patients reported minor adverse reactions like rashes or kidney discomfort that disappeared causing no sequelae. Uptake was observed in kidneys for all patients. Few patients also presented liver, spleen or gallbladder uptake. Two nuclear medicine physicians were charged with reading images based on two approaches: masked *vs.* unmasked. The images were read without (*i.e.*, masked) or with (*i.e.*, masked) complementary data of anatomic imaging studies (CT, sonography, MRI). For the masked study, 78% and 75% of the patient's diseases were correctly diagnosed, compared to 82% and 81% for the unmasked one. All malignant masses were correctly diagnosed. However, two false positive diagnoses of malignant tumors were made for two patients (*i.e.*, one suffering from endometriosis and one from adenomatoid tumor/hilar Leydig cell hyperplasia). For the recurrent malignancies only, the correct diagnostic ratio was only of 35% for the masked study and increased to 85% in the unmasked one. This indicated the importance of the correlation between the complementary data obtained with previous anatomical imaging studies and scintigraphy images. **[^{111}In]In-4** radiopharmaceutical was safe and effective for ovarian malignancies imaging because injection was safe and rapid uptake in the tumor and quick clearance from non-targeting tissues were observed. Images were similar and malignant tumors were well diagnosed by both nuclear medicine physicians.

2.4.2. [^{99m}Tc]Tc-EC20

Phase I clinical study was performed on 6 healthy untreated males (aged 20–65 years old) with no renal and hepatic misfunction [143–145]. Subjects were i.v. pre-treated with FA before i.v. injection of **[^{99m}Tc]Tc-23**. Health constants was then monitored up to 7 days, highlighting dizziness, diarrhea and increased white blood cells percentage in 50% of subjects. These events were related to radioconjugate injection but not considered as severe events to stop the study. Pharmacokinetic was evaluated during 24 h by measuring activity in blood and activity decreased rapidly as the half-life resident time in blood was of 12 min. Urine was also collected for 24 h to evaluate activity absorbed dose in organs. It was showed that urinary bladder and kidneys were the two organs absorbing the most radioconjugate. Whole-body planar imaging

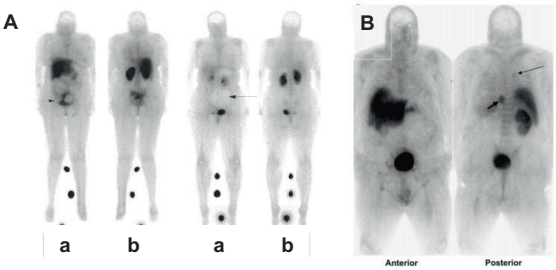

Fig. 15. (A) Planar scintigrams of patients at 4 h p.i. of **[^{111}In]In-4** (183 MBq) (a: anterior, b: posterior). Reprinted with permission from [141]. Copyright 2022 SNMMI, (B) SPECT images of 57-year-old man with pulmonary metastases from renal cell carcinoma at 1–2 h p.i. of **[^{99m}Tc]Tc-23** (555 MBq). Reprinted with permission from [142]. Copyright 2022 SNMMI.

was performed at 5 min to 24 h p.i.. Activity was clearly visualized in liver, kidneys and urinary bladder up to 24 h p.i. but also moderately in the bone marrow at 1 and 4 h p.i.. Imaging confirmed results of pharmacokinetics. Other phase I clinical trials were pursued in 2014 leading to the same results. **[^{99m}Tc]Tc-23** was well tolerated by subjects leading to the succeed of phase I.

Fisher *et al.* published phase II clinical trials results of **[^{99m}Tc]Tc-23** imaging to identify patients with FRα-positive tumors [142]. 154 patients with proven (CT, MRI) or suspected renal, ovarian, endometrial, breast or pituitary cancer participated in this study. Chosen patients should have lesions >1.5 cm, no renal misfunction and a tissue sample from surgery or biopsy. This latter was necessary to perform immunohistochemistry assay for analyzing FRα expression in tumors. Pre-treatment with FA before i.v. injection of **[^{99m}Tc]Tc-23** was necessary to obtain images with good tumor-to-background contrast. SPECT imaging was performed at 1 to 2 h p.i. (Fig. 15B) and, for most patients, specific uptake was observed in tumors and kidneys, which was not the case in bladder, liver and spleen. The monitoring of patient's health for 7 days p.i. revealed abdominal pain, nausea and vomiting for 8% of patients and were considered relative to radioconjugate injection. These non-severe events allowed to conclude that one injection of **[^{99m}Tc]Tc-23** was well tolerated by patients. 66.7% of patients were diagnosed with a cancer after nuclear imaging against 68% regarding immunohistochemistry assay results. Comparison of imaging and immunohistochemistry results showed an agreement in diagnostic of only 61%. This poor value is explained by the time spending between cancerous tissues sampling and imaging (from few days to few years). To conclude, clinical trial results were promising, and the team conducted further clinical tests to prove the suitability and efficiency of **[^{99m}Tc]Tc-23** to diagnose FRα-positive tumors.

2.5. Conclusion

First folate-based radioconjugates were developed in the late 90s for SPECT devices using gallium-67 and indium-111. These searches conducted to the first application of a folate-based radiopharmaceuticals for clinical diagnostic of ovarian and endometrial tumors. The first radiofolate **[^{67}Ga]Ga-1** described in the literature presented one of the best tumor-to-kidney ratio observed for radiofolate injection in FRα-positive tumor-bearing mice. Nevertheless, ^{67}Ga-folate-based radioconjugates also showing non-significant advantages in image and diagnostic quality compared to **[^{111}In]In-4**, which may be one of the reasons why no new folate-based tracers using gallium-67 were developed since 2011. Moreover, studies on ^{67}Ga-radioconjugates helped the development of ^{68}Ga-radiochemistry for PET applications. **[^{111}In]In-4** was used for first-in-human application and its clinical use led to the development of new folate-based radioconjugates using indium-111, but without significant improvement in diagnostic quality. The disinterest to develop new folate-based tracers using gallium-67 and indium-111 was also probably caused by the keen interest for technetium-99 m which was the most affordable radionuclide for SPECT imaging. Huge numbers of ^{99m}Tc-folate-based-radioconjugates were developed within the last 20 years. Different chelating strategies were implemented such as the use of chelating agents with or without co-ligand like $(CO)_3$ or TPPTS. These experimentations led to the discovery of **[^{99m}Tc]Tc-23** which is now used in clinical routine to diagnose ovarian tumors and other tumors overexpressing FRα. Most representative radiofolates developed for SPECT imaging have been depicted in this section and main results are described in Table 4. Following, classical folate-based tracers labelled with β^+-emitted isotopes to diagnose FRα-positive tumors by PET imaging will be described.

Table 4
Summary of radiochemistry, *in vitro* and *in vivo* results of radiofolates depicted in this section.

Radiofolate	RCY (%)	Log P	K_d for FRα (nM)	Tumor uptake (%IA/g) (4 h)	Tumor-to-kidney ratio (4 h)	References
[^{67}Ga]Ga-1	NC	NC	2	5.2 ± 1.5	2.6	[100,120]
[^{67}Ga]Ga-2	>90	NC	1.6[d]	NC	NC	[101]
[^{67}Ga]Ga-3	NC	NC	NC	6.08 ± 0.89	0.07 ± 0.01	[121]
[^{111}In]In-4	>98	NC	NC	3.1 ± 0.6	1.00 ± 0.34	[122,123]
[^{99m}Tc]Tc-4	>97	NC	NC	3.65 ± 0.23	0.14 ± 0.01	[146]
[^{111}In]In-5	>90	−4.21 ± 0.11[c]	NC	5.80 ± 0.55	0.10 ± 0.01	[125]
[^{177}Lu]Lu-5	>90	NC	NC	7.51 ± 1.25	0.13 ± 0.02	[125]
[^{99m}Tc]Tc-6	NC	NC	NC	17.84 ± 11.23	0.26 ± 0.03	[126]
[^{99m}Tc]Tc-7	>90	−2.34 ± 0.01	NC	0.19 ± 0.05	0.05	[127]
[^{99m}Tc]Tc-8	>90	−3.23 ± 0.08	NC	9.79 ± 1.66	0.09	[127]
[^{99m}Tc]Tc-9	>90	−3.40 ± 0.12	NC	11.35 ± 0.67[b]	0.08[b]	[128]
[^{99m}Tc]Tc-10	>90	−2.46 ± 0.04	NC	1.24 ± 0.01[b]	0.05[b]	[128]
[^{99m}Tc]Tc-11	>90	−3.05 ± 0.35	NC	5.52 ± 0.58[b]	0.05[b]	[128]
[^{99m}Tc]Tc-12	>95	−2.40 ± 0.17	NC	8.14 ± 0.45	0.14	[129]
[^{99m}Tc]Tc-13	NC	−2.89 ± 0.06	NC	7.85 ± 1.37	0.09	[130]
[^{99m}Tc]Tc-14	>94 dc	NC	NC	3.12 ± 0.06	NC	[131]
[^{99m}Tc]Tc-15	NC	NC	NC	0.147 ± 0.026[a]	0.036[a]	[132]
[^{99m}Tc]Tc-16	>95	NC	5000 ± 06	4.26 ± 1.3	0.27 ± 0.10	[133]
[^{99m}Tc]Tc-17	>97	NC	4.2 ± 0.8	6.26 ± 0.4	0.47	[134]
[^{99m}Tc]Tc-18	92 dc	NC	2.51[d]	1.24 ± 0.19	0.10 ± 0.00	[102,135,136]
[^{99m}Tc]Tc-19	92 dc	NC	2.09[d]	2.33 ± 0.36	0.13 ± 0.02	[102,135,136]
[^{99m}Tc]Tc-20	92 dc	NC	14.52[d]	0.43 ± 0.17	0.13 ± 0.05	[102,135,136]
[^{99m}Tc]Tc-21	95 dc	−3.41 ± 0.06	NC	4.84 ± 0.10	0.18	[137]
[^{99m}Tc]Tc-22	95 dc	−3.47 ± 0.05	NC	4.29 ± 0.67	0.17	[137]
[^{99m}Tc]Tc-23	95 dc	NC	0.92	17.68 ± 1.95	0.20 ± 0.01	[139,140]
[^{99m}Tc]Tc-24	95 dc	NC	0.23	11.77 ± 4.26	0.2 ± 0.1	[140]

RCY: Radiochemical yield; Log P: Logarithm of the Partition coefficient; NC: Not communicated; dc: Decay corrected; [a]: 1 h; [b]: 2 h; [c]: Log $D_{7.4}$ (Logarithm of the Distribution coefficient at pH 7.4); [d]: IC_{50} (nM).

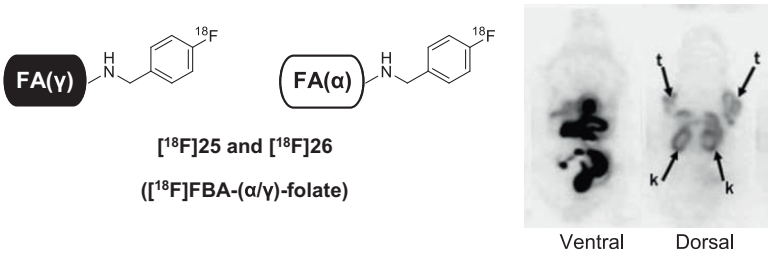

Fig. 16. Chemical structures of **[^{18}F]25** and **[^{18}F]26**, and microPET image of mice bearing KB tumor with **[^{18}F]25/26** (12.5 MBq). Reprinted with permission from [147]. Copyright 2022 SNMMI.

3. Radiofolates developed for PET imaging application

3.1. Fluorine-18 radiofolates

3.1.1. ^{18}F-folates synthesized using the conjugation approach

Bettio *et al.* presented the first radiofolate labelled with fluorine-18 for visualization of FRα-positive cells using PET [147]. 4-fluorobenzylamine was fixed to α- or γ-carboxylate function of glutamate residue of FA to obtain the **[^{18}F]25/26** ([^{18}F]FBA-(α/γ)-folates) regioisomer mixture (Fig. 16). Postmortem biodistribution and *in vivo* microPET imaging were achieved using KB tumor-bearing athymic nude mice. Postmortem biodistribution results at 125 min p.i. of **[^{18}F]25/26** presented a major uptake in kidneys (40.65 ± 12.81 %IA/g) following by tumors (6.56 ± 1.80 %IA/g) and duodenum (5.01 ± 2.01 %IA/g). High biodistribution of **[^{18}F]25/26** found in bile, urine and feces let conclude on both hepatobiliary and renal clearance ways. MicroPET imaging highlighted high activity in gallbladder, bladder and part of intestines that confirmed also hepatobiliary and renal elimination pathways. The dorsal image had a good contrast and showed that KB tumors were quite visible using **[^{18}F]25/26** (Fig. 16). To conclude, even if **[^{18}F]25/26** was not the ideal PET radiofolate, these first results demonstrated that fluorine-18 radiotracers were promising to diagnose FRα-positive tumors.

Ross *et al.* synthesized **[^{18}F]27** ([^{18}F]F-click-fluorobutyl-(γ)-folate) with CuAAC click reaction between azide-FA and [^{18}F]fluoro-1-hexyne-propargyl (Fig. 17) [148]. *In vitro* experiment in KB cells allowed to determine a low radiotracer affinity coefficient of 9.76 ± 3.13 nM, which boded well for the good radiotracer specificity. *In vivo* experiments were performed in KB tumor-bearing male NMRI nude mice. Tissue distribution at 45 min p.i. of **[^{18}F]27** revealed a massive uptake in kidney (16.53 ± 2.22 %IA/g) contrary to tumor uptake (3.13 ± 0.93 %IA/g). High uptake was also observed in the intestines (19.59 ± 59 %IA/g) concluding on the hepatobiliary clearance of **[^{18}F]27**, which could reduce diagnostic accuracy. Moreover, a renal clearance was by far preferred. Higher doses of **[^{18}F]27** was injected to perform microPET imaging at 15–45 min. Images demonstrated high radioactivity concentrations in gallbladder, intestines, urinary bladder and kidneys, but moderate level in the tumor. The imaging study revealed too important non-specific accumulations impeding the clear visualization of potential ovarian tumors. Unsatisfactory *in vivo* results depleted the possibility to push further preclinical study using this radiotracer.

Fisher *et al.* developed **[^{18}F]28** ([^{18}F]-click-FDG-(γ)-folate), based on the original combination of 2-deoxy-2-[^{18}F]fluoroglucopyranosyl azide with propargyl-γ-FA (Fig. 17) [149]. Binding affinity assay demonstrated an affinity of 0.63 ± 0.05 nM meaning that **[^{18}F]28** was more affine to FRα than FA. Biodistribution study

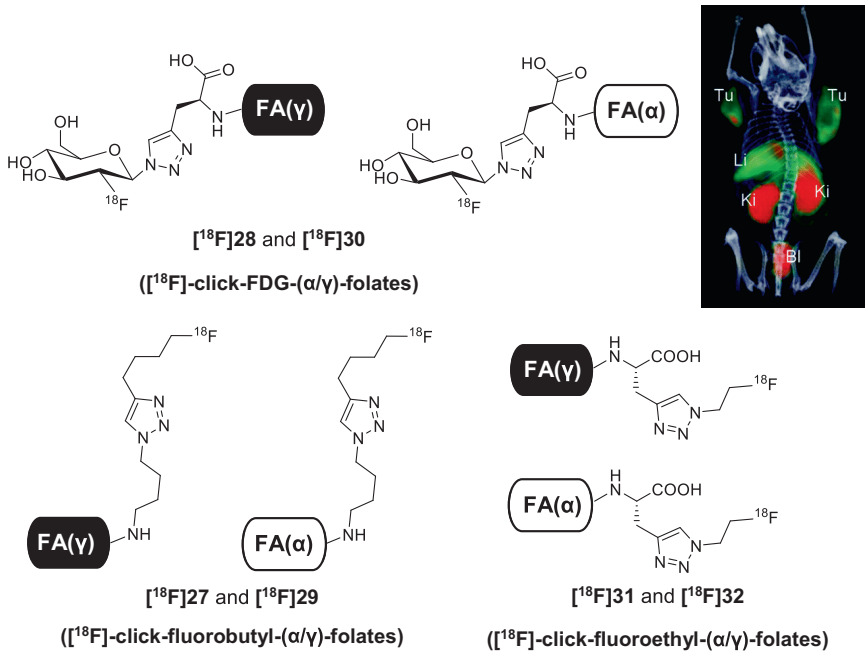

Fig. 17. Chemical structures of **[^{18}F]27**, **[^{18}F]28**, **[^{18}F]29**, **[^{18}F]30**, **[^{18}F]31** and **[^{18}F]32**, and microPET/CT image of KB tumor-bearing mice at 75–105 min p.i. of **[^{18}F]28** (10–14 MBq). Reprinted with permission from [149]. Copyright 2022 SNMMI.

was performed in KB tumor-bearing nude mice. Major uptake was found in kidney and gallbladder (27.08 ± 1.53 and 27.42 ± 7.57 %IA/g, respectively) followed by tumors and liver (9.05 ± 2.12 and 8.37 ± 1.19 %IA/g, respectively) at 90 min p.i. of **[^{18}F]28**, thus reflecting a moderate non-specific uptake. MicroPET imaging was performed at 75–105 min p.i. of **[^{18}F]28**. Images revealed a high accumulation of **[^{18}F]28** in kidneys and urinary bladder and, to a lesser extent, in KB tumors and liver. These results confirmed also that a huge **[^{18}F]28** accumulation in liver, kidneys and gallbladder could complicate the diagnostic *via* imaging tools. In conclusion, the innovative **[^{18}F]28** is a hopeful radiotracer which has to be improved with future research to become an even more specific radiotracer.

Boss *et al.* studied 3 pairs of α- and γ-^{18}F-radiofolate regioisomers synthesized by CuAAC click chemistry: [^{18}F]-click-fluorobutyl-(α/γ)-folates (**[^{18}F]27** and **[^{18}F]29**), [^{18}F]-click-FDG-(α/γ)-folates (**[^{18}F]28** and **[^{18}F]30**), and [^{18}F]-click-fluoroethyl-(α/γ)-folates (**[^{18}F]31** and **[^{18}F]32**) (Fig. 17) [105]. *In vitro* binding assay on KB cells confirmed the high affinity to FRα for each radiotracer (1.4–2.2 nM). Biodistribution and microPET imaging studies were performed in KB tumor-bearing athymic nude mice. All radiofolates showed highest uptake at 90 min p.i. (16.9–52.9 %IA/g). Tumor and liver exhibited a slightly and significantly higher uptake, respectively, for α-analogs compared to γ-analogs, thereby inducing a lower clearance of α-analogs from the body by hepatobiliary way. MicroPET images recorded at 75–105 min p.i. confirmed that **[^{18}F]27** and **[^{18}F]29** were not suitable for nuclear imaging as no activity was detected in tumor region. The most important activity in tumor areas was detected with **[^{18}F]31** and **[^{18}F]32** which both conducted to the best tumor-to-background contrast images. Using **[^{18}F]28**, **[^{18}F]31** and **[^{18}F]32**, major activity intensities were detected in kidneys and urinary bladder. The highest activity intensity was observed in intestines and bladder for **[^{18}F]30** and intestines were also quite visible on microPET images using **[^{18}F]32**. Nevertheless, images contrast was sufficient for tumor detection. MicroPET/CT scans revealed that **[^{18}F]28**, **[^{18}F]30**, **[^{18}F]31** and **[^{18}F]32** were suitable for FRα-positive tumor detection. To conclude, site conjugation has no impact on the *in vitro* characteristics of these six ^{18}F-radiofolates but has a real impact on *in vivo* distribution patterns. This work highlighted the importance of the prosthetic group choice to improve the biodistribution ability of the radiotracer.

Based on a CuAAC click chemistry strategy, Schieferstein *et al.* designed **[^{18}F]33** ([^{18}F]fluoro-OEG-(γ)-folate) which had an oligoethylene glycol (OEG) spacer between fluorine-18 and FA to improve its pharmacokinetics properties (Fig. 18) [150]. **[^{18}F]33** exhibited a reduced lipophilicity compared **[^{18}F]27** (capacity factor k' of 1.12 and 2.28, respectively) and showed an excellent FRα affinity (K_i of 1.6 nM). Biodistribution and microPET imaging were performed in KB tumor-bearing nude mice. Biodistribution results at 90 min p.i. of **[^{18}F]33** showed a tumor uptake of 3.54 ± 0.68 %IA/g, and the higher uptake was observed in gallbladder and kidneys (55.13 and 41.04 ± 7.04 %IA/g, respectively). As expected, **[^{18}F]33** exhibited a better tumor-to-background contrast than **[^{18}F]27**. MicroPET images at 90 min p.i. of **[^{18}F]33** revealed major accumulation in kidneys, liver, urinary bladder and intestines and, to a lesser extent, in tumor. This research proved the benefits of incorporating the OEG spacer in ^{18}F-radiofolate, such as improved tumor-to-background contrast. Nevertheless, results obtained with **[^{18}F]40** and **[^{18}F]41** presented section 3.1.2. are better.

After experimentation using **[^{18}F]33**, the team concluded that a too lipophilic profile was unfavorable as it favored hepatobiliary excretion. Kettenbach *et al.* pursued their investigations around lipophilicity impact on *in vivo* distribution patterns using two ^{18}F-radiofolates: **[^{18}F]34** ([^{18}F]fluoro-dibenzocyclooctyne-(γ)-folate) and **[^{18}F]35** ([^{18}F]fluoro-Alakyne-(γ)-folate) (Fig. 19) [151,152]. **[^{18}F]34** is more lipophilic (Log $D_{7.4}$ of 0.6) than **[^{18}F]35** (log $D_{7.4}$ of −1.4) as it contains a four cycles formation. Binding affinity assay was performed on KB cells and high FRα-affinity was achieved with **[^{18}F]34** and **[^{18}F]35** (IC_{50} of 11.2 ± 3.7 and 6.4 ± 0.5 nM, respectively). *Ex vivo* biodistribution was carried out in KB tumor-bearing BALB/c nude mice and a 3-times higher tumor uptake was observed for **[^{18}F]35** compared to **[^{18}F]34**. The main uptake was found in kidneys and a low tumor-to-kidney ratio was observed for **[^{18}F]34** (0.05) compared to that generally found in literature (0.12), which was the case for **[^{18}F]35**. Significant non-specific uptake in intestines and liver was also observed for both radiotracers. Background contrast was bad for **[^{18}F]34** as it was excreted by hepatobiliary way due to its lipophilic character. Finally, *in vivo* microPET imaging showed a massive activity in intestines for **[^{18}F]34**, followed by bladder, kidneys and liver. No

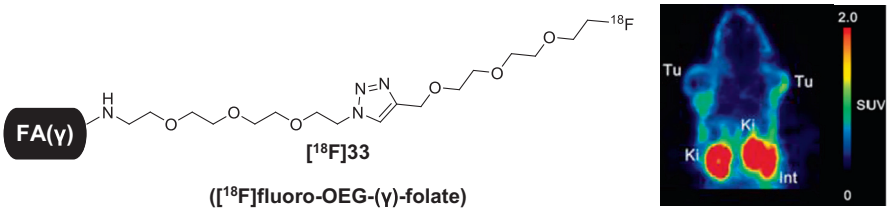

Fig. 18. Chemical structure of **[^{18}F]33** and microPET image of KB tumor-bearing mice at 60–90 min p.i. of **[^{18}F]33** (13 MBq). Image in open access from [150].

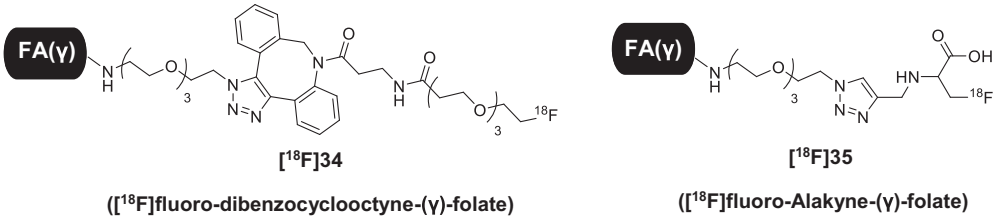

Fig. 19. Chemical structures of **[^{18}F]36** and **[^{18}F]37** [152].

activity was found in KB tumor. On the contrary, important activity was found in KB tumor using **[^{18}F]35** but main activity was visualized in bladder, intestines, and kidneys. To sum up, **[^{18}F]34** was not suitable for PET imaging. On its stands, **[^{18}F]35** was more appropriate for future observations and experiments for scanning FRα-positive tumors, but the tracer design should be optimized to improve its hydrophilicity character and to reduce intestines uptake and hepatobiliary clearance.

Boss *et al.* wished to know whether the 5-Me-THF could replace FA to target FRα-positive cells. The team synthesized α- and γ-regioisomers (both in enantiomeric pure forms) of a ^{18}F-5-Me-THF-radiotracer using CuAAC click reaction: **[^{18}F]36** ((6*S*)-(α)-[^{18}F]fluoro-5-Me-THF), **[^{18}F]37** ((6*S*)-(γ)-[^{18}F]fluoro-5-Me-THF), **[^{18}F]38** ((6*R*)-(α)-[^{18}F]fluoro-5-Me-THF) and **[^{18}F]39** ((6*R*)-(γ)-[^{18}F]fluoro-5-Me-THF) (Fig. 20) [153]. *In vitro* binding assay with KB cells revealed similar affinity to FRα in the range of 17.7 to 25.8 nM with close affinity to 5-Me-THF (20.6 to 25.8 nM). 5-Me-THF and its four derivatives had less affinity to FRα than FA and **[^{18}F]41** (Fig. 21) but stayed sufficiently affine to be highly specific radiofolates with a cellular uptake of about 50–60%. Tissue distribution was performed in nude mice bearing KB tumors. Similar tumor uptake was found at 1 h p.i. for all compounds (**[^{18}F]36**: 8.28 ± 1.2, **[^{18}F]37**: 8.20 ± 2.4, **[^{18}F]38**: 10.6 ± 2.8 and **[^{18}F]39**: 8.69 ± 1.5 %IA/g). The tumor-to-kidney ratio was 0.5 for (6*S*)-compounds (**[^{18}F]36** and **[^{18}F]37**) and 2-fold higher than for (6*R*)-analogs. α- And γ-compounds presented similar biodistribution patterns which was not the case for (6*R*)- and (6*S*)-compounds (**[^{18}F]38** and **[^{18}F]39**). Kidney uptake was 2-fold higher for (6*R*)-compared to (6*S*)-compounds (**[^{18}F]38**: 35.5 ± 2.0 and **[^{18}F]36**: 15.1 ± 1.8 %IA/g)) whereas liver uptake was 5-fold higher for (6*S*)- compared to (6*R*)-compound (**[^{18}F]37**: 14.1 ± 2.2 and **[^{18}F]39**: 2.48 ± 0.4 %IA/g). MicroPET/CT data was recorded at 1 h p.i.. α-Compounds had bad tumor-to-background contrast as liver, kidneys, intestines, gallbladder, and urinary bladder expressed higher activity level than tumors. Contrast was better for γ-compounds. Tumor expressed the highest activity level for **[^{18}F]39**. This compound gave the better images quality as liver and intestines were not visible. To conclude, (6*R*)-analogs showed better *in vivo* properties than (6*S*)-analogs. No significant differences could be observed between α- and γ-compounds. These four compounds and more specifically **[^{18}F]39** are suitable for clinical trials.

3.1.2. ^{18}F-folates synthesized by pendent approach

Ross *et al.* and Betzel *et al.* were the first to implement an integrated approach using a direct labelling strategy by nucleophilic aromatic substitution [154,155]. Ross *et al.* developed **[^{18}F]40** (2′-[^{18}F]fluorofolic acid or 2′-[^{18}F]FFA) (Fig. 21). *In vitro* binding assay using KB cells demonstrated the high affinity of **[^{18}F]40** to FRα. *In* and *ex vivo* studies were performed in KB tumor-bearing NMRI nude mice at 75 min p.i. of **[^{18}F]40**. The major uptake was measured in kidneys followed by gallbladder, tumor and liver (46.06 ± 13.39, 17.69 ± 10.35, 9.37 ± 1.76 and 7.79 ± 1.23 %IA/g, respectively). High activity in urine concluded on the renal excretion way of **[^{18}F]40**. MicroPET study was performed at 10 min p.i. of **[^{18}F]40** and helped to determine non-specific organ uptake. Tumor and kidneys were well visualized as they presented the highest activity. Minor activity was also measured in abdominal region due to uptake in liver and intestines. Until now, microPET images presented one of the best tumor-to-background contrasts and gave promising results to pursue experimentation on fluorinated-radiofolate.

The radiofolate **[^{18}F]41** (3′-Aza-2′–[^{18}F]fluorofolic acid ([^{18}F]-AzaFol)) developed by Betzel *et al.* is a derivative of **[^{18}F]40** where fluorine-18 is attached by nucleophilic aromatic substitution onto a pyridine ring for **41** instead of a phenyl ring for **40** (Fig. 21). *In vitro* stability studies on KB cells demonstrated that affinity to

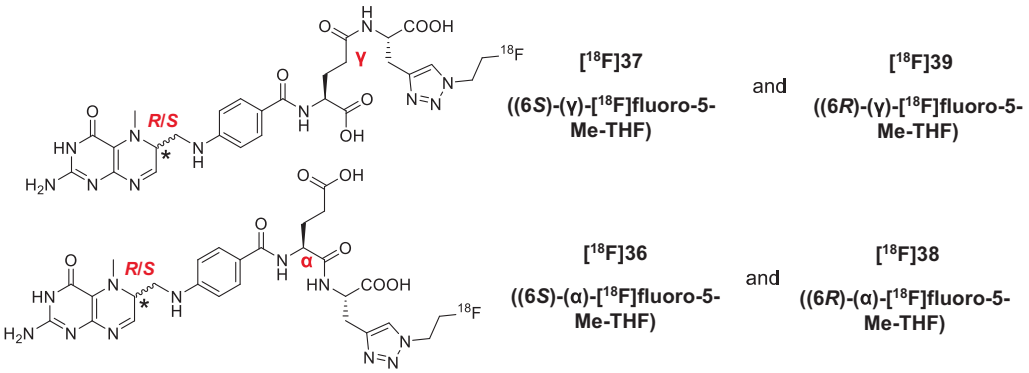

Fig. 20. Chemical structures of **[^{18}F]36**, **[^{18}F]37**, **[^{18}F]38** and **[^{18}F]39** [153].

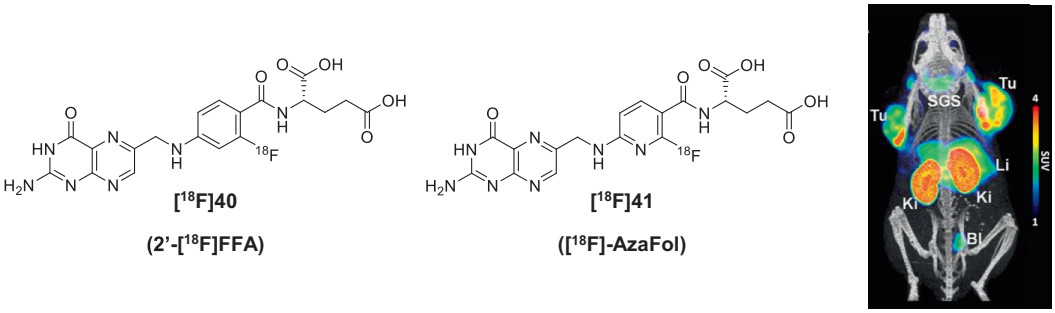

Fig. 21. Chemical structures of **[^{18}F]40** [154] and **[^{18}F]41** and microPET/CT image of KB tumor-bearing mice at 120–150 min p.i. of **[^{18}F]41** (13 MBq). Reprinted with permission from [155]. Copyright 2022 American Chemical Society.

FRα of **[^{18}F]41** was not affected by backbone modification as IC_{50} was of 1.4 ± 0.5 nM. Another promising finding was obtained with biodistribution studies showing a high KB tumor uptake (12.59 ± 1.77 %IA/g) at 90 min p.i. of **[^{18}F]41** in KB tumor-bearing athymic nude mice. Organs such as kidneys, liver, salivary glands and gallbladder also taken up significant amount of radiofolate (57.33 ± 8.40, 10.31 ± 2.37, 14.09 ± 0.93 and 9.26 ± 0.59 %IA/g, respectively) which could be due to the short time between injection and collecting data. Indeed, clearance was still ongoing and folate derivative accumulation in gallbladder and feces demonstrated a partial hepatobiliary clearance. Compared to previous results, no significant uptake in intestines was observed which is a good point for a well visualization of tumors in the abdominal area. Furthermore, microPET images recorded at 120–150 min p.i. of **[^{18}F]41** presented good quality as major activity was detected in tumor and kidneys followed by moderate activity in liver and bladder (Fig. 21). The results were the more convincing ones until now and a new synthesis strategy was implemented to considerably decrease total synthesis time. Moreover, less non-specific uptake was observed, and the higher tumor uptake was registered. High contrasts images were the most encouraging results. Regarding all these promising results, clinical study using **[^{18}F]41** was allowed and presented in section 3.3.

Boss *et al.* modified 5-Me-THF to create a new FA derivative: 3′-Aza-5-Me-THF by changing the 3-C of the phenyl ring by a nitrogen. This new FA derivative exists in two diastereomeric forms: (6*S*)- (**42**) and (6*R*)- (**43**) derivatives (Fig. 22A). **[^{18}F]42** ((6*S*)-3′-Aza-2′-[^{18}F]fluoro-5-Me-THF) and **[^{18}F]43** ((6*R*)-3′-aza-2′-[^{18}F]fluoro-5-Me-THF) were synthetized using substitution approach [156]. FRα affinity of (6*R*)- and (6*S*)-analogs (27.1 and 23.8 nM, respectively) were close to 5-Me-THF one. *In vivo* properties were described and compared to results obtained in a previous study involving **[^{18}F]41** [155]. The biodistribution study started with the injection of **[^{18}F]41**, **[^{18}F]43** and **[^{18}F]42** in KB tumor-bearing nude mice. Final data at 3 h p.i. showed the highest tumor uptake ever observed for a radiofolate with a value of 32.3 ± 6.1 and 34.8 ± 6.0 %IA/g for **[^{18}F]43** and **[^{18}F]42**, respectively. Tissue distribution profile using **[^{18}F]41** was the same as previous results and showed tumor internalization 2-times lower than for **[^{18}F]42** and **[^{18}F]43** (15.0 ± 2.3 %IA/g). **[^{18}F]43** showed a high tumor-to-kidney ratio of 1.63 ± 0.32 and this is the best ratio ever observed. MicroPET/CT imaging recorded at 3 h p.i. allowed well visualization of tumors and kidneys with a huge tumor-to-background contrast (Fig. 22B–D). Biodistribution results were confirmed by imaging study ones as the major activity intensity in tumors was found for **[^{18}F]43** followed by **[^{18}F]42** and the lowest kidney uptake was found with **[^{18}F]43**. Moreover, liver was not visible with **[^{18}F]42** compared to **[^{18}F]43** which is an advantage for tumor detection. Therefore, **[^{18}F]42** and **[^{18}F]43** are suitable for clinical trials as they provide images of a rare quality and contrast. Their use could significantly improve medical experiments for the FRα–positive tumors detection and could also be used for therapy monitoring and patient surveillance. Müller and co-workers pursued their study of **[^{18}F]42** and **[^{18}F]43** on another FRα-positive cell line RT16 (chinese hamster ovary cells transfected with FRα)[157]. High affinity of both radiotracers was observed for FRα (IC_{50} of 2.1 ± 0.4 and 1.8 ± 0.1 nM, respectively) but lower than **[^{18}F]41** (0.6 ± 0.3 nM). RT16 tumor-bearing mice was imaged 1 h p.i. of **[^{18}F]41**, **[^{18}F]42** and **[^{18}F]43**. The three radioconjugates presented excellent tumor uptake but **[^{18}F]43** showed the best tumor uptake and tumor-to-background contrast. These results supported previous ones and confirming the suitability of **[^{18}F]43** to enter into phase I clinical trial.

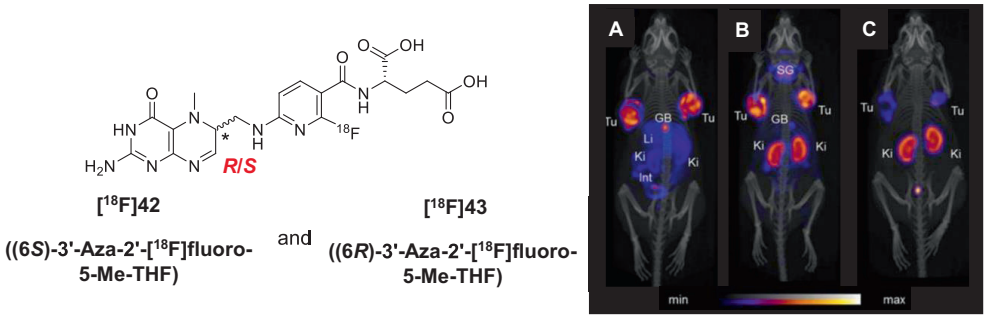

Fig. 22. Chemical structures of **[^{18}F]42** and **[^{18}F]43**. MicroPET/CT images of KB tumor-bearing mice at 3 h p.i. of (A) **[^{18}F]43**, (B) **[^{18}F]42** and (C) **[^{18}F]41** (5 MBq). Reprinted with permission from [156]. Copyright 2022 SNMMI.

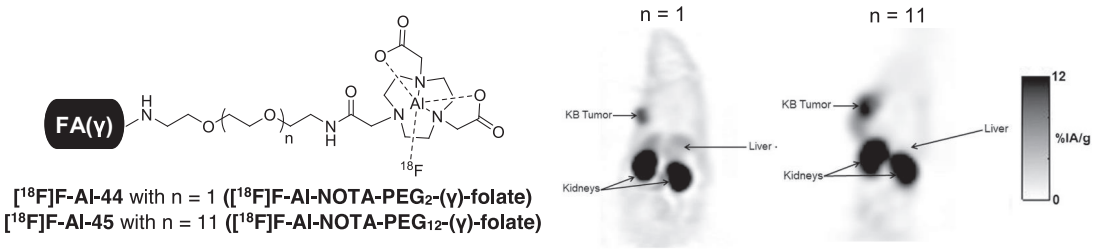

Fig. 23. Chemical structures of **[^{18}F]F-Al-44** and **[^{18}F]F-Al-45**, and microPET/CT images of KB tumor-bearing mice at 90 min p.i. of **[^{18}F]F-Al-44** or **[^{18}F]F-Al-45** (4–11 MBq). Reprinted with permission from [158]. Copyright 2022 American Chemical Society.

3.1.3. [^{18}F]F-Al-NOTA-folates

Conjugation approach has the drawback to require long synthesis time that is not in adequation with the short half-life time of fluorine-18. Low and co-workers has perceived the need to explore another radiofluorination approach based on Al-^{18}F-coordination. Consequently, this team synthesized and explored *in vitro* and *in vivo* characteristics of **[^{18}F]F-Al-44** ([^{18}F]F-Al-NOTA-(γ)-folate) to assess the relevance of using this as an alternative radiofluorination approach [158]. Compound **44** was composed of a PEG_2 spacer inserted between NOTA chelator and FA (Fig. 23). The binding affinity coefficient determined using KB cells illustrated the good binding ability of the design radiofolate (IC_{50} of 18.7 nM). *In vivo* studies were performed in KB tumor-bearing nude mice. MicroPET data collected at 90 min p.i. of **[^{18}F]F-Al-44** showed that KB tumor and kidneys were the only two tissues visible on imaging with an important background contrast. Biodistribution data revealed a significant uptake only in tumor and kidneys (10.9 ± 2.7 and 78.6 ± 5.1 %IA/g, respectively) and a moderate one in liver (5.3 ± 0.5 %IA/g). Those preclinical results with **[^{18}F]F-Al-44** are the best observed for a radiofluorinated folate tracer by far. These conclusions open new investigation perspectives since **[^{18}F]F-Al-44** development is at its early stage.

Regarding promising results obtained with **[^{18}F]F-Al-44**, the team decided to replace PEG_2 by a PEG_{12} spacer to improve its *in vivo* behavior and thus synthesized **[^{18}F]F-Al-45** ([^{18}F]F-Al-NOTA-PEG_{12}-(γ)-folate) (Fig. 23) [159]. The IC_{50} of **[^{18}F]F-Al-45** determined with KB cells was 33.8 nM and KB or A549 cells were inoculated into right shoulder of female nu/nu mice for *in vivo* studies. MicroPET data was collected at 90 min p.i. of **[^{18}F]F-Al-45** or **[^{18}F]F-Al-44**. For both radiopharmaceuticals, only KB tumors and kidneys expressed high activity intensity. Background contrast was better with PEG_{12}-analog as liver was no more visible (Fig. 23). *Ex vivo* distribution was performed at 120 min p.i. of **[^{18}F]F-Al-45** or **[^{18}F]F-Al-44** and, as generally observed, the highest uptake was found in kidneys (55.25 ± 7.38 and 87.86 ± 4.42 %IA/g, respectively). Tumor uptake was similar for both radiofolates. Liver uptake was significantly weaker for **[^{18}F]F-Al-45** than **[^{18}F]F-Al-44** (1.64 ± 0.3 *vs.* 5.40 ± 0.75 %IA/g) due to the most important hydrophilicity of PEG_{12} compared to PEG_2. To conclude, the team successfully improved the *in vivo* properties of **[^{18}F]F-Al-44** by increasing the spacer hydrophilicity. In conclusion, **[^{18}F]F-Al-45** possesses good characteristics and constitutes an improved diagnostic agent to detect FRα-positive tumors. This novel radiopharmaceutical possesses all the required qualities to participate in clinical trials.

3.2. Gallium-68 radiofolates

3.2.1. [^{68}Ga]Ga-DOTA-folates

Fani *et al.* developed the two first ^{68}Ga-radiofolates consisting in γ-conjugation of DOTA chelator to FA through an EDA linker (**[^{68}Ga]Ga-46**, [^{68}Ga]Ga-P3026) or a 3-{2-[2-(3-amino-propoxy)-ethoxy]-ethoxy}-propylamine linker (**[^{68}Ga]Ga-47**, [^{68}Ga]Ga-P1254) (Fig. 24) [160]. *In vitro* studies were performed in KB tumor cells and both radiofolates showed a rapid and high cell uptake and retention. **[^{68}Ga]Ga-46** revealed highest cell surface binding compared to **[^{68}Ga]Ga-47**. The internalization rate followed the order **[^{68}Ga]Ga-46** > **[^{68}Ga]Ga-47**. **[^{68}Ga]Ga-46** and **[^{68}Ga]Ga-47** showed high FRα affinity with a K_d value of 4.65 ± 0.82 and 4.27 ± 0.42 m M, respectively. *In vivo* experiments were performed in nude mice bearing a dual KB and HT1080 tumor model. Biodistribution profiles for each radioconjugates were similar and characterized by efficient clearance from the blood. The major uptake at 2 h p.i. was found in kidneys resulting in a low tumor-to-kidney ratio of 0.12 ± 0.02 for **[^{68}Ga]Ga-46** and 0.11 for **[^{68}Ga]Ga-47**. MicroPET/CT images were performed with **[^{68}Ga]Ga-46** on mice at 1 h p.i. with surgically kidney removal. MicroPET images confirmed biodistribution results with a good visualization of FRα-positive tumor and negligible uptake in FRα-negative tumor. High uptake in salivary gland was also observed. To sum up, these two radiofolates give promising results but further investigations are necessary to develop a suitable ^{68}Ga-radioconjugate for clinical trials.

3.2.2. [^{68}Ga]Ga-HBED-CC-EDBE-folate

Choi *et al.* described the synthesis of the new ^{68}Ga-folate-radioconjugate **[^{68}Ga]Ga-48** ([^{68}Ga]Ga-HBED-CC-EDBE-(γ)-folate) consisting in γ-conjugation of HBED-CC chelator to FA through an 2,2′-ethylenedioxy-bis-ethylamine linker (Fig. 24) [72]. *In vitro* cellular uptake of **[^{68}Ga]Ga-48** was evaluated in CT-26, KB and A549 cells. Binding percentage was determined over 2 h and showed a higher cellular uptake of **[^{68}Ga]Ga-48** in CT-26 and KB cells which expressed FRα than in FRα-negative A549 cells. MicroPET imaging performed on CT-26 tumor-bearing BALB/c mice at 2 h p.i. of **[^{68}Ga]Ga-48** indicated significant uptake in tumor, but also in other organs leading to a poor image quality. Thus, this radiofolate is not suitable for further investigations.

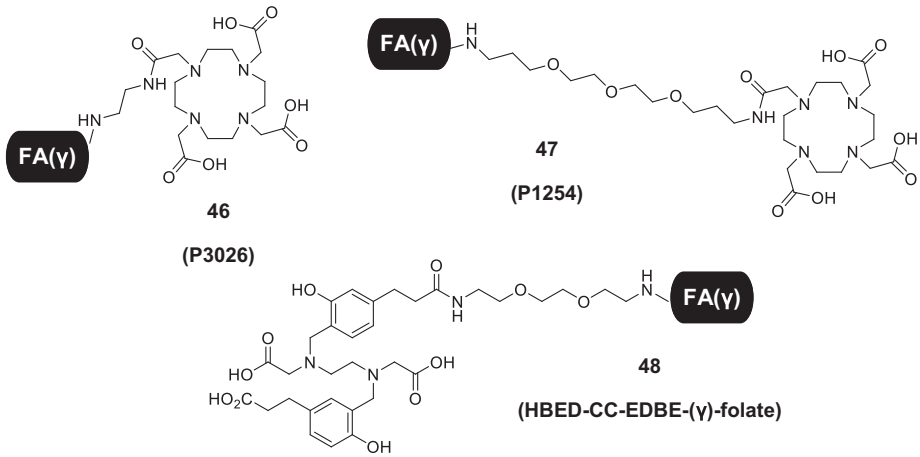

Fig. 24. Chemical structures of **46**, **47** and **48** [72,160].

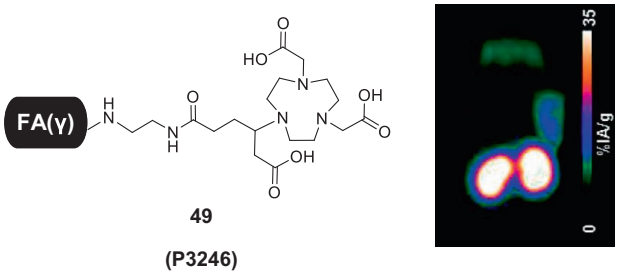

Fig. 25. Chemical structure of **49** and microPET image of KB tumor-bearing mice at 1 h p.i. of **[^{68}Ga]Ga-49** (10–12 MBq). Reprinted with permission from [160]. Copyright 2022 American Chemical Society.

3.2.3. [^{68}Ga]Ga-NODAGA-folate

Fani *et al.* pursued their studies on ^{68}Ga-radiofolates with the synthesis of **[^{68}Ga]Ga-49** ([^{68}Ga]Ga-P3246) (Fig. 25) using a NODAGA chelator compared to **[^{68}Ga]Ga-52** (see section 3.2.5.) [161]. A saturation binding study was conducted on KB cells using different concentrations of **[^{68}Ga]Ga-49** and revealed its high affinity binding to FRα (K_d = 5.61 ± 0.96 nM). *In vivo* biodistribution and PET/CT studies were performed in KB tumor-bearing athymic female nude mice. The biodistribution profile was characterized by high tumor uptake (16.56 ± 3.67 %IA/g) and high activity accumulation in kidneys (91.52 ± 21.05 %IA/g) at 1 h p.i., resulting in tumor-to-kidney ratio of 0.18. The blood clearance was fast while the concentration of activity was low in non-targeted organs, such as lungs, spleen, stomach, and muscles. Concerning MicroPET tests (Fig. 25), time activity curves obtained on the dynamic acquisition with regions of interest (ROIs) analyses showed an increase of activity in tissues which express FRα like tumor, salivary glands and kidneys.

3.2.4. [^{68}Ga]Ga-DOTA-pteroate

Zhang *et al.* described the synthesis of two novel radioconjugates named **[^{68}Ga]Ga-50** ([^{68}Ga]Ga-DOTA-Lys-pteroate) and **[^{68}Ga]Ga-51** ([^{68}Ga]Ga-DOTA-DAV-Lys-pteroate) (Fig. 26) in which glutamic acid of FA was replaced by a lysine (*i.e.*, Lys-pteroate ligand) and linked to a DOTA chelator [162]. In **51**, a δ-aminovaleric acid spacer was added between Lys-pteroate and DOTA. *In vitro* cellular uptake was performed in KB cells and showed a high cellular uptake of **[^{68}Ga]Ga-50** and **[^{68}Ga]Ga-51** with a cell binding of 52.52 ± 1.64% and 33.11 ± 0.85%, respectively, and also a rapid cellular internalization. Biodistribution and microPET imaging were carried out on Kunming mice bearing KB tumor. Both ^{68}Ga-complexes displayed a fast clearance and low activity accumulation in most organs except kidneys. Indeed tumor-to-kidney ratio was 0.11 for both ^{68}Ga-radioconjugates at 2 h p.i.. **[^{68}Ga]Ga-51** showed a better biodistribution and *in vivo* results: higher cellular uptake, faster clearance, higher tumor-to-muscle (6.76 *vs.* 4.34) and tumor-to-blood ratio (28.65 *vs.* 17.93) at 2 h p.i.. This could be explained by a higher distance between the chelating agent and the targeting moiety allowing it to better interact with FRα. MicroPET images using **[^{68}Ga]Ga-51** at 2 h p.i. showed clear visualization of tumor and kidneys, and poor activity in non-specific organs leading to a good tumor-to-background contrast. To conclude, **[^{68}Ga]Ga-51** is suitable for further investigations contrary to **[^{68}Ga]Ga-50.**

3.2.5. [^{68}Ga]Ga-NODAGA-dideaza-folate

[^{68}Ga]Ga-52 described by Fani *et al.* ([^{68}Ga]Ga-NODAGA-EDA-(γ)-5,8-dideaza-folate) consisted of 5,8-dideaza-folate linked on its γ-carboxylic acid to the spacer EDA functionalized by NODAGA (Fig. 27) [161]. *In vitro* and *in vivo* results of **[^{68}Ga]Ga-52** were compared to those of **[^{68}Ga]Ga-49** (analogue possessing a folate entity instead of dideaza-folate, see section 3.2.3.). Evaluation in KB cell culture showed an higher cell-associated uptake *in vitro* for **[^{68}Ga]Ga-49** compared to **[^{68}Ga]Ga-52** (60–72% *vs.* 50–60%). Internalized and binding fraction were higher for **[^{68}Ga]Ga-49** (14.8 ± 0.2%) compared to **[^{68}Ga]Ga-52** (11.5 ± 1.0%) at 4 h. The cellular retention was slightly higher for **[^{68}Ga]Ga-49** (76.3 ± 10.2%) compared to **^{68}Ga]Ga-52** (70.9 ± 3.9%). Soft modification of the FA entity resulted in the decrease in affinity to FRα (K_d = 7.21 ± 2.46 nM). Biodistribution and microPET/CT imaging were carried out on KB tumor-bearing athymic female nude mice. Biodistribution profile was similar to that of **[^{68}Ga]Ga-49** (tumor and kidneys uptake values of 10.95 ± 2.12 and 62.26 ± 14.32 %IA/g at 1 h p.i., respectively), resulting in tumor-to-kidney ratio of 0.18. The clearance from the blood and the specificity of **[^{68}Ga]Ga-52** were also similar to those of **[^{68}Ga]Ga-49**. To sum up, modification of the FA entity does not improve properties of the radioconjugate.

3.3. Clinical evaluation of PET radiofolate

Gnesin *et al.* exposed the first clinical trial of a PET radiotracer for FRα-overexpressing tumor imaging [163,164]. 6 patients with lung adenocarcinoma were involved in this study. Lung cancers

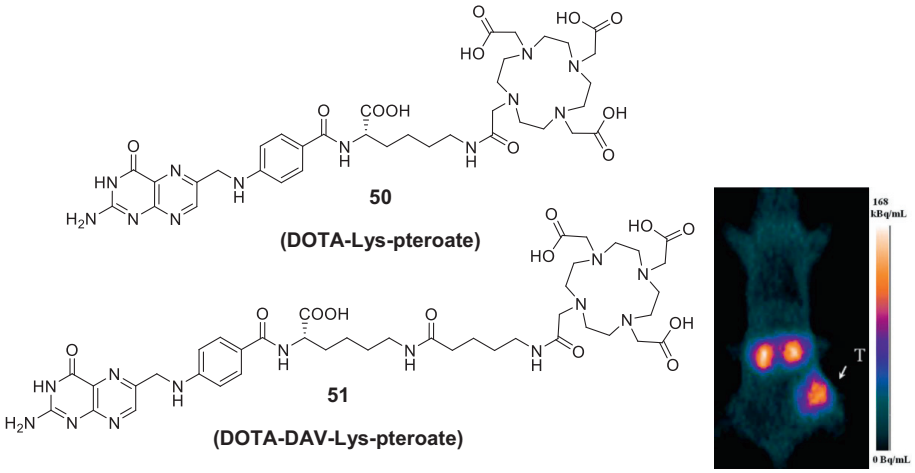

Fig. 26. Chemical structures of **50** and **51** and microPET/CT image of KB tumor-bearing mice at 2 h p.i. of **[^{68}Ga]Ga-51** (7.4 MBq). Reprinted with permission from [162]. Copyright 2022 John Wiley and Sons.

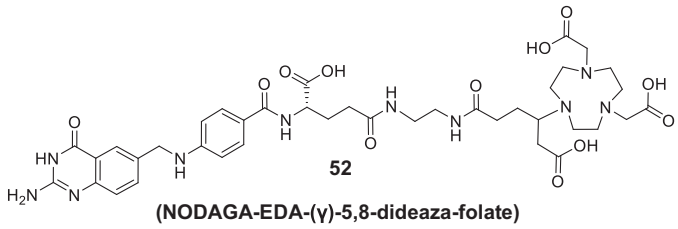

Fig. 27. Chemical structure of **52** [161].

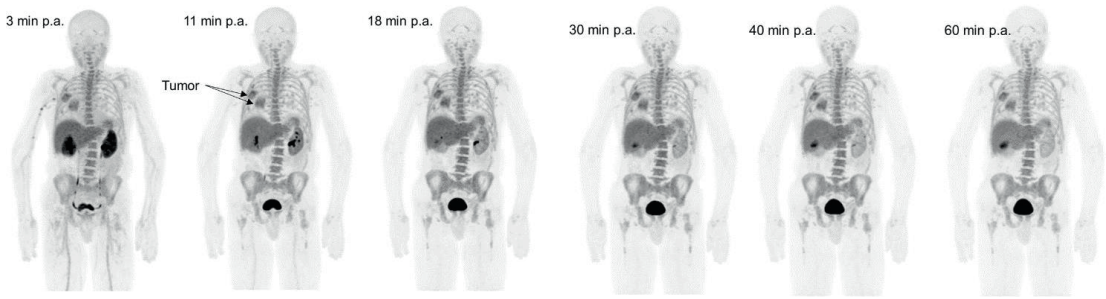

Fig. 28. PET images of patient with lung adenocarcinoma at 3, 11, 18, 30, 40 and 60 min p.i. of **[^{18}F]41** (299–399 MBq). Image in open access from [163].

were previously histologically confirmed for each patient. FA (1 mg) was i.v. injected before injection of 299–399 MBq of **[^{18}F]41** and PET/CT was recorded during 1 h after tracer injection (Fig. 28). Kidneys were quite visible on imaging only at 3 min p.i. and became moderately visible such as liver and tumor. Tumor-to-lung ratio slightly increased during image acquisition before reaching a plateau between 4.8 and 5 at 40 min. This high tumor-to-lung ratio allowed high tumor-to-background contrast and a good visualization of tumors in the thoracic area. Dosimetric study highlighted that the most irradiated organs were liver, kidney, bladder wall and spleen. Extrapolation from preclinical data differed from clinical results as in mice model, the highest exposure was in kidneys followed by liver. The effective dose taken by patients were comparable to the one taken during a |^{18}F]FDG PET imaging. To conclude, **[^{18}F]41** is suitable to diagnose lung adenocarcinoma by PET imaging as it is safe and an effective radiotracer with good dosimetric properties. Nevertheless, regarding the low number of patients, this study has to be pursued to reinforce these promising results. **[^{18}F]41** could also be employed in future clinical trials to diagnose ovarian and endometrial cancer or peritoneal carcinosis.

3.4. Conclusion

As PET imaging for tumor diagnostic was implemented in clinical routine more recently than SPECT imaging, the development of folate-based radiopharmaceuticals has started later. Thus, the first radiofolate using β^+-emitting isotope **[^{18}F]27/26** was developed in 2006 whereas the first SPECT radiofolate **[^{67}Ga]Ga-1** was introduced ten years earlier, in 1996. ^{18}F-folate-tracers developed using substitution or chelating approach give better *in vivo* results than those developed using conjugation approach. In fact, less uptake in non-specific organs was observed and those radiopharmaceuticals are more excreted from body using renal clearance way. They also allow to record images with better tumor-to-background contrast and thus with better qualities. Until now, only [^{18}F]-AzaFol (**[^{18}F]41**) radiofolate using β^+–emitting isotope has been tested in clinical phase I trials to detect FRα-positive tumors by PET/CT (NCT0342993) [164]. Results of this clinical trial were very promising to diagnose lung adenocarcinoma and should be used in another clinical study in a few years. Moreover, regarding promising results already obtained concerning ^{68}Ga-radiofolates, the ease to produce gallium-68 thanks to germanium-68/gallium-68 generator and the generalization of the use of PET compared to SPECT, future clinical trials could also be conducted soon. Main results for each radiofolate are described in Table 5.

4. Albumin-binding radiofolates for nuclear imaging

As FRα is present on proximal tubule cells of kidneys, all developed radiofolates are well internalized into them. This uptake makes kidneys quite visible on nuclear images and deplete the tumor-to-background contrast. Radiopharmaceuticals with the best tumor-to-kidney ratio are presented in this section which increase diagnostic's quality. High kidney uptake is also an issue for TRT and theranostic approach. Radionuclides used in therapy emit α or β^- radiations which are destructive for DNA. Thus, with a massive uptake in kidneys, these radiofolates can be nephrotoxic. Mathias *et al.* were the first to discover that moderate injection of FA before the injection of radiofolate improve the tumor-to-background ratio by decreasing the uptake of non-specific organs and kidneys [123]. Müller and co-workers were the main ones to work on solutions to decrease kidney uptake [165] by pre-injection of FA derivatives like antifolates [166–169] or by conjugation of an albumin-binding entity to radiofolates for preparing albumin binder entity (AB)-radiofolates [170]. So, this section is dedicated to these radiofolates, and the addition of an AB entity is aimed at improving the pharmacokinetic properties. Thanks to this addition, the affinity of the AB-radiofolates to plasma proteins increases and provides an enhancement of the circulation time in the blood. Enhancement of the blood circulating time allows radiofolates to fix more tumor and less kidneys. It exists different types of AB entities [171] like peptides [172] and portable binders like 4-(*p*-iodophenyl)butyric acid derivatives [173] which can be easily conjugated to drugs or tracers.

Table 5
Summary of radiochemistry, *in vitro* and *in vivo* results of radiofolates depicted in this section.

Radiofolate	RCY (%)	Log P	K_d for FRα (nM)	Tumor uptake (%IA/g)	Tumor-to-kidney ratio	References
[^{18}F]25/26	15–45	NC	71 ± 8[b] 62 ± 6[b]	6.56 ± 1.80 (125 min)	0.16	[147]
[^{18}F]27	19–23 dc	−2.7 ± 0.1[a]	2.1 ± 0.2[b]	3.22 ± 1.05 (90 min)	0.10	[105,148]
[^{18}F]38	19–23 dc	−2.7 ± 0.1[a]	2.2 ± 0.1[b]	3.73 ± 0.62 (90 min)	0.08	[105]
[^{18}F]29	3–10 dc	−4.2 ± 0.1[a]	1.5 ± 0.3[b]	9.05 ± 2.12 (90 min)	0.34	[105,149]
[^{18}F]30	3–10 dc	−4.2 ± 0.1[a]	1.6 ± 0.2[b]	10.9 ± 0.52 (90 min)	0.2 ± 0.07	[105]
[^{18}F]31	2–4 dc	−3.0 ± 0.1[a]	1.4 ± 0.2[b]	7.24 ± 0.99 (90 min)	0.43	[105]
[^{18}F]32	2–4 dc	−3.0 ± 0.1[a]	1.6 ± 0.2[b]	12.5 ± 1.04 (90 min)	0.38	[105]
[^{18}F]33	8.7 dc	NC	1.6	3.54 ± 0.68 (90 min)	0.09 ± 0.01	[150]
[^{18}F]34	3.2 ± 1.8	0.6 ± 0.07[a]	6.3 ± 1.4	1.68 ± 0.13 (1 h)	0.05	[151]
[^{18}F]35	19.3 ± 2.8	−1.43 ± 0.08[a]	5.5 ± 0.4	0.56 ± 0.13 (1 h)	0.12	[151]
[^{18}F]36	1–4 dc	−2.2 ± 0.1[a]	24.0 ± 4.6[b]	8.28 ± 1.2 (1 h)	0.55 ± 0.08	[153]
[^{18}F]37	5–7 dc	−2.2 ± 0.1[a]	17.7 ± 7.2[b]	8.20 ± 2.4 (1 h)	0.44 ± 0.12	[153]
[^{18}F]38	2–3 dc	−2.6 ± 0.2[a]	22.3 ± 3.0[b]	10.6 ± 2.8 (1 h)	0.30 ± 0.08	[153]
[^{18}F]39	2–4 dc	−2.5 ± 0.2[a]	22.2 ± 6.9[b]	8.69 ± 1.5 (1 h)	0.22 ± 0.04	[153]
[^{18}F]40	8 dc	0.53 ± 0.2	1.8 ± 0.1	9.37 ± 1.76 (75 min)	0.20	[154]
[^{18}F]41	9 dc	−4.2 ± 0.1	1.4 ± 0.5	12.59 ± 1.77 (90 min)	1.4 ± 0.5	[155]
[^{18}F]42	1–5 dc	−4.2 ± 0.1[a]	23.8 ± 4.0[b]	34.8 ± 6.0 (3 h)	0.84 ± 0.12	[156]
[^{18}F]43	1–5 dc	−4.8 ± 0.1[a]	27.1 ± 3.7[b]	32.3 ± 6.1 (3 h)	1.63 ± 0.32	[156]
[^{18}F]F-Al-44	18.6 ± 4.5 dc	1.0	18.7[b]	10.9 ± 2.7 (90 min)	0.10 ± 0.03	[158]
[^{18}F]F-Al-45	8.4 ± 1.3 dc	0.4	3.38[b]	9.20 ± 0.62 (90 min)	0.18 ± 0.02	[159]
[^{68}Ga]Ga-46	>95	NC	4.65 ± 0.82	14.29 ± 4.14 (4 h)	0.12 ± 0.01	[160]
[^{68}Ga]Ga-47	>95	NC	4.27 ± 0.82	13.10 ± 0.65 (4 h)	0.13 ± 0.03	[160]
[^{68}Ga]Ga-48	>98 dc	1.61	NC	NC	NC	[72]
[^{68}Ga]Ga-49	>95 dc	NC	5.61 ± 0.96	16.56 ± 3.67 (1 h)	0.18	[161]
[^{68}Ga]Ga-50	84 ± 3	−3.22 ± 0.11	NC	11.05 ± 0.59 (2 h)	0.11	[162]
[^{68}Ga]Ga-51	93 ± 2	−3.64 ± 0.19	NC	0.06 ± 0.60 (2 h)	0.10	[162]
[^{68}Ga]Ga-52	>95 dc	NC	7.21 ± 2.46	10.95 ± 2.12 (1 h)	0.18	[161]

RCY: Radiochemical yield; Log P: Logarithm of the Partition coefficient; NC: Not communicated; dc: Decay corrected; [a]: Log $D_{7.4}$ (Logarithm of the Distribution coefficient at pH 7.4); [b]: IC_{50} (nM).

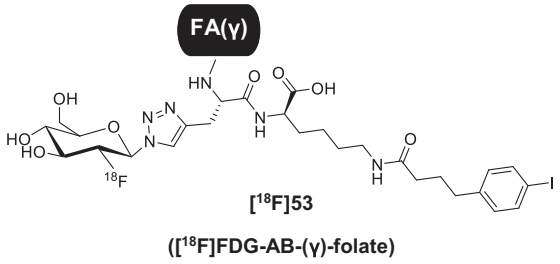

Fig. 29. Chemical structure of **[^{18}F]53** [174].

4.1. Albumin-binding ^{18}F-folate

In 2013, Fischer *et al.* were the first to design and evaluate an AB-radiofolate called **[^{18}F]53** ([^{18}F]FDG-AB-(γ)-folate) [174]. **53** was synthesized through CuAAC click chemistry approach from propargyl-AB-(γ)-folate and [^{18}F]FDG-azide (Fig. 29). *In vitro* and *in vivo* experiments were carried out on KB tumor cells and KB tumor-bearing mice, respectively. A FRα-specific binding of **[^{18}F]53** to KB tumor cells was observed. The role of AB entity was tested by comparison between **[^{18}F]53** and **[^{18}F]28** (studied in section 3.1.1.) [149]. The addition of the AB entity showed an increase in the partition coefficient (Log $D_{7.4}$ of − 3.2 ± 0.4 for **[^{18}F]53** *vs.* − 4.2 ± 0.1 for **[^{18}F]28**), which led to slightly increase the hydrophilicity of compound **53**. As expected, biodistribution tests revealed a high blood circulation time for **[^{18}F]53** as blood uptake was still of 2.21 ± 0.15 %IA/g at 4 h p.i. whereas it was only of 0.44 ± 0.09 %IA/g at 1 h p.i.. This confirmed that AB entity had a real impact on biodistribution. *In vivo* tumor uptake of **[^{18}F]53** increased over time to reach a maximum at 4 h p.i. (15.2 ± 0.53 %IA/g). Kidneys uptake was reduced by four using AB entity (13.4 ± 3.62 %IA/g compared to 42.9 ± 1.13 %IA/g without). The tumor-to-kidney ratio was 0.88 at 1 h p.i., whereas a much lower ratio of 0.23 was seen at 1 h p.i. for **[^{18}F]28**. Nonetheless, non-specific uptake was observed in gallbladder, salivary glands and liver. SPECT/CT scan images of mouse taken at 4 h p.i. of **[^{18}F]53** clearly showed tumors. The addition of the AB entity improved hepatobiliary elimination leading to a good visualization of gallbladder and abdominal region that could decrease the reliability of imaging diagnostics.

4.2. Albumin-binding ^{152}Tb-, ^{155}Tb- and ^{161}Tb-folates

Müller and co-workers developed compound **54** (cm09) composed of a DOTA chelator, FA and AB entities that were assembled around a modified lysine thanks to amide bond and CuAAC click reaction. Their objective was to investigate for the first time, in parallel, the respective contributions of each terbium radioisotopes on PET and SPECT imaging in KB tumor-bearing nude mice [81]. *In vivo* biodistribution studies for **[^{161}Tb]Tb-54** revealed a high tumor uptake at 4 h p.i. (23.8 ± 2.5 %IA/g) and persisting at 7 days p.i. (5.7 ± 1.9 %IA/g). No uptake was found in non-FRα-expressing organs and good tumor-to-tissue ratios were measured in blood, liver and kidneys (15, 6 and 0.8, respectively, at 24 h p.i.), demonstrating the potential interest of **[^{161}Tb]Tb-54** as contrast agent for SPECT imaging. Excellent microPET and SPECT images with **[^{152}Tb]Tb-54**, **[^{155}Tb]Tb-54** and **[^{161}Tb]Tb-54** were obtained at 24 h p.i., allowing clear visualization of the tumor (Fig. 30A,B,C). Interestingly, the relatively long half-life of terbium-155 allowed the acquisition with high longitudinal SPECT imaging resolution, leading to a clear visualization of the activity accumulation in the tumor and kidneys at 4 days p.i.. Müller *et al.* completed the evaluation of **[^{155}Tb]Tb-54** properties using SPECT images on IGROV-1 tumor-bearing mice [175]. SPECT/CT images at 2 days p.i. of **[^{155}Tb]Tb-54** revealed excellent activity accumulation in IGROV-1 tumors

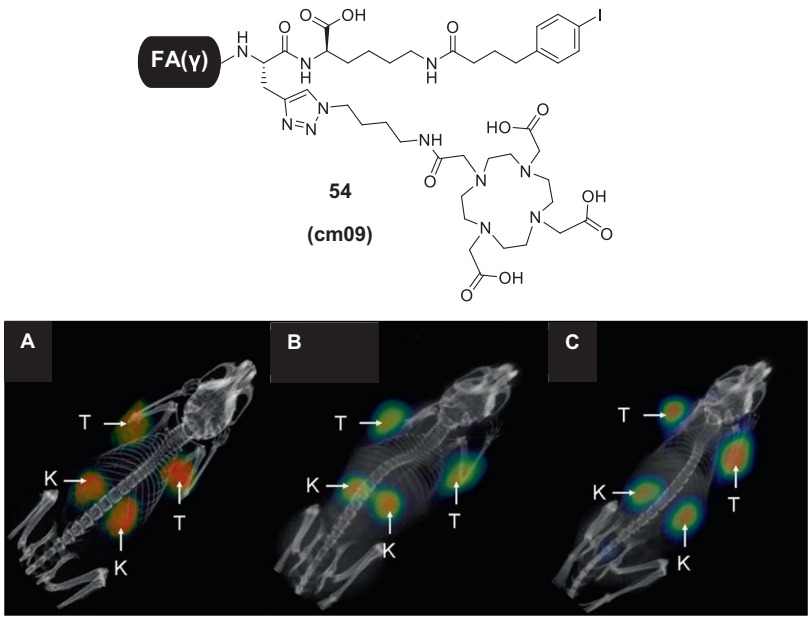

Fig. 30. Chemical structure of **54**, (A) microPET/CT image of KB tumor-bearing mice at 24 h p.i. of **[^{152}Tb]Tb-54** (9 MBq), and SPECT/CT images of KB tumor-bearing mice at 24 h p.i. of **[^{155}Tb]Tb-54** (B) 4 MBq and (C) 30 MBq. Reprinted with permission from [81]. Copyright 2022 SNMMI.

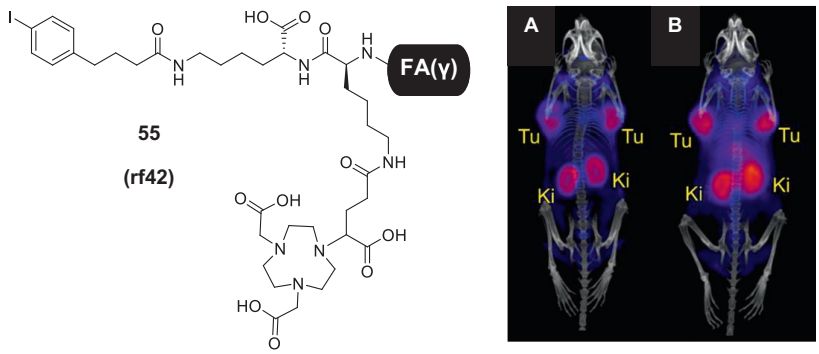

Fig. 31. Chemical structure of **55** and microPET/CT images of KB tumor-bearing mice at 2 h p.i. of **[^{64}Cu]Cu-55** (3.5–7 MBq) (A) and **[^{68}Ga]Ga-55** (5 MBq) (B). Reprinted with permission from [176]. Copyright 2022 American Chemical Society.

and kidneys. To sum up, the three terbium radiofolates are suitable for their respective applications.

4.3. Albumin-binding ^{68}Ga-, ^{64}Cu-, and ^{55}Co-folates

Ocak *et al.* used **[^{68}Ga]Ga-54** to evaluate its diagnostic potential for a FRα-positive ovarian tumor cell line (MKP-L) [176]. Biodistribution analysis was performed at 4 h p.i. of **[^{68}Ga]Ga-54** and showed a high fixation of the radioconjugate in tumors (4.2 ± 1.5 %IA/g) and kidneys (16.7 ± 4.7 %IA/g), conducted to a tumor-to-kidney ratio of 0.25. MicroPET/CT images acquisition on mice C57BL/6 bearing MKP-L tumors at different stages of disease was performed with injection of **[^{68}Ga]Ga-54** and compared to control mice. Imaging of peritoneal tumors at 3–3.5 h p.i. showed specificity of **[^{68}Ga]Ga-54** and high tumor uptake. **[^{68}Ga]Ga-54** showed its suitability to monitor over time (between 2 and 7 weeks p.i.) the evolution of tumor size on the same mice model using microPET imaging.

Müller and co-workers developed compound **55** (rf42) composed of a lysine residue functionalized with FA at its γ-position, AB entity and NODAGA chelator (Fig. 31) [177]. *In vivo* and *in vitro* results were compared to those obtained with its DOTA analogue **56** (cm10, Fig. 34). Compounds **55** and **56** were radiolabelled with gallium-68 and copper-64. Biodistribution data in KB tumor-bearing mice were acquired over a period of 4 h for **[^{68}Ga]Ga-55** and 72 h for **[^{64}Cu]Cu-55**. For **[^{64}Cu]Cu-55**, tumor, kidneys, salivary glands and liver showed significantly uptake at 4 h p.i. with values of 14.52 ± 0.99, 26.71 ± 2.34, 7.08 ± 4.56 and 6.24 ± 0.56 %IA/g, respectively, leading to a tumor-to-kidney ratio of 0.55. Similar results were obtained for **[^{68}Ga]Ga-55**. **[^{64}Cu]Cu-55** showed accumulation in liver over the time (*i.e.*, 6.02 ± 0.41 %IA/g at 72 h p.i.), thereby having a negative impact on the tumor-to-background contrast that could contribute to incorrect diagnoses. Chelating agent effect on the imaging efficiency was investigated by taking microPET/CT images at 2 h p.i. of **[^{68}Ga]Ga-55**, **[^{68}Ga]Ga-56**, **[^{64}Cu]Cu-55** and **[^{64}Cu]Cu-56**. MicroPET/CT imaging results with **[^{68}Ga]Ga-55** and **[^{64}Cu]Cu-55** exhibited distinct tumor and kidneys visualization (Fig. 31A,B). **[^{68}Ga]Ga-55** and **[^{68}Ga]Ga-56** gave similar microPET/CT images. Conversely, image comparison with **[^{64}Cu]Cu-55** and **[^{64}Cu]Cu-56** clearly showed a massive accumulation of activity of **[^{64}Cu]Cu-56** in liver due to a loss of copper-64 from DOTA and its transfer to Cu-binding proteins induced by a limited *in vivo* stability of the ^{64}Cu-DOTA complex. Clear visualization of the tumor and kidneys on microPET images accompanied by a low accumulation in the liver was obtained with **[^{64}Cu]Cu-55** even at

72 h p.i.. **[^{64}Cu]Cu-55** was identified as the most promising ^{64}Cu-radiofolate for PET imaging of FRα-positive tumors.

In 2019, the same team developed and pre-clinically evaluated **[^{55}Co]Co-55** and **[^{55}Co]Co-56** [178]. Their biodistribution profiles were evaluated in KB tumor-bearing mice and compared to those of **[^{64}Cu]Cu-55** and **[^{68}Ga]Ga-55** [76,79,177,179–183]. The results showed that both ^{55}Co-radiofolates displayed higher tumor uptake at 4 h p.i. (17 %IA/g) compared to ^{68}Ga- and ^{64}Cu-analogs. In addition, the biodistribution data at 4 h p.i. revealed a higher renal uptake and a lower distribution in blood for **[^{55}Co]Co-55** compared to **[^{55}Co]Co-56** (53 ± 12 *vs.* 36 ± 7 %IA/g for kidney and 8 ± 3 *vs.* 14 ± 1 %IA/g for blood), which could be explained by the slightly higher lipophilicity of **[^{55}Co]Co-56** compared to **[^{55}Co]Co-55**. This data underlined the versality importance of the chelating agent used for cobalt-55 labelling. The high affinity to FRα-expressing tissues was also evidenced by microPET/CT imaging of KB tumor-bearing mice at 4 h p.i..

4.4. Albumin-binding ^{44}Sc-folate

In a proof-of-concept study published in 2013, Müller and co-workers focused on the use of scandium-44 for PET imaging and dosimetry using compound **54** [184,185]. The resulted **[^{44}Sc]Sc-54** was *in vitro* and *in vivo* compared to **[^{177}Lu]Lu-54** which showed a high KB tumor uptake (section 5.2.). High KB cellular uptake and internalization in KB cells (30–50% of total FRα-bound fraction) was observed. Biodistribution studies in KB tumor-bearing mice using **[^{44}Sc]Sc-54** revealed a high tumor accumulation at 2 h p.i. (8.37 ± 0.41 %IA/g) that reached a maximum at 20 h p.i. (14.05 ± 2.29 %IA/g). In addition, specific salivary and kidney accumulations of **[^{44}Sc]Sc-54** were observed (3–7 and 19–23 %IA/g from 2 to 20 h p.i., respectively), indicating specificity of **[^{44}Sc]Sc-54** for organs expressing FRα. The biodistribution study showed a good tumor-to-kidney ratio between 0.44 and 0.65. All these tissue distribution data were broadly comparable, or even similar at 1 day p.i., to those of **[^{177}Lu]Lu-54**. MicroPET/CT images with **[^{44}Sc]Sc-54** at 4 h p.i. showed clear visualization of KB tumor and kidneys (Fig. 32A). The activity distribution profile of **[^{44}Sc]Sc-54** was similar to that observed on SPECT/CT images with **[^{177}Lu]Lu-54** at 4 h p.i. (Fig. 32B).

4.5. Conclusion

Addition of an AB entity to radiofolate successfully decrease kidney uptake and lead to a significant improvement of tumor-to-kidney ratio of AB-radiofolate reaching 0.44 to 1.03 (Table 6). These results are similar with those obtained with the other strategy involving antifolate pre-injection [124,125]. In addition, regarding images, both strategies lead to a better tumor-to-background contrast resulting in more accurate diagnostic. It is interesting to note that the combination strategy showed a synergistic effect on tumor-to-kidney ratio (*i.e.*, reaching 1.79 and on image contrast [165]. However, as the addition of AB entity to radiofolate is not toxic compared to antifolate pre-injection, this strategy is more suitable and AB-radiofolates could be validated by authorities to perform clinical trials. Moreover, by decreasing kidney uptake, TRT experimentations to treat FRα-positive tumors become possible as nephrotoxicity could be limited.

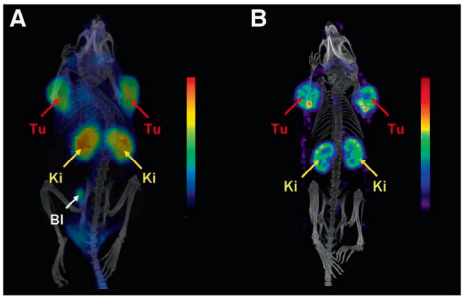

Fig. 32. (A) microPET/CT images of KB tumor-bearing mice at 4 h p.i. of **[^{44}Sc]Sc-54** (25 MBq) and (B) SPECT/CT images of KB tumor-bearing mice at 4 h p.i. of **[^{177}Lu]Lu-54** (35 MBq). Reprinted with permission from [184]. Copyright 2022 SNMMI.

5. Evaluation of radiofolates used in theranostic approach

This section describes radiofolates design for diagnostic imaging (SPECT or PET) and/or for TRT in the viewpoint of developing a theranostic approach. Regarding its energy properties, lutetium-177 is a radionuclide of choice for TRT and treatment monitoring or dosimetry using SPECT/CT imaging. Moreover, lutetium-177 can be easily complexed by the versatile DOTA chelator. Thus, it is favored for mismatched pair theranostic agents' development using gallium-68 as diagnostic radionuclide [73,95–97]. Concerning FRα-positive tumors, [^{177}Lu]Lu-MOv18 [187] and ^{177}Lu-folates have been developed for therapy. For over ten years now, lutetium-177 is used as radionuclide and ^{177}Lu-radiofolates have been developed by Schibli and co-workers. The matched pairs (scandium-44/scandium-47) and (technetium-99 m/rhenium-188) and the matched quadruplet (terbium-152/terbium-155/terbium-149/terbium-161) have also been tested in a theranostic approach using one radionuclide for diagnostic and the corresponding α or β$^-$-emitting-radionuclide for TRT. Finally, the ^{90}Y-radiofolate depicted here for TRT can be used in a mismatched pair with ^{64}Cu- or ^{68}Ga-radiofolate using the same precursor for theranostic use [177].

5.1. Lutetium-177 radiofolate evaluation

Müller *et al.* completed the study of **5** by replacing indium-111 by lutetium-177 to observe the impact of the radionuclide choice on *in vivo* characteristics [125]. Radiolabelling and *in vitro* results were similar to those obtained with **[^{111}In]In-5**. *In vivo* study was performed with the same experimental conditions previously described in section 2.2.2.. At 4 h p.i. of **[^{177}Lu]Lu-5**, biodistribution data revealed massive uptake in kidneys (57.22 ± 11.05 %IA/g) and moderate uptake in KB tumors, liver and salivary glands (7.51 ± 1.25, 4.63 ± 1.12, 5.02 ± 1.07 %IA/g, respectively). Kidneys and non-specific uptakes in liver and salivary glands were similar to those observed with **[^{111}In]In-5** (55.88 ± 3.91, 5.20 ± 2.00 and 6.13 ± 1.84 %IA/g, respectively) while tumor uptake was significantly higher (5.80 ± 0.55 %IA/g). This led to a higher tumor-to-kidney ratio of 0.15. Thus, the radionuclide type has a slightly but significant impact on the tracer biodistribution. SPECT/CT imaging showed moderate activity in KB tumors whereas high activity was detected in kidneys for both tracers. Small differences observed in biodistribution study did not have a significant impact on the image quality. Thus, **[^{177}Lu]Lu-5** is as suitable as **[^{111}In]In-5** for clinical trials.

5.2. Technetium-99 m/rhenium-188 approach for theranostic folate application

Kim *et al.* worked on the matched pair (technetium-99 m/rhenium-188) to develop a theranostic approach with folate tracer. Rhenium-188 is a γ- and β$^-$-emitter which confer to him SPECT imaging and therapy properties. Technetium and rhenium have similar chemical properties and can be chelated on same molecules. Thus, authors synthetized two radiofolates **[^{99m}Tc]Tc-57** and **[^{188}Re]Re-57** [188]. Compound **57** ((γ)-folate-Gly-Gly-Cys-

Table 6
Summary of radiochemistry, *in vitro* and *in vivo* results of radiofolates depicted in this section.

Radiofolate	RCY (%)	Log P	Tumor uptake (%IA/g) (4 h)	Tumor-to-kidney ratio (4 h)	References
[^{18}F]53	15–22	−3.2 ± 0.4	15.2 ± 0.53	0.88 ± 0.04	[174]
[^{68}Ga]Ga-54	>98 dc	NC	4.2 ± 1.5	0.25	[176]
[^{44}Sc]Sc-54	96	−4.49 ± 0.12	12.51 ± 1.74	0.59 ± 0.06	[184]
[^{152}Tb]Tb-54	>96	NC	NC	NC	[81,186]
[^{155}Tb]Tb-54	>96	NC	NC	NC	[81,186]
[^{161}Tb]Tb-54	>98	NC	23.81 ± 2.53	0.87 ± 0.12	[81,186]
[^{55}Co]Co-55	>95	NC	17.0 ± 4.0	0.32	[178]
[^{55}Co]Co-56	>95	NC	17.0 ± 2.0	0.47	[178]
[^{68}Ga]Ga-55	95	−3.85 ± 0.09[a]	11.92 ± 1.68	0.47 ± 0.06	[177]
[^{64}Cu]Cu-55	>95	−4.04 ± 0.48[a]	14.52 ± 0.99	0.55 ± 0.08	[177]

RCY: Radiochemical yield; Log P: Logarithm of the Partition coefficient; NC: Not communicated; dc: Decay corrected; [a]: Log $D_{7.4}$ (Logarithm of the Distribution coefficient at pH 7.4).

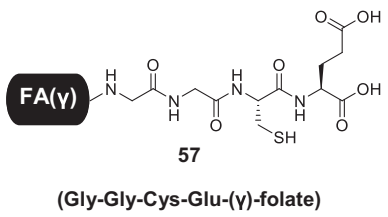

Fig. 33. Chemical structure of **57** [188].

Glu) was composed of FA linked to the peptidic chelating agent H-Gly-Gly-Cys-Glu-OH *via* an amide bond on the *N*-terminal glycine (Fig. 33). They performed *in vitro* studies in KB and HT1080 cells and *in vivo* studies in BALB/c nude mice bearing both KB and HT1080 tumors. Identical biodistribution patterns were obtained with **[^{99m}Tc]Tc-57** and **[^{188}Re]Re-57**. *In vivo* HT1080 tumors showed very low uptake as expected. At 4 h p.i., uptake of **[^{99m}Tc]Tc-57** in kidneys was 57.04 ± 18.58 and 17.59 ± 7.40 %IA/g in KB tumor (ratio: 0.30). When **[^{188}Re]Re-57** was used, kidneys and KB tumor uptake were respectively 63.71 ± 5.86 and 24.10 ± 7.28 %IA/g (ratio: 0.37). At 32 h p.i., tumor-to-kidney ratio reached 1.04 meaning that KB tumor uptake was higher than kidney uptake. For therapy, it is mandatory to have the highest tumor-to-kidney ratio as possible, and a value above 1 is a promising result. γ-Scintigraphy using **[^{99m}Tc]Tc-57** showed intense activity in KB tumor, kidneys and bladder at 4 h p.i., but this activity was significantly low at 16 h p.i. expect for KB-tumor making it the most visible tissue. SPECT/CT scan images showed intense activity in kidneys, urinary bladder and moderate activity in KB tumors at 4 and 16 h p.i. of **[^{99m}Tc]Tc-57** or **[^{188}Re]Re-57**. At last, **[^{99m}Tc]Tc-57** displayed tumor-to-normal organ ratio at 4 h p.i. much higher (2- to 5-fold) than those reported with **[^{99m}Tc]Tc-23** which is currently undergoing clinical trials. Nevertheless, no preclinical study on the therapeutic effect of **[^{188}Re]Re-57** have been reported.

The same team worked on the radiolabelling of **18** with rhenium-188 to determine if this compound could be suitable for therapy [86]. They already worked on **[^{99m}Tc]Tc-18** and wanted to see if the pair (**[^{188}Re]Re-18**/**[^{99m}Tc]Tc-18**) could be suitable as theranostic radioconjugates. Biodistribution tests were performed in KB tumor-bearing mice with **[^{188}Re]Re-18** and **[^{99m}Tc]Tc-18**. Similar significant uptake was observed at 4 h p.i. in kidneys (12.04 ± 0.62 *vs.* 18.48 ± 0.72 %IA/g, respectively), liver (2.96 ± 0.49 *vs.* 2.37 ± 2.85 %IA/g, respectively) and tumors (1.87 ± 0.04 *vs.* 2.33 ± 0.36 %IA/g, respectively). Competition tests were performed with FA and significant uptake was observed only on liver (2.00 ± 1.74 %IA/g) for **[^{188}Re]Re-18** confirming the non-specific uptake in liver for this radioconjugate. As kidney uptake was too important and could lead to renal toxicity, the team decided not to pursue investigations with **[^{188}Re]Re-18** for TRT.

5.3. Albumin-binding ^{177}Lu-folates evaluation

Müller and co-workers published three articles concerning **[^{177}Lu]Lu-54** and compared it with the conventional radiofolate **[^{177}Lu]Lu-3** without AB entity [185,186,189]. The aims of this study were to clarify whether the **[^{177}Lu]Lu-54** could be compared to **[^{177}Lu]Lu-3** and to highlight the effect of the presence of an AB entity on the tumor uptake and retention in kidneys. *In vitro* tests were performed on KB cells. High FRα affinities obtained with **[^{177}Lu]Lu-54** and **[^{177}Lu]Lu-3** were comparable to those of other radiofolates evaluated by the same team [190]. An increase in lipophilicity was observed with the addition of the AB entity (– 4.25 ± 0.41 for **[^{177}Lu]Lu-54** *vs.* – 4.81 ± 0.36 for **[^{177}Lu]Lu-3**). The biodistribution studies with KB tumor-bearing mice showed a high tumor uptake of **[^{177}Lu]Lu-54** (10.8 ± 1.32 %IA/g at 1 h p.i.). At 24 h p.i., tumor uptake of **[^{177}Lu]Lu-3** was 7.00 ± 1.22 %IA/g concluding to a significant tumor uptake increase by adding an AB entity. For **[^{177}Lu]Lu-54**, kidney uptake was 30.09 ± 4.04 at 24 h p.i. Comparatively, the kidney uptake of **[^{177}Lu]Lu-3** at 24 h p.i. was 57.95 ± 3.75 %IA/g confirming that a longer blood circulation time decreased the kidney uptake. Consequently, the tumor-to-kidney ratio was found to be higher for **[^{177}Lu]Lu-54** compared to **[^{177}Lu]Lu-3** (0.65 *vs.* 0.12). No significant uptake was observed in other tested organs for both radiofolates. SPECT/CT images showed a significant increase of the tumor-to-kidney ratio (~1.0 *vs.* ~ 0.2) in mice that received **[^{177}Lu]Lu-54** (Fig. 34), compared with **[^{177}Lu]Lu-3**.

Müller and co-workers developed four [^{177}Lu]Lu-DOTA-(γ)-folate conjugates deriving from **[^{177}Lu]Lu-54** to increase pharmacokinetic properties of **[^{177}Lu]Lu-54** and its interaction with

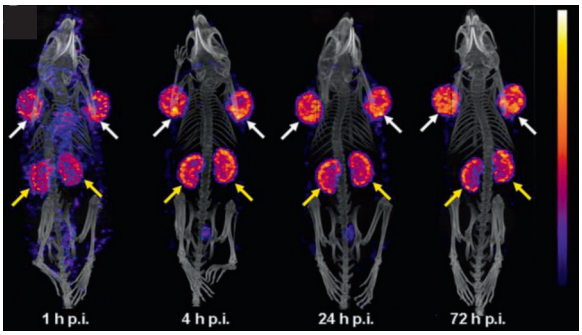

Fig. 34. SPECT/CT images of KB tumor-bearing mice at 1, 4, 24 and 72 h p.i. of **[^{177}Lu]Lu-54** (35 MBq). Reprinted with permission from [185]. Copyright 2022 SNMMI.

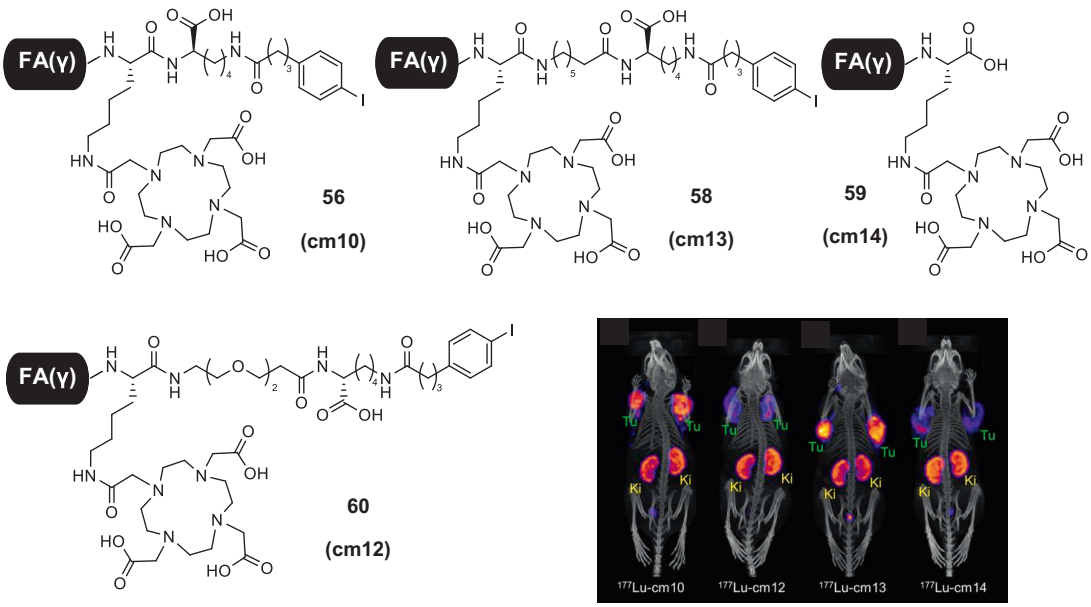

Fig. 35. Chemical structures of **56**, **58**, **59** and **60** and SPECT/CT images of KB tumor-bearing mice at 24 h p.i. of **[^{177}Lu]Lu-56**, **[^{177}Lu]Lu-58**, **[^{177}Lu]Lu-59** and **[^{177}Lu]Lu-60** (50 MBq). Reprinted with permission from [188]. Copyright 2022 American Chemical Society.

albumin by modification of the linker between DOTA chelator and FA. They developed **56** (cm10: lead compound designed with a lysine residue functionalized with DOTA, FA and the AB entity), **58** (cm12: with a PEG_{11} spacer between AB entity and lysine), **59** (cm13: with a short alkyl chain instead of PEG_{11} spacer) and **60** (cm14: **56** without the AB entity) (Fig. 35) [190]. *In vitro* experiments were performed in KB and IGROV-1 tumor cells. Cell uptake was in the range of 13 to 22% at 30 min p.i. All four radiofolates showed high FRα affinities in a range of 4.0–7.2 nM. *In vivo* experiments were conducted in KB and IGROV-1 tumor-bearing mice. At 24 h p.i., the kidneys uptake in KB tumor-bearing mice was between 19.5 and 46.6 %IA/g while tumor uptake was between 4.80 and 17.6 %IA/g. These led to tumor-to-kidney ratios between 0.43 and 0.63 for AB-radiofolates and 0.10 for **[^{177}Lu]Lu-60**. Comparatively slightly high tumor-to-kidney ratio was found in IGROV-1 tumor-bearing mice. These results clearly indicated an increase in tumor uptake and a decrease in kidney uptake when an AB entity was employed. Results also revealed that the presence or not of a spacer and its length played a role in the biodistribution profile. The biodistribution study concluded that a short alkyl chain spacer gave better results than a long PEG_{11} spacer for this type of radiofolate. SPECT/CT imaging was performed at 24 h p.i. of the four radiofolates (Fig. 35) and an excellent visualization of tumors and kidneys was observed. Tumor-to-kidney ratios were calculated and confirmed results of biodistribution as tumor-to-kidney ratios of **[^{177}Lu]Lu-56** (1.0) and **[^{177}Lu]Lu-58** (1.1) were superior to those of **[^{177}Lu]Lu-59** (0.7) and **[^{177}Lu]Lu-60** (0.7).

5.4. Treatment evaluation of FRα-positive tumors using radiofolates

The therapeutic application of **[^{177}Lu]Lu-54** was evaluated by Müller *et al.* in KB tumor-bearing mice. Tumor growth inhibition was much better with a single injection of 20 MBq compared to a fractionated injection (2 × 10 MBq or 3 × 7 MBq) [185]. Using a single injection of 20 MBq, the SPECT imaging revealed the disappearance of the tumor for 4 of the 5 mice of the group. Moreover, radiotoxic side effects were not observed. The good survival rate (80%) observed for mice injected with 20 MBq in one time gave promising results to push further investigations. To conclude **[^{177}Lu]Lu-54** was suitable for therapeutic clinical trials. Hence, the impact of the addition of an AB entity on the antitumor activity of radiofolate, and on the long-term kidney damage by comparison with **[^{177}Lu]Lu-3** properties was achieved [189]. The addition of the AB entity increased the absorbed radiation dose for tumors by a factor of three (1.4 Gy/MBq for **[^{177}Lu]Lu-54** *vs.* 0.444 Gy/MBq for **[^{177}Lu]Lu-3**) and reduced the absorbed radiation dose for kidneys by a factor of two (2.3 Gy/MBq for **[^{177}Lu]Lu-54** *vs.* 4.8 Gy/MBq for **[^{177}Lu]Lu-3**). The best tumor growth inhibition was observed with **[^{177}Lu]Lu-54** (≥20 MBq (≥28 Gy) per mouse), resulting in complete tumor remission. The long-term side effects were studied and showed a lower renal toxicity with **[^{177}Lu]Lu-54**. A threshold dose limit for the kidneys of 25 Gy in mice was obtained for **[^{177}Lu]Lu-54** [191].

^{149}Tb-folate was used in preclinical therapeutic tests to heal FRα-positive tumor-bearing mice [192]. *In vitro* study **[^{149}Tb]Tb-54** using KB cells were fulfilled to determine the killing potential of this radionuclide. MTT assay was performed using increasing concentration of **[^{149}Tb]Tb-54** (0–500 kBq/mL) in cell culture media. Cell viability was reduced by 20% with 0.5 kMq/mL and by 80% with 500 kBq/mL. 3 groups of KB tumor-bearing female athymic nude mice were used for therapeutic tests. Group A was the control, group B was injected with 2.2 MBq of **[^{149}Tb]Tb-54** and group C by 3 MBq of radiofolate. 14 days after the beginning of the therapy, blood urea nitrogen (damage of kidneys) and alkaline phosphate and total bilirubin (liver misfunction) were controlled in each group and revealed no kidneys and liver misfunction. At 21 days p.i. of radiofolate, the first mice (group A) had to be euthanized. At this time point, tumor growth was decreased by 62% and 85% for the group B and C, respectively (Fig. 36A). In the case of the survival time, it was increased by 45% and 105%, respectively (Fig. 36B). These results seemed promising as survival time was increased by 2 but a total remission would be ideal. Nevertheless, for now, other therapy studies including radiofolate showed similar results.

Thanks to identical chemical characteristics and complementary physical decay characteristics, terbium-149 and terbium-161 could be used to compare the effectiveness of α *vs.* β^- therapy for a same compound **54**. Therapy with **[^{149}Tb]Tb-54** (2.4 MBq) and **[^{161}Tb]Tb-54** (11 MBq) in KB tumor-bearing mice induced a marked tumor growth delay or a total remission (33% for **[^{149}Tb]**

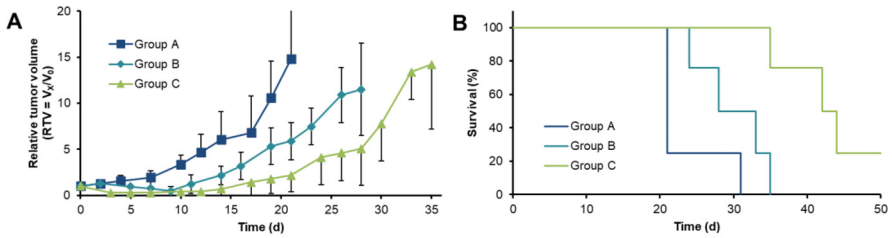

Fig. 36. (A) Relative tumor volume and (B) survival rate of KB tumor-bearing mice injected with saline (group A), 2.2 MBq (group B) and 3 MBq (group C) of **[^{149}Tb]Tb-54**. Adapted from [192]

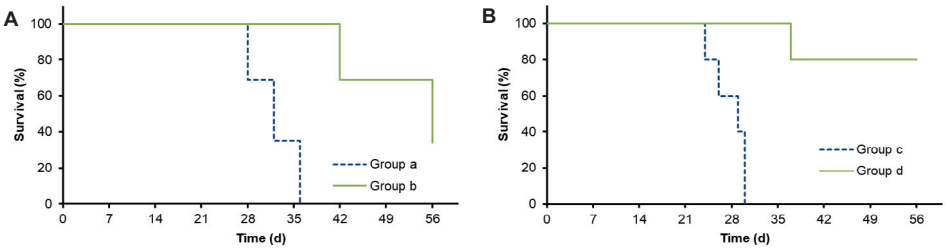

Fig. 37. Survival rate of mice treated (A) with **[^{149}Tb]Tb-54** (a: control, b: 2.4 MBq) and (B) **[^{161}Tb]Tb-54** (c: control, d: 11 MBq). . Adapted from [81]

Tb-54 and 80% for **[^{161}Tb]Tb-54**) and was accompanied by a significant survival improvement (Fig. 37A and B) [81]. In a second study, *in vitro* and *in vivo* antitumor effects of **[^{161}Tb]Tb-54** and **[^{177}Lu]Lu-54** in KB and IGROV-1 cells and in KB or IGROV-1-tumor-bearing mice were compared [186]. They also compared renal side effects after β^- therapy [186,193]. Biodistribution profiles of **[^{161}Tb]Tb-54** and **[^{177}Lu]Lu-54** in IGROV-1 tumor-bearing mice were found to be very close to those previously described on KB tumor-bearing mice (sections 4.2. and 5.3.). SPECT/CT images were performed in KB tumor-bearing mice at 24 h p.i. of **[^{161}Tb]Tb-54** or **[^{177}Lu]Lu-54** and showed a clear visualization of the tumor and the kidneys in both cases. After injection of 10 MBq of **[^{161}Tb]Tb-54** or **[^{177}Lu]Lu-54** in KB and IGROV-1 tumors-bearing mice, higher absorbed doses in tumors and kidneys of **[^{161}Tb]Tb-54** (3.3 and 4.5 Gy/MBq, respectively) were estimated in comparison with those of **[^{177}Lu]Lu-54** (2.4 and 3.4 Gy/MBq, respectively). These results might explain why a more marked tumor growth delay and an enhanced antitumor effect were observed after injection of **[^{161}Tb]Tb-54** compared to **[^{177}Lu]Lu-54**. The renal side effects (*i.e.* radionephrotoxicity) of **[^{161}Tb]Tb-54** and **[^{177}Lu]Lu-54** were studied in non-tumor-bearing mice at therapeutic doses (10, 20, and 30 MBq) over an 8-months period. β^- particles emission from terbium-161 and lutetium-177 had the same impact on kidney function. At 15 weeks p.i. (20 and 30 MBq), a significant impairment of kidney function was observed whereas this impairment appeared after 8 months when 10 MBq was injected [193]. This study demonstrates that **[^{161}Tb]Tb-54** and **[^{177}Lu]Lu-54** are suitable for theranostic approach to diagnose and treat FRα-overexpressing tumors. Further biological investigations would be necessary to envision future clinical trials.

Müller *et al.* investigated the potential of ^{47}Sc-radioconjugate containing a DOTA chelator and an AB entity (**[^{47}Sc]Sc-56**) for TRT [98]. Biodistribution studies of **[^{47}Sc]Sc-56** showed a high blood uptake in the first 4 h due to the increase in circulation time. High accumulation in KB tumor, kidneys and salivary glands (17.96 ± 2.17, 35.4 ± 1.1 and 7.40 ± 0.97 %IA/g at 4 h p.i., respectively) was observed with a good retention of activity for 72 h. Consequently the tumor-to-kidney ratio reached a maximum of 0.56 ± 0.07 at 72 h p.i.. SPECT/CT imaging of a KB tumor-bearing mouse at 48 h p.i. showed an excellent visualization of tumor. Activity uptake was also clearly seen in kidneys but in a lower intensity than tumor. Preclinical therapy study was achieved on KB tumor-bearing mice. 10 MBq of **[^{47}Sc]Sc-56** was injected in 6 mice. Compared to KB tumor-bearing mice receiving PBS injection, tumor growth was reduced by 2 and survival time was increased of 54% (Fig. 38A). Nevertheless, no remission was observed (Fig. 38B and C). For a single injection of 10 MBq of **[^{47}Sc]Sc-56**, a tumor dose of 10 Gy and a kidney dose of 20 Gy were determined. Since the kidney dose limit was approximately 23 Gy, this new therapeutic radiofolate would drastically minimize kidney toxicities. To conclude, scandium-47 is suitable for PET diagnostic and will be potentially used in clinical trials within a few years. These results

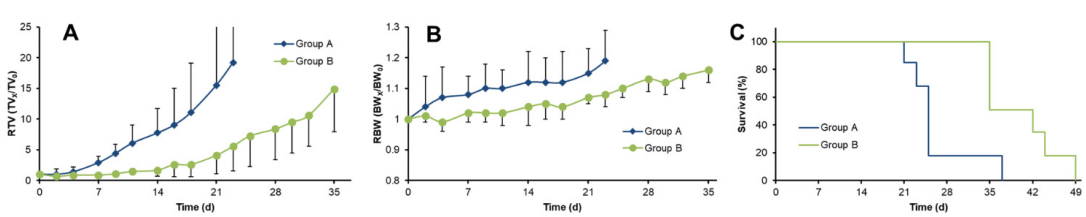

Fig. 38. (A) Relative tumor volume (RTV), (B) Relative body weight and (C) survival rate of KB tumor-bearing mice injected with saline (group A) or with **[^{47}Sc]Sc-56** (10 MBq) (group B). . Adapted from [98]

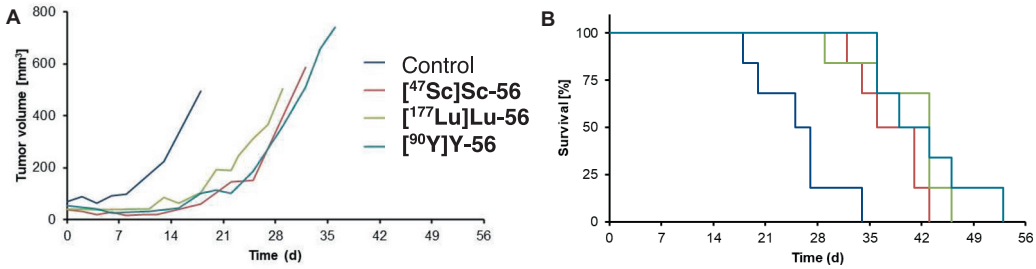

Fig. 39. (A) Tumor volume and (B) survival rate of IGROV-1 tumor-bearing mice injected with PBS, **[^{47}Sc]Sc-56** (12.5 MBq), **[^{177}Lu]Lu-56** (10 MBq) and **[^{90}Y]Y-56** (5 MBq). . Adapted from [194]

are also promising for the use of the matched pair scandium-44/scandium-47 in a theranostic approach.

Siwowska *et al.* evaluated the β^- therapeutic potential of scandium-47, lutetium-177 and yttrium-90 chelated to **56** [194]. MTT assay was performed using increasing doses (5–40 MBq/mL) of radiofolates in IGROV-1 cell culture to establish the killing ability of these three radiofolates. Cell viability was determined 4 h after incubation and revealed a total cell death with 20 MBq/mL of **[^{90}Y]Y-56** whereas 20% and 25% of cell were viable with 40 MBq of **[^{177}Lu]Lu-56** and **[^{47}Sc]Sc-56**, respectively. This result confirmed the killing ability of those radiofolates and particularly of **[^{90}Y]Y-56**. *In vivo* experiments were performed using IGROV-1 tumor-bearing nude mice. For therapy study, 4 groups of mice received respectively PBS, 12.5 MBq of **[^{47}Sc]Sc-56**, 10 MBq of **[^{177}Lu]Lu-56** and 5 MBq of **[^{90}Y]Y-56**. Doses were adapted regarding respective emission energy to reach the same absorbed tumor dose per radiofolate. Body weight of all mice stayed stable for the whole experiment period. A tumor growth inhibition of respectively 69%, 6% and 76% was observed leading to an increase in survival time (26%, 35% and 65%, respectively) (Fig. 39A and B). Plasma parameters like blood urea nitrogen, alkaline phosphate and total bilirubin were evaluated. As concentration in blood was the same before therapy, non-nephrotoxicity of the three radiofolates for tested doses was concluded. These *in vitro* and *in vivo* results showed that **[^{90}Y]Y-56** presents the best FRα-positive tumor cell killing ability. Nonetheless, regarding these promising results, all tested radionuclides could be used in TRT following the nature of the tumor.

Recent improvement in kidney uptake decrease was obtained with **[^{18}F]42** and **[^{18}F]43** with the use of the reduced form of FA, 5-Me-THF. Thus, Guzik *et al.* translated this concept to develop a suitable TRT ^{177}Lu-radioconjugate [195]. Thus, they replaced FA of **56** by 6*S*-Me-THF and 6*R*-Me-THF to obtained **61** and **62**, respectively. **[^{177}Lu]Lu-61** and **[^{177}Lu]Lu-62** ([^{177}Lu]Lu-6*S*-RedFol-1 and [^{177}Lu]Lu-6*R*-RedFol-1) (Fig. 40) showed higher KB cellular uptake (42–53% and 28–30%, respectively) and internalization (14–19% and 14–15%, respectively) compared to **[^{177}Lu]Lu-56** (uptake of 20–26% and internalization of 10–11%). Regarding biodistribution tests conducted in KB tumor-bearing mice, high uptake was only observed in tumor and kidneys demonstrating a good specificity of the radioconjugates to tumor cells. Tumor-to-kidney ratio was below 1 for **[^{177}Lu]Lu-61** and **[^{177}Lu]Lu-56** (0.66 and 0.64, respectively) whereas one of the best tumor-to-kidney ratio ever observed was obtained for **[^{177}Lu]Lu-62** (1.96). High tumor and kidney accumulations were visible on SPECT/CT images recorded 24 h p.i. of the three radioconjugates in KB tumor-bearing mice. For **[^{177}Lu]Lu-62**,

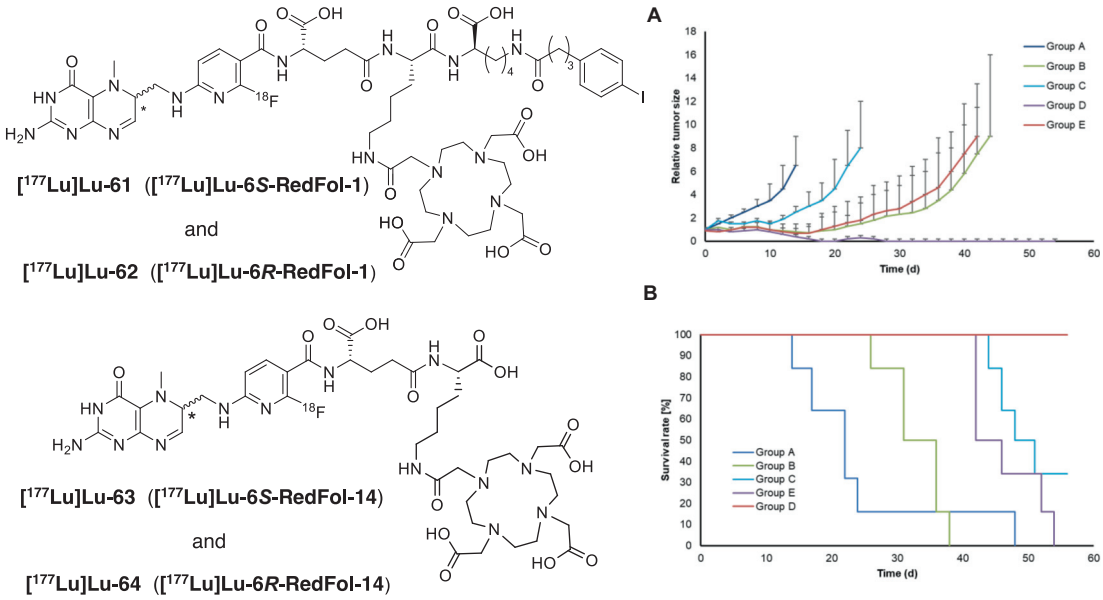

Fig. 40. Chemical structure of **61**, **62**, **63** and **64**, (A) Relative tumor size and (B) survival rate of KB tumor-bearing mice injected with PBS, **[^{177}Lu]Lu-62** (10 MBq), **[^{177}Lu]Lu-56** (10 MBq), **[^{177}Lu]Lu-62** (10 MBq) and **[^{177}Lu]Lu-56** (15 MBq). . Adapted from [195]

Table 7
Summary of radiochemistry, *in vitro* and *in vivo* results of radiofolates depicted in this section.

Radiofolate	RCY (%)	Log P	K_d for FRα (nM)	Tumor uptake (%IA/g) (4 h)	Tumor-to-kidney ratio (4 h)	References
[^{177} Lu]Lu-5	>90	NC	NC	7.51 ± 1.25	0.67 ± 0.01	[125]
[^{177}Lu]Lu-3	>98	−4.81 ± 0.36[a]	NC	7.52 ± 1.15	0.10 ± 0.01	[169,185,189]
[^{177}Lu]Lu-54	>98	−4.25 ± 0.41[a]	NC	18.12 ± 1.80	0.65 ± 0.07	[185,186,189]
[^{177}Lu]Lu-56	>97	−4.40 ± 0.23[a]	5.1 ± 2.1	14.3 ± 1.94	1.2 ± 0.5	[190,194]
[^{177}Lu]Lu-57	NC	−4.10 ± 0.14[a]	7.4 ± 1.2	19.5 ± 3.21	0.61 ± 0.10	[190]
[^{177}Lu]Lu-58	NC	−4.10 ± 0.20[a]	4.0 ± 3.4	16.0 ± 1.58	0.63 ± 0.12	[165,190]
[^{177}Lu]Lu-59	NC	< −5.5[a]	4.9 ± 2.7	8.56 ± 2.09	0.12 ± 0.00	[190]
[^{99m}Tc]Tc-60	>93	NC	5.19	17.59 ± 7.40	0.30	[188]
[^{188}Re]Re-60	>93	NC	5.19	21.74 ± 4.41	0.28	[188]
[^{99m}Tc]Tc-18	>95	NC	NC	2.33 ± 0.36	0.13 ± 0.02	[86]
[^{188}Re]Re-18	>95	NC	NC	1.87 ± 0.04	0.15 ± 0.01	[86]
[^{149}Tb]Tb-54	>96	−4.25 ± 0.41[a]	NC	NC	NC	[81,192]
[^{161}Tb]Tb-54	>98	NC	NC	23.8 ± 2.5	0.87 ± 0.12	[81,186]
[^{47}Sc]Sc-56	>96	NC	NC	17.96 ± 2.17	0.51 ± 0.03	[98,194]
[^{90}Y]Y-56	>97	NC	NC	NC	NC	[194]
[^{177}Lu]Lu-61	NC	−3.70 ± 0.10	1.0 ± 2.4	26 ± 1	0.66	[195]
[^{177}Lu]Lu-62	NC	−3.92 ± 0.11	2.0 ± 3.5	20 ± 2	1.96	[195]
[^{177}Lu]Lu-63	NC	< −5	2.0 ± 3.4	14 ± 3	0.09 ± 0.01	[196]
[^{177}Lu]Lu-64	NC	< −5	2.2 ± 3.9	9.5 ± 1.7	0.09 ± 0.02	[196]

RCY: Radiochemical yield; Log P: Logarithm of the Partition coefficient; NC: Not communicated; dc: Decay corrected; [a]: Log $D_{7.4}$ (Logarithm of the Distribution coefficient at pH 7.4).

tumor was more visible than kidneys confirming biodistribution results. These results was in accordance with those obtained with **[^{18}F]41**, **[^{18}F]42** and **[^{18}F]43** where the best tumor-to-kidney ratio was observed for **[^{18}F]43** ((6*R*)-3′-aza-2′-[^{18}F]fluoro-5-Me-THF). Thus, 6*R*-5-Me-THF derivative seems less internalized into kidney cells which is promising for TRT. To observe the impact of the AB entity on biodistribution, free AB-analogues of **[^{177}Lu]Lu-61** and **[^{177}Lu]Lu-62** were evaluated (**[^{177}Lu]Lu-63** ([^{177}Lu]Lu-6*S*-RedFol-14) and **[^{177}Lu]Lu-64** ([^{177}Lu]Lu-6*R*-RedFol-14), respectively) [196]. **[^{177}Lu]Lu-63** and **[^{177}Lu]Lu-64** had different pharmacokinetic properties compared to their AB-analogues as they expressed fast blood clearance. Thus, tumor-to-kidney ratios were low (0.08 and 0.09, respectively). Regarding SPECT/CT imaging, conclusions were similar to those obtained for biodistribution. With AB entity, higher tumor accumulation and lower kidney accumulation were slightly visible and confirmed that ^{177}Lu-AB-5-Me-THF radioconjugates are suitable for TRT evaluation. To evaluate TRT ability of **[^{177}Lu]Lu-62**, the radioconjugate was injected in KB tumor-bearing mice and compared to **[^{177}Lu]Lu-56**. Total remission was observed for mice injected with 15 MBq of **[^{177}Lu]Lu-62** whereas tumor growth inhibition of 44% was observed for **[^{177}Lu]Lu-56** (15 MBq). No significant body weight loss was observed for mice treated with radioconjugates (Fig. 40 A,B). Blood plasma parameters did not change during TRT and were similar for treated and untreated mice demonstrating no nephrotoxicity. Thus, **[^{177}Lu]Lu-62** is the most promising radioconjugate for FRα TRT**.**

5.5. Conclusion

TRT to treat FRα-positive tumor-bearing mice was experimented using mainly lutetium-177 but also rhenium-188, terbium-149, terbium-161, scandium-47 and yttrium-90. Main results are described in Table 7. Radiofolates containing an AB entity are the most promising radiofolates to treat FRα-overexpressing tumors. Based on the tumor models and injected activities, all published radiofolates showed a positive impact on tumor regression with the addition of an AB entity even if complete remission was not achieved. As for AB-radiofolates for nuclear imaging (Section 4.), a synergistic effect on tumor regression was also demonstrated by the combination of an AB entity and antifolate pre-injection though without attaining remission [165]. Nevertheless, these preclinical tests are quite promising as survival time was increased by 50% in average with a tumor growth reduced by 2. Regarding radioconjugates using Me-THF as targeting entity and particularly **[^{177}Lu]Lu-62**, therapy results are different but positive. Thus, folate-tracer could be radiolabelled with different radionuclides depending on the characteristics of the tumor's patients to personally adapt treatments to patients.

6. Conclusions and perspectives

In the late 90 s, the first radiofolates were successfully developed for scintigraphy. The [^{111}In]In-DTPA-folate ([**^{111}In]In-4**) was the first-in-human study to diagnose ovarian cancer. Then, with the advent of technetium, plethora of ^{99m}Tc-radiofolates were developed for FRα-overexpressing tumor diagnosis. Most of them showed similar results with good tumor uptake and good tumor-to-background ratio whereas low tumor-to-kidney ratio was observed. With the emergence of PET imaging, ^{18}F-, ^{68}Ga-, ^{64}Co-, ^{44}Sc-radiofolates was developed and a decline of interest for ^{99m}Tc-radiofolate occurs. Numerous of them also demonstrate great specificity to FRα-overexpressing tumor cells allowing the record of good quality images. The targeting moieties of radiofolates are based on FA. FA and folates are essential nutrients for the organism, so stable radiofolates had to be developed to avoid their elimination *via* metabolism before to get a chance to proceed with the imaging or the therapy. Stability tests was successfully performed for described radiopharmaceuticals as no significant degradation was observed.

Regarding chemical structure of folate-based-radiopharmaceuti cals, a great willingness to improve radiopharmaceutical designs and synthesis strategies has been noticed. For ^{18}F-radiofolate structures, some of them are now synthesized using the click chemistry approach. This effective approach allows reduction of costs of synthesis thanks to a decrease in the number of steps and an increase in yields. Müller and co-workers developed radioconjugates based on a lysine functionalized by FA or derivatives, DOTA and AB. Moreover, some teams demonstrate that functionalization of FA at the α- and/or or γ-position of the glutamate moiety have no impact on binding affinity. In this way, it is no longer necessary to use regioselective reactions that also ease the synthesis of the tracer precursors. When one of the two diastereoisomers has to

be selected, the use of pteroate entity is preferred compared to non-selective reaction followed by separative purification.

The two nuclear imaging modalities depend on the isotopes used for the radiolabelling of folate derivatives. For scintigraphy or SPECT/CT examinations, almost all nuclear medicine departments have a molybdenum-99/technetium-99 m generator. The low cost and high availability of this generator make possible the development and the use of ^{99m}Tc-radiofolates in clinical routine such as FolateScan (**[^{99m}Tc]Tc-23**) [139]. Less frequently, some nuclear medicine departments are equipped with a germanium-68/gallium-68 generator to produce gallium-68 or with a cyclotron to produce fluorine-18 used in the production of PET radiopharmaceuticals. Different radiofolates labelled with β^+-emitters have been described in the literature. The sensitivity of PET not only allows the detection of small amounts of radiofolate (more sensitive than MRI imaging for example [197]), it is also an excellent tool for quantifying the overall absorption of the tracer and therefore to monitor the evolution of the lesions or the efficacy of a treatment, by quantifying the expression of FRα correlated with the presence of tumor cells.

Numerous folate-based radiopharmaceuticals have succeeded *in vitro* and *in vivo* tests, and further preclinical tests could be conducted before considering clinical trials. KB cells might not be the most representative cell line for FRα-overexpressing human cancerous cells, but KB cell line is the most referenced cell line in literature for this use, as it is a well-known and available line (subclone of HeLa), easy to expand *in vitro* and to implant *in vivo*. Some studies were carried out with more representative cell lines from human FRα-overexpressing tumors (SKOV-3ip and IGROV-1 for ovarian cancer, HT29 and LoVo for colorectal cancer, CT-26 for colon cancer, M109 for non-small cell lung cancer and MT-1 for breast cancer). However, the transplant of cells from patient derived xenograft (PDX) would be the best alternative to mimic the tumor characteristics and the architectural properties of original patient tumors and then be a better model to study these specific tracers and therefore being able to move forward successful clinical trials. The culture and the implantation of PDX are not easy tasks as, it is known, depending on the type of cancer, that not all the PDX cultures are successful. In the attempt to proceed with a clinical trial, more specific cancer cells should be studied in animal models, the best candidates being PDX cells.

Among all developed radiofolates, the ones that give the most promising results are those with a high hydrophilicity, high tumor-to-liver ratio, high FRα affinity and a strong stability complex. High hydrophobicity radiopharmaceuticals are eliminated by the hepatobiliary way which increase the intestines, gallbladder and liver dosimetry and decrease tumor-to-background ratio entailing poor image quality and tough diagnosis. Moreover, a high signal-to-noise ratio facilitates the imaging of small lesions and peritoneal metastasis. Three radiofolates have satisfied all *in vitro* and *in vivo* specifications and have been studied under clinical trials, FolateScan (**[^{99m}Tc]Tc-23**) and [^{111}In]In-DTPA-folate ([**^{111}In]In-4**) for SPECT imaging and [^{18}F]-Azafol (**[^{18}F]41**) for PET imaging. However, only FolateScan is currently used in clinical routine to diagnose ovarian or endometrial cancer. Promising results of [^{18}F]-Azafol could allow its use in clinical routine in a few years. Nevertheless, despite the constant increase in spatial resolution of imaging technology, detection of metastases of epithelial ovarian cancer remains a challenge.

Concerning TRT, one of the big challenges of its development is the good biodistribution of radiopharmaceuticals and more precisely, a low kidney uptake. As FRα is highly expressed by the tubule cells of kidneys, radiofolates are highly internalized into these cells entailing high tumor-to-kidney ratio. Due to the intense fixation and renal topology, several strategies have been developed to limit this unwanted fixation and reduce the adverse effects caused by non-specific targeting. The first strategy is a chemical modification of the radiopharmaceutical structure by adding an AB entity to increase the circulation time of the radiofolate and reduce renal uptake. Thus, TRT has been intended with ^{177}Lu-, ^{161}Tb-, ^{149}Tb-AB-radiofolates. Only one preclinical trial (**[^{177}Lu]Lu-56**) showed complete remission. Nonetheless, delay in tumor growth and increase in survival rate have been observed for all TRT studies involving radiofolates which is encouraging in the development of such a therapy to treat FRα-overexpressing cancers. In fact, treatment with **[^{177}Lu]Lu-56** allows 100% survival rate whereas treatment with **[^{177}Lu]Lu-54** or **[^{161}Tb]Tb-56** showed the second best survival rates. No significant nephrotoxicity was observed for all treatment strategies tested giving hope to see one day a TRT clinical trials using radiofolate. Moreover, monitoring of the injected dose and dose number constraint nephrotoxicity.

The second strategy, not depicted in this review, consists in a prior injection of antifolates such as pemetrexed, to reduce renal binding of radiofolate by a competition for the FRα [166,169]. Nevertheless, this does not prevent the kidneys from being exposed to radiation, but significantly reduce it as huge increase in tumor-to-kidney ratio is observed. The evaluation of the impact of the combination of pemetrexed pre-injection and the presence of an AB entity in the radiopharmaceutical structure on the tissue distribution give encouraging results with a positive synergistic effect as an increase of around 30–50% of the tumor-to-kidney ratio (~1.79) [165]. Finally, a last strategy is being explored to target another biological markers such as anti-Müllerian hormone type II receptor (AMHRII) or Müllerian-inhibiting substance receptor type II (MISRII) for targeted diagnosis of target gynecological cancers. In fact, a first-in-human study is currently ongoing using GM102 mAb (NCT02978755) to diagnose gynecologic cancers by targeting AMHRII [198–200].

Moreover, the development of folate-based-radiopharmaceuti cals using high energy radiation isotopes (α and β^- emission) allows their use in nuclear medicine in a theranostic approach. Müller and co-workers successfully employed AB-radiofolates (**54**, **55** and **56**) in PET giving high quality images with low activity intensity in kidneys and high intensity in tumors and for TRT giving high survival rate and tumor growth delay. Theranostic works could be push further by the radiolabelling of **55** with fluorine-18 using aluminum-fluorine-18 innovative strategy or with the radiolabelling of **54** and **56** by gallium-68 to produce gallium-68/lutetium-177 mismatched pair. Concerning treatment monitoring, SPECT or PET radiofolates could be employed to follow the evaluation of tumor characteristics. In fact, the clinical study of the treatment of ovarian cancer using Vintafolide has been monitored with success using [^{99m}Tc]Tc-EC20 in SPECT imaging [201].

Regarding the use of radiofolates under clinical trials, the identification of the patient, who potentially will respond to these types of agents, represents a crucial step. The level of FRα expression is particularly important to evaluate. FRα expression could be routinely evaluated in anatomopathology on patient tumor biopsies, giving a hint at the patients overexpressing the receptor. Then, as [^{99m}Tc]Tc-EC20 is a gold standard diagnostic radiopharmaceutical for the imaging of FRα-overexpressing tumor, clinical trials involving diagnostic radiofolates might include SPECT/CT imaging with [^{99m}Tc]Tc-EC20. Even if the targeting agent is different from the one in [^{99m}Tc]Tc-EC20 (FA, Me-THF or 3′-Aza-2′–FA), the comparison of both images might be relevant as the same receptor is targeted. For therapeutic clinical trials, patient should be identified using SPECT/CT with [^{99m}Tc]Tc-EC20 to confirm standard staining and immunohistopathology results following a biopsy. As preclinical results on radiofolate use for diagnosis and therapy are promising, some clinical trials might be starting in the near future.

Declaration of Competing Interest

The authors declare that they have no known competing financial interests or personal relationships that could have appeared to influence the work reported in this paper.

Acknowledgments

We thank Dr. Francis Baros for his assistance in the bibliography research procedure. We thank Doxaca for the realization of the graphical abstract. This work was supported by the "Ministère de l'Enseignement Supérieur, de la Recherche et de l'Innovation" (MSERI) and Nancyclotep with a Doctoral fellowship for Laurène Wagner.

References

[1] H. Azaïs, C. Schmitt, M. Tardivel, O. Kerdraon, A. Stallivieri, C. Frochot, N. Betrouni, P. Collinet, S. Mordon, Assessment of the specificity of a new folate-targeted photosensitizer for peritoneal metastasis of epithelial ovarian cancer to enable intraperitoneal photodynamic therapy. A preclinical study, Photodiagnosis Photodyn. Ther. 13 (2016) 130–138, https://doi.org/10.1016/j.pdpdt.2015.07.005.

[2] N. Parker, M.J. Turk, E. Westrick, J.D. Lewis, P.S. Low, C.P. Leamon, Folate receptor expression in carcinomas and normal tissues determined by a quantitative radioligand binding assay, Anal. Biochem. 338 (2005) 284–293, https://doi.org/10.1016/j.ab.2004.12.026.

[3] K.R. Kalli, A.L. Oberg, G.L. Keeney, T.J.H. Christianson, P.S. Low, K.L. Knutson, L. C. Hartmann, Folate receptor alpha as a tumor target in epithelial ovarian cancer, Gynecol. Oncol. 108 (2008) 619–626, https://doi.org/10.1016/j.ygyno.2007.11.020.

[4] S. Markert, S. Lassmann, B. Gabriel, M. Klar, M. Werner, G. Gitsch, F. Kratz, A. Hasenburg, Alpha-folate receptor expression in epithelial ovarian carcinoma and non-neoplastic ovarian tissue, Anticancer Res. 28 (2008) 3567–3572.

[5] H. Elnakat, M. Ratnam, Distribution, functionality and gene regulation of folate receptor isoforms: implications in targeted therapy, Folate Recept.-Target, Drugs Cancer Inflamm. Dis. 56 (2004) 1067–1084, https://doi.org/10.1016/j.addr.2004.01.001.

[6] D.J. O'Shannessy, E.B. Somers, R. Smale, Y.-S. Fu, Expression of Folate Receptor-α (FRA) in Gynecologic Malignancies and its Relationship to the Tumor Type, Int. J. Gynecol. Pathol. 32 (2013) 258–268, https://doi.org/10.1097/PGP.0b013e3182774562.

[7] X. Zhao, H. Li, R.J. Lee, Targeted drug delivery via folate receptors, Expert Opin. Drug Deliv. 5 (2008) 309–319, https://doi.org/10.1517/17425247.5.3.309.

[8] H. Azaïs, G. Queniat, C. Bonner, O. Kerdraon, M. Tardivel, G. Jetpisbayeva, C. Frochot, N. Betrouni, P. Collinet, S. Mordon, Fischer 344 Rat: A Preclinical Model for Epithelial Ovarian Cancer Folate-Targeted Therapy, Int. J. Gynecol. Cancer. 25 (2015) 1194–1200, https://doi.org/10.1097/IGC.0000000000000497.

[9] H. Azaïs, C. Frochot, A. Grabarz, S. Khodja Bach, L. Colombeau, N. Delhem, S. Mordon, P. Collinet, Photosensibilisateur spécifique pour la thérapie photodynamique ciblée des métastases péritonéales des cancers ovariens, Gynécologie Obstétrique Fertil. Sénologie. 45 (2017) 190–196, https://doi.org/10.1016/j.gofs.2017.02.010.

[10] H. Azaïs, C. Rebahi, M. Baydoun, B. Serouart, L. Ziane, O. Moralès, C. Frochot, L. Colombeau, E. Thécua, P. Collinet, N. Delhem, S. Mordon, A global approach for the development of photodynamic therapy of peritoneal metastases regardless of their origin, Photodiagnosis Photodyn. Ther. 30 (2020), https://doi.org/10.1016/j.pdpdt.2020.101683 101683.

[11] H. Azaïs, A. Moussaron, S. Khodja Bach, A. Bassil, N. Betrouni, C. Frochot, P. Collinet, S. Mordon, FRα : une cible pour la thérapie photodynamique prophylactique des métastases péritonéales ovariennes ?, Bull Cancer (Paris). 101 (2014) 1109–1113, https://doi.org/10.1684/bdc.2014.1977.

[12] M. Baydoun, O. Moralès, C. Frochot, C. Ludovic, B. Leroux, E. Thecua, L. Ziane, A. Grabarz, A. Kumar, C. de Schutter, P. Collinet, H. Azais, S. Mordon, N. Delhem, Photodynamic Therapy Using a New Folate Receptor-Targeted Photosensitizer on Peritoneal Ovarian Cancer Cells Induces the Release of Extracellular Vesicles with Immunoactivating Properties, J. Clin. Med. 9 (2020) 1185, https://doi.org/10.3390/jcm9041185.

[13] A. Quilbe, O. Moralès, M. Baydoun, A. Kumar, R. Mustapha, T. Murakami, B. Leroux, C. de Schutter, E. Thecua, L. Ziane, L. Colombeau, C. Frochot, S. Mordon, N. Delhem, An Efficient Photodynamic Therapy Treatment for Human Pancreatic Adenocarcinoma, J. Clin. Med. 9 (2020) 192, https://doi.org/10.3390/jcm9010192.

[14] A. Stallivieri, F. Baros, G. Jetpisbayeva, B.M. and C. Frochot, The Interest of Folic Acid in Targeted Photodynamic Therapy, Curr. Med. Chem. (2015). http://www.eurekaselect.com/133566/article (accessed April 15, 2020).

[15] R. Schneider, F. Schmitt, C. Frochot, Y. Fort, N. Lourette, F. Guillemin, J.-F. Müller, M. Barberi-Heyob, Design, synthesis, and biological evaluation of folic acid targeted tetraphenylporphyrin as novel photosensitizers for selective photodynamic therapy, Bioorg. Med. Chem. 13 (2005) 2799–2808, https://doi.org/10.1016/j.bmc.2005.02.025.

[16] M.J. Turk, G.J. Breur, W.R. Widmer, C.M. Paulos, L.-C. Xu, L.A. Grote, P.S. Low, Folate-targeted imaging of activated macrophages in rats with adjuvant-induced arthritis, Arthritis Rheum. 46 (2002) 1947–1955, https://doi.org/10.1002/art.10405.

[17] D.M.S.H. Chandrupatla, G. Jansen, E. Mantel, P.S. Low, T. Matsuyama, R.P. Musters, A.D. Windhorst, A.A. Lammertsma, C.F.M. Molthoff, C.J. van der Laken, Imaging and Methotrexate Response Monitoring of Systemic Inflammation in Arthritic Rats Employing the Macrophage PET Tracer [18F] Fluoro-PEG-Folate, Contrast Media Mol. Imaging. 2018 (2018), https://doi.org/10.1155/2018/8092781.

[18] T.M. Piscaer, C. Müller, T.L. Mindt, E. Lubberts, J.A.N. Verhaar, E.P. Krenning, R. Schibli, M. De Jong, H. Weinans, Imaging of activated macrophages in experimental osteoarthritis using folate-targeted animal single-photon–emission computed tomography/computed tomography, Arthritis Rheum. 63 (2011) 1898–1907, https://doi.org/10.1002/art.30363.

[19] M. Siebelt, J.H. Waarsing, H.C. Groen, C. Müller, S.J. Koelewijn, E. de Blois, J.A. N. Verhaar, M. de Jong, H. Weinans, Inhibited osteoclastic bone resorption through alendronate treatment in rats reduces severe osteoarthritis progression, Bone. 66 (2014) 163–170, https://doi.org/10.1016/j.bone.2014.06.009.

[20] A. Müller, K. Beck, Z. Rancic, C. Müller, C.R. Fischer, T. Betzel, P.A. Kaufmann, R. Schibli, S.D. Kramer, S.M. Ametamey, Imaging Atherosclerotic Plaque Inflammation via Folate Receptor Targeting Using a Novel 18F-Folate Radiotracer, Mol. Imaging. 13 (2014) 7290.2013.00074. 10.2310/7290.2013.00074.

[21] W. Ayala-López, W. Xia, B. Varghese, P.S. Low, Imaging of Atherosclerosis in Apoliprotein E Knockout Mice: Targeting of a Folate-Conjugated Radiopharmaceutical to Activated Macrophages, J. Nucl. Med. 51 (2010) 768–774, https://doi.org/10.2967/jnumed.109.071324.

[22] A. Coliva, A. Zacchetti, E. Luison, A. Tomassetti, I. Bongarzone, E. Seregni, E. Bombardieri, F. Martin, A. Giussani, M. Figini, S. Canevari, 90 Y Labeling of monoclonal antibody MOv18 and preclinical validation for radioimmunotherapy of human ovarian carcinomas, Cancer Immunol. Immunother. 54 (2005) 1200–1213, https://doi.org/10.1007/s00262-005-0693-2.

[23] F. Crippa, G.L. Buraggi, E. Di Re, M. Gasparini, E. Seregni, S. Canevari, M. Gadina, M. Presti, A. Marini, E. Seccamani, Radioimmunoscintigraphy of ovarian cancer with the MOv18 monoclonal antibody, Eur. J. Cancer Clin. Oncol. 27 (1991) 724–729, https://doi.org/10.1016/0277-5379(91)90174-C.

[24] C. Brand, A. Sadique, J.L. Houghton, K. Gangangari, J.F. Ponte, J.S. Lewis, N.V.K. Pillarsetty, J.A. Konner, T. Reiner, Leveraging PET to image folate receptor α therapy of an antibody-drug conjugate, EJNMMI Res. 8 (2018) 87, https://doi.org/10.1186/s13550-018-0437-x.

[25] G.S. Heo, L. Detering, H.P. Luehmann, T. Primeau, Y.-S. Lee, R. Laforest, S. Li, J. Stec, K.-H. Lim, A.C. Lockhart, Y. Liu, Folate Receptor α-Targeted 89Zr-M9346A Immuno-PET for Image-Guided Intervention with Mirvetuximab Soravtansine in Triple-Negative Breast Cancer, Mol. Pharm. 16 (2019) 3996–4006, https://doi.org/10.1021/acs.molpharmaceut.9b00653.

[26] L. Xing, Y. Xu, K. Sun, H. Wang, F. Zhang, Z. Zhou, J. Zhang, F. Zhang, B. Caliskan, Z. Qiu, M. Wang, Identification of a peptide for folate receptor alpha by phage display and its tumor targeting activity in ovary cancer xenograft, Sci. Rep. 8 (2018) 1–13, https://doi.org/10.1038/s41598-018-26683-z.

[27] G. Sgouros, L. Bodei, M.R. McDevitt, J.R. Nedrow, Radiopharmaceutical therapy in cancer: clinical advances and challenges, Nat. Rev. Drug Discov. 19 (2020) 589–608, https://doi.org/10.1038/s41573-020-0073-9.

[28] J.R. Whetstine, R.M. Flatley, L.H. Matherly, The human reduced folate carrier gene is ubiquitously and differentially expressed in normal human tissues: identification of seven non-coding exons and characterization of a novel promoter, Biochem. J. 367 (2002) 629–640, https://doi.org/10.1042/bj20020512.

[29] H. Yuasa, K. Inoue, Y. Hayashi, Molecular and Functional Characteristics of Proton-Coupled Folate Transporter, J. Pharm. Sci. 98 (2009) 1608–1616, https://doi.org/10.1002/jps.21515.

[30] L.H. Matherly, Z. Hou, Y. Deng, Human reduced folate carrier: translation of basic biology to cancer etiology and therapy, Cancer Metastasis Rev. 26 (2007) 111–128, https://doi.org/10.1007/s10555-007-9046-2.

[31] S.K. Desmoulin, L. Wang, E. Hales, L. Polin, K. White, J. Kushner, M. Stout, Z. Hou, C. Cherian, A. Gangjee, L.H. Matherly, Therapeutic Targeting of a Novel 6-Substituted Pyrrolo [2,3-d]pyrimidine Thienoyl Antifolate to Human Solid Tumors Based on Selective Uptake by the Proton-Coupled Folate Transporter, Mol. Pharmacol. 80 (2011) 1096–1107, https://doi.org/10.1124/mol.111.073833.

[32] J. Kuten, I. Fahoum, Z. Savin, O. Shamni, G. Gitstein, D. Hershkovitz, N.J. Mabjeesh, O. Yossepowitch, E. Mishani, E. Even-Sapir, Head-to-Head Comparison of 68Ga-PSMA-11 with 18F-PSMA-1007 PET/CT in Staging Prostate Cancer Using Histopathology and Immunohistochemical Analysis as a Reference Standard, J. Nucl. Med. 61 (2020) 527–532, https://doi.org/10.2967/jnumed.119.234187.

[33] K.G. Rothberg, Y.S. Ying, J.F. Kolhouse, B.A. Kamen, R.G. Anderson, The glycophospholipid-linked folate receptor internalizes folate without entering the clathrin-coated pit endocytic pathway, J. Cell Biol. 110 (1990) 637–649, https://doi.org/10.1083/jcb.110.3.637.

[34] J.F. Ross, P.K. Chaudhuri, M. Ratnam, Differential regulation of folate receptor isoforms in normal and malignant tissues in vivo and in established cell lines, Physiologic and clinical implications, Cancer. 73 (1994) 2432–2443, https://doi.org/10.1002/1097-0142(19940501)73:9<2432::AID-CNCR2820730929>3.0.CO;2-S.
[35] J. Holm, S.I. Hansen, M. Høier-Madsen, L. Bostad, A high-affinity folate binding protein in proximal tubule cells of human kidney, Kidney Int. 41 (1992) 50–55, https://doi.org/10.1038/ki.1992.7.
[36] J. Holm, S.I. Hansen, M. Høier-Madsen, L. Bostad, High-affinity folate binding in human choroid plexus. Characterization of radioligand binding, immunoreactivity, molecular heterogeneity and hydrophobic domain of the binding protein, Biochem. J. 280 (1991) 267–271. 10.1042/bj2800267.
[37] J. Holm, S.I. Hansen, M. HØIer-Madsen, C.W. Nichols, Characterization of a folate receptor in parotid gland and a folate binding protein in saliva from humans: Epitope relatedness to human milk folate binding protein, APMIS. 108 (2000) 517–524, https://doi.org/10.1034/j.1600-0463.2000.01087-8517.x.
[38] M. Ratnam, H. Marquardt, J.L. Duhring, J.H. Freisheim, Homologous membrane folate binding proteins in human placenta: cloning and sequence of a cDNA, Biochemistry. 28 (1989) 8249–8254, https://doi.org/10.1021/bi00446a042.
[39] J. Holm, S.I. Hansen, C.W. Nichols, M. Høier-Madsen, P.E. Helkjær, Characterization of the folate receptor in human molar placenta, Biosci. Rep. 16 (1996) 379–389, https://doi.org/10.1007/BF01207263.
[40] W. Xia, A.R. Hilgenbrink, E.L. Matteson, M.B. Lockwood, J.-X. Cheng, P.S. Low, A functional folate receptor is induced during macrophage activation and can be used to target drugs to activated macrophages, Blood. 113 (2009) 438–446, https://doi.org/10.1182/blood-2008-04-150789.
[41] Y. Ren, J. Tang, M.Y. Mok, A.W.K. Chan, A. Wu, C.S. Lau, Increased apoptotic neutrophils and macrophages and impaired macrophage phagocytic clearance of apoptotic neutrophils in systemic lupus erythematosus, Arthritis Rheum. 48 (2003) 2888–2897, https://doi.org/10.1002/art.11237.
[42] Y.V. Bobryshev, Monocyte recruitment and foam cell formation in atherosclerosis, Micron. 37 (2006) 208–222, https://doi.org/10.1016/j.micron.2005.10.007.
[43] F. Shen, M. Wu, J.F. Ross, D. Miller, M. Ratnam, Folate Receptor Type.gamma. Is Primarily a Secretory Protein Due to Lack of an Efficient Signal for Glycosylphosphatidylinositol Modification: Protein Characterization and Cell Type Specificity, Biochemistry. 34 (1995) 5660–5665, https://doi.org/10.1021/bi00016a042.
[44] E. Bianchi, B. Doe, D. Goulding, G.J. Wright, Juno is the egg Izumo receptor and is essential for mammalian fertilization, Nature. 508 (2014) 483–487, https://doi.org/10.1038/nature13203.
[45] C. Chen, J. Ke, X.E. Zhou, W. Yi, J.S. Brunzelle, J. Li, E.-L. Yong, H.E. Xu, K. Melcher, Structural basis for molecular recognition of folic acid by folate receptors, Nature. 500 (2013) 486–489, https://doi.org/10.1038/nature12327.
[46] K.N. Bell, G.P. Oakley Jr., Update on prevention of folic acid-preventable spina bifida and anencephaly, Birt, Defects Res. A. Clin. Mol. Teratol. 85 (2009) 102–107, https://doi.org/10.1002/bdra.20504.
[47] L.B. Bailey, R.J. Berry, Folic acid supplementation and the occurrence of congenital heart defects, orofacial clefts, multiple births, and miscarriage, Am. J. Clin. Nutr. 81 (2005) 1213S-1217S. 10.1093/ajcn/81.5.1213.
[48] T.D. Nilaweera, M. Saeed, A. Kohen, Targeting the de Novo Biosynthesis of Thymidylate for the Development of a PET Probe for Pancreatic Cancer Imaging, Biochemistry. 54 (2015) 1287–1293, https://doi.org/10.1021/bi501481n.
[49] W.F. Jiemy, P. Heeringa, J.A.A.M. Kamps, C.J. van der Laken, R.H.J.A. Slart, E. Brouwer, Positron emission tomography (PET) and single photon emission computed tomography (SPECT) imaging of macrophages in large vessel vasculitis: Current status and future prospects, Autoimmun. Rev. 17 (2018) 715–726, https://doi.org/10.1016/j.autrev.2018.02.006.
[50] S.L. Pimlott, A. Sutherland, Molecular tracers for the PET and SPECT imaging of disease, Chem. Soc. Rev. 40 (2010) 149–162, https://doi.org/10.1039/B922628C.
[51] M.R. Stacy, M.W. Maxfield, A.J. Sinusas, Targeted Molecular Imaging of Angiogenesis in PET and SPECT: A Review, Yale J. Biol. Med. 85 (2012) 75–86.
[52] X. Wang, H. Feng, S. Zhao, J. Xu, X. Wu, J. Cui, Y. Zhang, Y. Qin, Z. Liu, T. Gao, Y. Gao, W. Zeng, SPECT and PET radiopharmaceuticals for molecular imaging of apoptosis: from bench to clinic, Oncotarget. 8 (2017) 20476–20495. 10.18632/oncotarget.14730.
[53] J.P. Holland, M.J. Williamson, J.S. Lewis, Unconventional Nuclides for Radiopharmaceuticals, Mol. Imaging. 9 (2010) 1–20, https://doi.org/10.2310/7290.2010.00008.
[54] E.W. Price, C. Orvig, Matching chelators to radiometals for radiopharmaceuticals, Chem. Soc. Rev. 43 (2013) 260–290, https://doi.org/10.1039/C3CS60304K.
[55] H. Kasban, M. El-bendary, D. Salama, A Comparative Study of Medical Imaging Techniques, Int. J. Inf. Sci. Intell. Syst. 4 (2015) 37–58.
[56] A. Rahmim, H. Zaidi, PET versus SPECT: strengths, limitations and challenges, Nucl. Med. Commun. 29 (2008) 193–207, https://doi.org/10.1097/MNM.0b013e3282f3a515.
[57] K. Lameka, M.D. Farwell, M. Ichise, Chapter 11 – Positron Emission Tomography, in: J.C. Masdeu, R.G. González (Eds.), Handb. Clin. Neurol., Elsevier, 2016: pp. 209–227. 10.1016/B978-0-444-53485-9.00011-8.
[58] M. Moghbel, A. Newberg, A. Alavi, Chapter 12 – Positron emission tomography: ligand imaging, in: J.C. Masdeu, R.G. González (Eds.), Handb. Clin. Neurol., Elsevier, 2016: pp. 229–240. 10.1016/B978-0-444-53485-9.00012-X.
[59] T.I. Kostelnik, C. Orvig, Radioactive Main Group and Rare Earth Metals for Imaging and Therapy, Chem. Rev. 119 (2019) 902–956, https://doi.org/10.1021/acs.chemrev.8b00294.
[60] B.F. Hutton, K. Erlandsson, K. Thielemans, Advances in clinical molecular imaging instrumentation, Clin. Transl. Imaging. 6 (2018) 31–45, https://doi.org/10.1007/s40336-018-0264-0.
[61] T. Jones, D.W. Townsend, History and future technical innovation in positron emission tomography, J. Med. Imaging. 4 (2017), https://doi.org/10.1117/1.JMI.4.1.011013 011013.
[62] D. van der Born, A. Pees, A.J. Poot, R.V.A. Orru, A.D. Windhorst, D.J. Vugts, Fluorine-18 labelled building blocks for PET tracer synthesis, Chem. Soc. Rev. 46 (2017) 4709–4773, https://doi.org/10.1039/C6CS00492J.
[63] H.S. Krishnan, L. Ma, N. Vasdev, S.H. Liang, 18F-Labeling of Sensitive Biomolecules for Positron Emission Tomography, Chem. – Eur. J. 23 (2017) 15553–15577, https://doi.org/10.1002/chem.201701581.
[64] R. Schirrmacher, B. Wängler, J. Bailey, V. Bernard-Gauthier, E. Schirrmacher, C. Wängler, Small Prosthetic Groups in 18F-Radiochemistry: Useful Auxiliaries for the Design of 18F-PET Tracers, Semin. Nucl. Med. 47 (2017) 474–492, https://doi.org/10.1053/j.semnuclmed.2017.07.001.
[65] R. Bejot, V. Gouverneur, 18F-Radionuclide Chemistry, in: Fluor. Pharm. Med. Chem., IMPERIAL COLLEGE PRESS, 2011: pp. 335–382. 10.1142/9781848166363_0010.
[66] C. Fersing, A. Bouhlel, C. Cantelli, P. Garrigue, V. Lisowski, B. Guillet, A Comprehensive Review of Non-Covalent Radiofluorination Approaches Using Aluminum [18F]fluoride: Will [18F]AlF Replace 68Ga for Metal Chelate Labeling?, Molecules 24 (2019) 2866, https://doi.org/10.3390/molecules24162866.
[67] W.J. McBride, R.M. Sharkey, H. Karacay, C.A. D'Souza, E.A. Rossi, P. Laverman, C.-H. Chang, O.C. Boerman, D.M. Goldenberg, A Novel Method of 18F Radiolabeling for PET, J. Nucl. Med. 50 (2009) 991–998, https://doi.org/10.2967/jnumed.108.060418.
[68] N. Viola-Villegas, A. Vortherms, R.P. Doyle, Targeting Gallium to Cancer Cells through the Folate Receptor, Drug Target Insights. 3 (2008) 13–25, https://doi.org/10.4137/DTI.S651.
[69] I. Aljammaz, B. Al-Otaibi, N. Al-Hokbany, S. Amer, S. Okarvi, Development and pre-clinical evaluation of new 68Ga-NOTA-folate conjugates for PET imaging of folate receptor-positive tumors, Anticancer Res. 34 (2014) 6547–6556.
[70] A. Jain, A. Mathur, U. Pandey, J. Bhatt, A. Mukherjee, R. Ram, H.D. Sarma, A. Dash, Synthesis and evaluation of a 68Ga labeled folic acid derivative for targeting folate receptors, Appl. Radiat. Isot. 116 (2016) 77–84, https://doi.org/10.1016/j.apradiso.2016.07.024.
[71] S. Isal, J. Pierson, L. Imbert, A. Clement, C. Collet, S. Pinel, N. Veran, A. Reinhard, S. Poussier, G. Gauchotte, S. Frezier, G. Karcher, P.-Y. Marie, F. Maskali, PET imaging of 68Ga-NODAGA-RGD, as compared with 18F-fluorodeoxyglucose, in experimental rodent models of engrafted glioblastoma, EJNMMI Res. 8 (2018) 51, https://doi.org/10.1186/s13550-018-0405-5.
[72] P.S. Choi, J.Y. Lee, J.H. Park, S.W. Kim, Synthesis and evaluation of 68Ga-HBED-CC-EDBE-folate for positron-emission tomography imaging of overexpressed folate receptors on CT26 tumor cells, J. Label. Compd. Radiopharm. 61 (2018) 4–10, https://doi.org/10.1002/jlcr.3563.
[73] Z. Talip, C. Favaretto, S. Geistlich, N.P. van der Meulen, A Step-by-Step Guide for the Novel Radiometal Production for Medical Applications: Case Studies with 68Ga, 44Sc, 177Lu and 161Tb, Mol. Basel Switz. 25 (2020) 966, https://doi.org/10.3390/molecules25040966.
[74] C.J. Anderson, R. Ferdani, Copper-64 Radiopharmaceuticals for PET Imaging of Cancer: Advances in Preclinical and Clinical Research, Cancer Biother. Radiopharm. 24 (2009) 379–393, https://doi.org/10.1089/cbr.2009.0674.
[75] B.M. Zeglis, J.L. Houghton, M.J. Evans, N. Viola-Villegas, J.S. Lewis, Underscoring the Influence of Inorganic Chemistry on Nuclear Imaging with Radiometals, Inorg. Chem. 53 (2014) 1880–1899, https://doi.org/10.1021/ic401607z.
[76] C.L. Ferreira, S. Lapi, J. Steele, D.E. Green, T.J. Ruth, M.J. Adam, C. Orvig, 55Cobalt complexes with pendant carbohydrates as potential PET imaging agents, Appl. Radiat. Isot. 65 (2007) 1303–1308, https://doi.org/10.1016/j.apradiso.2007.06.003.
[77] O. Morris, M. Fairclough, J. Grigg, C. Prenant, A. McMahon, A review of approaches to 18F radiolabelling affinity peptides and proteins, J. Label. Compd. Radiopharm. 62 (2019) 4–23, https://doi.org/10.1002/jlcr.3634.
[78] C. Müller, K.A. Domnanich, C.A. Umbricht, N.P. van der Meulen, Scandium and terbium radionuclides for radiotheranostics: current state of development towards clinical application, Br. J. Radiol. 91 (2018) 20180074, https://doi.org/10.1259/bjr.20180074.
[79] T. Mastren, B.V. Marquez, D.E. Sultan, E. Bollinger, P. Eisenbeis, T. Voller, S.E. Lapi, Cyclotron Production of High-Specific Activity 55Co and In Vivo Evaluation of the Stability of 55Co Metal-Chelate-Peptide Complexes, Mol. Imaging. 14 (2015) 526–532, https://doi.org/10.2310/7290.2015.00025.
[80] F. Rösch, Past, present and future of 68Ge/68Ga generators, Ga-68 Spec, Issue. 76 (2013) 24–30, https://doi.org/10.1016/j.apradiso.2012.10.012.
[81] C. Müller, K. Zhernosekov, U. Köster, K. Johnston, H. Dorrer, A. Hohn, N.T. van der Walt, A. Türler, R. Schibli, A Unique Matched Quadruplet of Terbium Radioisotopes for PET and SPECT and for α- and β−-Radionuclide Therapy: An In Vivo Proof-of-Concept Study with a New Receptor-Targeted Folate

Derivative, J. Nucl. Med. 53 (2012) 1951–1959, https://doi.org/10.2967/jnumed.112.107540.
[82] A. Cuocolo, S. Pappatà, E. Zampella, R. Assante, Chapter Three – Advances in SPECT Methodology, in: M. Politis (Ed.), Int. Rev. Neurobiol., Academic Press, 2018: pp. 77–96. 10.1016/bs.irn.2018.08.001.
[83] S. Melki, M.B. Chawki, P.-Y. Marie, L. Imbert, A. Verger, Augmented planar bone scintigraphy obtained from a whole-body SPECT recording of less than 20 min with a high-sensitivity 360° CZT camera, Eur. J. Nucl. Med. Mol. Imaging. 47 (2020) 1329–1331, https://doi.org/10.1007/s00259-019-04525-y.
[84] O. Israel, O. Pellet, L. Biassoni, D. De Palma, E. Estrada-Lobato, G. Gnanasegaran, T. Kuwert, C. la Fougère, G. Mariani, S. Massalha, D. Paez, F. Giammarile, Two decades of SPECT/CT – the coming of age of a technology: An updated review of literature evidence, Eur. J. Nucl. Med. Mol. Imaging. 46 (2019) 1990–2012, https://doi.org/10.1007/s00259-019-04404-6.
[85] D. Papagiannopoulou, Technetium-99m radiochemistry for pharmaceutical applications, J. Label. Compd. Radiopharm. 60 (2017) 502–520, https://doi.org/10.1002/jlcr.3531.
[86] C. Müller, P.A. Schubiger, R. Schibli, Isostructural folate conjugates radiolabeled with the matched pair 99mTc/188Re: a potential strategy for diagnosis and therapy of folate receptor-positive tumors, Nucl. Med. Biol. 34 (2007) 595–601, https://doi.org/10.1016/j.nucmedbio.2007.05.011.
[87] T. Hernández-Jiménez, G. Ferro-Flores, B. Ocampo-García, E. Morales-Avila, A. Escudero-Castellanos, E. Azorín-Vega, C. Santos-Cuevas, M. Luna-Gutiérrez, N. Jiménez-Mancilla, L.A. Medina, F. de M. Ramirez, M. Pedraza-López, 177 Lu-DOTA-HYNIC-Lys(Nal)-Urea-Glu: synthesis and assessment of the ability to target the prostate specific membrane antigen, J. Radioanal. Nucl. Chem. 318 (2018) 2059–2066, https://doi.org/10.1007/s10967-018-6239-9.
[88] B. Mitran, S.S. Rinne, M.W. Konijnenberg, T. Maina, B.A. Nock, M. Altai, A. Vorobyeva, M. Larhed, V. Tolmachev, M. de Jong, U. Rosenström, A. Orlova, Trastuzumab cotreatment improves survival of mice with PC-3 prostate cancer xenografts treated with the GRPR antagonist 177Lu-DOTAGA-PEG2-RM26, Int. J. Cancer. 145 (2019) 3347–3358, https://doi.org/10.1002/ijc.32401.
[89] C. Müller, N.P. van der Meulen, M. Benešová, R. Schibli, Therapeutic Radiometals Beyond 177Lu and 90Y: Production and Application of Promising α-Particle, β−-Particle, and Auger Electron Emitters, J. Nucl. Med. 58 (2017) 91S-96S. 10.2967/jnumed.116.186825.
[90] C. Müller, C. Vermeulen, U. Köster, K. Johnston, A. Türler, R. Schibli, N.P. van der Meulen, Alpha-PET with terbium-149: evidence and perspectives for radiotheragnostics, EJNMMI Radiopharm. Chem. 1 (2017) 1–5, https://doi.org/10.1186/s41181-016-0008-2.
[91] N. Lepareur, F. Lacœuille, C. Bouvry, F. Hindré, E. Garcion, M. Chérel, N. Noiret, E. Garin, F.F.R. Knapp, Rhenium-188 Labeled Radiopharmaceuticals: Current Clinical Applications in Oncology and Promising Perspectives, Front. Med. 6 (2019) 132, https://doi.org/10.3389/fmed.2019.00132.
[92] S. Sharma, PET Radiopharmaceuticals for Personalized Medicine, Curr. Drug Targets. 17 (2016) 1894–1907, https://doi.org/10.2174/1389450117666160720091233.
[93] A. Yordanova, E. Eppard, S. Kürpig, R.A. Bundschuh, S. Schönberger, M. Gonzalez-Carmona, G. Feldmann, H. Ahmadzadehfar, M. Essler, Theranostics in nuclear medicine practice, OncoTargets Ther. 10 (2017) 4821–4828, https://doi.org/10.2147/OTT.S140671.
[94] L.C. Pike, C.M. Thomas, T. Guerrero-Urbano, A. Michaelidou, T. Greener, E. Miles, D. Eaton, S.F. Barrington, Guidance on the use of PET for treatment planning in radiotherapy clinical trials, Br. J. Radiol. 92 (2019) 0190180, https://doi.org/10.1259/bjr.20190180.
[95] A. Dash, S. Chakraborty, M.R.A. Pillai, F.F. (Russ) Knapp, Peptide Receptor Radionuclide Therapy: An Overview, Cancer Biother. Radiopharm. 30 (2015) 47–71, https://doi.org/10.1089/cbr.2014.1741.
[96] S. Banerjee, M.R.A. Pillai, F.F. (Russ) Knapp, Lutetium-177 Therapeutic Radiopharmaceuticals: Linking Chemistry, Radiochemistry, and Practical Applications, Chem. Rev. 115 (2015) 2934–2974, https://doi.org/10.1021/cr500171e.
[97] J. Notni, H.-J. Wester, Re-thinking the role of radiometal isotopes: Towards a future concept for theranostic radiopharmaceuticals, J. Label. Compd. Radiopharm. 61 (2018) 141–153, https://doi.org/10.1002/jlcr.3582.
[98] C. Müller, M. Bunka, S. Haller, U. Köster, V. Groehn, P. Bernhardt, N. van der Meulen, A. Türler, R. Schibli, Promising Prospects for 44Sc-/47Sc-Based Theragnostics: Application of 47Sc for Radionuclide Tumor Therapy in Mice, J. Nucl. Med. 55 (2014) 1658–1664, https://doi.org/10.2967/jnumed.114.141614.
[99] J.M. Kelly, S. Ponnala, A. Amor-Coarasa, N.A. Zia, A. Nikolopoulou, C. Williams Jr., D.J. Schlyer, S.G. DiMagno, P.S. Donnelly, J.W. Babich, Preclinical evaluation of a high affinity sarcophagine-containing PSMA ligand for 64Cu/67Cu-based theranostics in prostate cancer, Mol. Pharm. 17 (2020) 1954–1962, https://doi.org/10.1021/acs.molpharmaceut.0c00060.
[100] S. Wang, R.J. Lee, C.J. Mathias, M.A. Green, P.S. Low, Synthesis, Purification, and Tumor Cell Uptake of 67Ga-Deferoxamine−Folate, a Potential Radiopharmaceutical for Tumor Imaging, Bioconjug. Chem. 7 (1996) 56–62, https://doi.org/10.1021/bc9500709.
[101] T.L. Mindt, C. Müller, F. Stuker, J.-F. Salazar, A. Hohn, T. Mueggler, M. Rudin, R. Schibli, A "Click Chemistry" Approach to the Efficient Synthesis of Multiple Imaging Probes Derived from a Single Precursor, Bioconjug. Chem. 20 (2009) 1940–1949, https://doi.org/10.1021/bc900276b.
[102] C. Müller, A. Hohn, P.A. Schubiger, R. Schibli, Preclinical evaluation of novel organometallic 99m Tc-folate and 99m Tc-pteroate radiotracers for folate receptor-positive tumour targeting, Eur. J. Nucl. Med. Mol. Imaging. 33 (2006) 1007–1016, https://doi.org/10.1007/s00259-006-0111-9.
[103] C.P. Leamon, R.B. Deprince, R.W. Hendren, Folate-mediated Drug Delivery: Effect of Alternative Conjugation Chemistry, J. Drug Target. 7 (1999) 157–169, https://doi.org/10.3109/10611869909085499.
[104] P. Wedeking, R. Wager, T. Arunachalam, K. Ramalingam, K. Linder, R. Ranganathan, A. Nunn, N. Raju, M. Tweedle, Metal Complexes Derivatized with Folate for Use in Diagnostic and Therapeutic Applications, WO9959640 (A2), 1999. https://worldwide.espacenet.com/publicationDetails/biblio?FT=D&date=19991125&DB=EPODOC&locale=en_EP&CC=WO&NR=9959640A2&KC=A2&ND=4 (accessed May 24, 2020).
[105] S.D. Boss, T. Betzel, C. Mueller, C.R. Fischer, S. Haller, J. Reber, V. Groehn, R. Schibli, S.M. Ametamey, Comparative Studies of Three Pairs of alpha- and gamma-Conjugated Folic Acid Derivatives Labeled with Fluorine-18, Bioconjug. Chem. 27 (2016) 74–86, https://doi.org/10.1021/acs.bioconjchem.5b00644.
[106] C. Müller, P.A. Schubiger, R. Schibli, Synthesis and in Vitro/in Vivo Evaluation of Novel 99mTc(CO)3-Folates, Bioconjug. Chem. 17 (2006) 797–806, https://doi.org/10.1021/bc050323q.
[107] B. Kühle, C. Müller, T.L. Ross, A. Novel, 68Ga-Labeled Pteroic Acid-Based PET Tracer for Tumor Imaging via the Folate Receptor, in: Theranostics Gallium-68 Radionucl, Springer, Berlin, Heidelberg, 2013, pp. 257–267, https://doi.org/10.1007/978-3-642-27994-2_13.
[108] D.J. O'Shannessy, E.B. Somers, J. Maltzman, R. Smale, Y.-S. Fu, Folate receptor alpha (FRA) expression in breast cancer: identification of a new molecular subtype and association with triple negative disease, SpringerPlus. 1 (2012) 22, https://doi.org/10.1186/2193-1801-1-22.
[109] D.C. Christoph, B.R. Asuncion, B. Hassan, C. Tran, J.D. Maltzman, D.J. O'Shannessy, M.W. Wynes, T.C. Gauler, J. Wohlschlaeger, M. Hoiczyk, M. Schuler, W.E. Eberhardt, F.R. Hirsch, Significance of Folate Receptor Alpha and Thymidylate Synthase Protein Expression in Patients with Non–Small-Cell Lung Cancer Treated with Pemetrexed, J. Thorac. Oncol. 8 (2013) 19–30, https://doi.org/10.1097/JTO.0b013e31827628ff.
[110] R.J. Lutz, Targeting the folate receptor for the treatment of ovarian cancer, Transl. Cancer Res. 4 (2015). 10.21037/3838.
[111] C.-Y. Ke, C.J. Mathias, M.A. Green, Folate-receptor-targeted radionuclide imaging agents, Folate Recept.-Target, Drugs Cancer Inflamm. Dis. 56 (2004) 1143–1160, https://doi.org/10.1016/j.addr.2004.01.004.
[112] P.S. Low, W.A. Henne, D.D. Doorneweerd, Discovery and Development of Folic-Acid-Based Receptor Targeting for Imaging and Therapy of Cancer and Inflammatory Diseases, Acc. Chem. Res. 41 (2008) 120–129, https://doi.org/10.1021/ar7000815.
[113] E.I. Sega, P.S. Low, Tumor detection using folate receptor-targeted imaging agents, Cancer Metastasis Rev. 27 (2008) 655, https://doi.org/10.1007/s10555-008-9155-6.
[114] C. Müller, Folate-Based Radiotracers for PET Imaging—Update and Perspectives, Molecules. 18 (2013) 5005–5031, https://doi.org/10.3390/molecules18055005.
[115] C. Müller, R. Schibli, Folate Receptor-Targeted Radionuclide Imaging Agents, in: A.L. Jackman, C.P. Leamon (Eds.), Target. Drug Strateg. Cancer Inflamm., Springer US, Boston, MA, 2011: pp. 65–92. 10.1007/978-1-4419-8417-3_4.
[116] H. Schieferstein, T.L. Ross, 18F-labeled folic acid derivatives for imaging of the folate receptor via positron emission tomography, J. Label. Compd. Radiopharm. 56 (2013) 432–440, https://doi.org/10.1002/jlcr.3104.
[117] C. Müller, R. Schibli, Folic Acid Conjugates for Nuclear Imaging of Folate Receptor-Positive Cancer, J. Nucl. Med. 52 (2011) 1–4, https://doi.org/10.2967/jnumed.110.076018.
[118] C. Muller, Folate Based Radiopharmaceuticals for Imaging and Therapy of Cancer and Inflammation, Curr. Pharm. Des. 18 (2012) 1058–1083, https://doi.org/10.2174/138161212799315777.
[119] S.D. Boss, S.M. Ametamey, Development of Folate Receptor−Targeted PET Radiopharmaceuticals for Tumor Imaging—A Bench-to-Bedside Journey, Cancers. 12 (2020) 1508, https://doi.org/10.3390/cancers12061508.
[120] C.J. Mathias, S. Wang, R.J. Lee, D.J. Waters, P.S. Low, M.A. Green, Tumor-Selective Radiopharmaceutical Targeting via Receptor-Mediated Endocytosis of Gallium-67-Deferoxamine-Folate, J. Nucl. Med. 37 (1996) 1003–1008.
[121] C. Müller, I.R. Vlahov, H.K.R. Santhapuram, C.P. Leamon, R. Schibli, Tumor targeting using 67Ga-DOTA-Bz-folate — investigations of methods to improve the tissue distribution of radiofolates, Nucl. Med. Biol. 38 (2011) 715–723, https://doi.org/10.1016/j.nucmedbio.2010.12.013.
[122] S. Wang, J. Luo, D.A. Lantrip, D.J. Waters, C.J. Mathias, M.A. Green, P.L. Fuchs, P. S. Low, Design and Synthesis of [111In]DTPA−Folate for Use as a Tumor-Targeted Radiopharmaceutical, Bioconjug. Chem. 8 (1997) 673–679, https://doi.org/10.1021/bc9701297.
[123] C.J. Mathias, S. Wang, D.J. Waters, J.J. Turek, P.S. Low, M.A. Green, Indium-111-DTPA-Folate as a Potential Folate Receptor-Targeted Radiopharmaceutical, J. Nucl. Med. 39 (1998) 1579–1585.
[124] C. Müller, R. Schibli, E.P. Krenning, M. de Jong, Pemetrexed Improves Tumor Selectivity of 111In-DTPA-Folate in Mice with Folate Receptor-Positive Ovarian Cancer, J. Nucl. Med. 49 (2008) 623–629, https://doi.org/10.2967/jnumed.107.047704.
[125] C. Müller, T.L. Mindt, M. de Jong, R. Schibli, Evaluation of a novel radiofolate in tumour-bearing mice: promising prospects for folate-based radionuclide

therapy, Eur. J. Nucl. Med. Mol. Imaging. 36 (2009) 938–946, https://doi.org/10.1007/s00259-008-1058-9.
[126] W. Guo, G.H. Hinkle, R.J. Lee, 99mTc-HYNIC-folate: a novel receptor-based targeted radiopharmaceutical for tumor imaging, J. Nucl. Med. 40 (1999) 1563–1569.
[127] J. Lu, Y. Pang, F. Xie, H. Guo, Y. Li, Z. Yang, X. Wang, Synthesis and in vitro/in vivo evaluation of 99mTc-labeled folate conjugates for folate receptor imaging, Nucl. Med. Biol. 38 (2011) 557–565, https://doi.org/10.1016/j.nucmedbio.2010.11.007.
[128] F. Xie, C. Zhang, Q. Yu, Y. Pang, Y. Chen, W. Yang, J. Xue, Y. Liu, J. Lu, Novel 99mTc radiolabeled folate complexes with PEG linkers for FR-positive tumor imaging: synthesis and biological evaluation, RSC Adv. 4 (2014) 32197–32206, https://doi.org/10.1039/C4RA03564J.
[129] Z. Guo, P. Zhang, M. Song, X. Wu, C. Liu, Z. Zhao, J. Lu, X. Zhang, Synthesis and preliminary evaluation of novel 99mTc-labeled folate derivative via click reaction for SPECT imaging, Appl. Radiat. Isot. 91 (2014) 24–30, forrer.
[130] H. Guo, F. Xie, M. Zhu, Y. Li, Z. Yang, X. Wang, J. Lu, The synthesis of pteroyl-lys conjugates and its application as Technetium-99m labeled radiotracer for folate receptor-positive tumor targeting, Bioorg. Med. Chem. Lett. 21 (2011) 2025–2029, https://doi.org/10.1016/j.bmcl.2011.02.014.
[131] M.H. Kim, W.H. Kim, C.G. Kim, D.-W. Kim, Synthesis and Evaluation of 99mTc-Labeled Folate-Tripeptide Conjugate as a Folate Receptor-Targeted Imaging Agent in a Tumor-Bearing Mouse Model, Nucl. Med. Mol. Imaging. 49 (2015) 200–207, https://doi.org/10.1007/s13139-015-0336-2.
[132] S. ligan, D.J. Yang, T. Higuchi, F. Zareneyrizi, H. Bayhan, D. Yu, E.E. Kim, D.A. Podoloff, 99mTc-Ethylenedicysteine-Folate: A New Tumor Imaging Agent. Synthesis, Labeling and Evaluation in Animals, Cancer Biother. Radiopharm. 13 (1998) 427–435. 10.1089/cbr.1998.13.427.
[133] P. Panwar, V. Shrivastava, V. Tandon, P. Mishra, K. Chuttani, R.K. Sharma, R. Chandra, A.K. Mishra, 99mTc-tetraethylenepentamine-folate a new 99mTc based folate derivative for the detection of folate receptor positive tumors: Synthesis and biological evaluation, Cancer Biol. Ther. 3 (2004) 995–1001, https://doi.org/10.4161/cbt.3.10.1138.
[134] G. Mishra, P.P. Hazari, N. Kumar, A.K. Mishra, In vitro and in vivo evaluation of 99mTc-DO3A-EA-Folate for receptor-mediated targeting of folate positive tumors, J. Drug Target. 19 (2011) 761–769, https://doi.org/10.3109/1061186X.2011.561857.
[135] C. Müller, C. Dumas, U. Hoffmann, P.A. Schubiger, R. Schibli, Organometallic 99mTc-technetium(I)- and Re-rhenium(I)-folate derivatives for potential use in nuclear medicine, Second Int, Symp. Bio-Organomet. Chem. – Dedic. Profr. Richard H Fish Occas. His 65th Birthd. 689 (2004) 4712–4721, https://doi.org/10.1016/j.jorganchem.2004.08.045.
[136] C. Müller, P.A. Schubiger, R. Schibli, In vitro and in vivo targeting of different folate receptor-positive cancer cell lines with a novel 99m Tc-radiofolate tracer, Eur. J. Nucl. Med. Mol. Imaging. 33 (2006) 1162–1170, https://doi.org/10.1007/s00259-006-0118-2.
[137] T.L. Mindt, C. Müller, M. Melis, M. de Jong, R. Schibli, "Click-to-Chelate". In Vitro and In Vivo Comparison of a 99mTc(CO)3-Labeled N(τ)-Histidine Folate Derivative with Its Isostructural, Clicked 1,2,3-Triazole Analogue, Bioconjug. Chem. 19 (2008) 1689–1695, https://doi.org/10.1021/bc800183r.
[138] C. Müller, F. Forrer, R. Schibli, E.P. Krenning, M. de Jong, SPECT Study of Folate Receptor-Positive Malignant and Normal Tissues in Mice Using a Novel 99mTc-Radiofolate, J. Nucl. Med. 49 (2008) 310–317, https://doi.org/10.2967/jnumed.107.045856.
[139] C.P. Leamon, M.A. Parker, I.R. Vlahov, L.-C. Xu, J.A. Reddy, M. Vetzel, N. Douglas, Synthesis and Biological Evaluation of EC20: A New Folate-Derived, 99mTc-Based Radiopharmaceutical, Bioconjug. Chem. 13 (2002) 1200–1210, https://doi.org/10.1021/bc0200430.
[140] J.A. Reddy, L.-C. Xu, N. Parker, M. Vetzel, C.P. Leamon, Preclinical Evaluation of 99mTc-EC20 for Imaging Folate Receptor-Positive Tumors, J. Nucl. Med. 45 (2004) 857–866.
[141] B.A. Siegel, F. Dehdashti, D.G. Mutch, D.A. Podoloff, R. Wendt, G.P. Sutton, R. W. Burt, P.R. Ellis, C.J. Mathias, M.A. Green, D.M. Gershenson, Evaluation of 111In-DTPA-Folate as a Receptor-Targeted Diagnostic Agent for Ovarian Cancer: Initial Clinical Results, J. Nucl. Med. 44 (2003) 700–707.
[142] R.E. Fisher, B.A. Siegel, S.L. Edell, N.M. Oyesiku, D.E. Morgenstern, R.A. Messmann, R.J. Amato, Exploratory Study of 99mTc-EC20 Imaging for Identifying Patients with Folate Receptor-Positive Solid Tumors, J. Nucl. Med. 49 (2008) 899–906, https://doi.org/10.2967/jnumed.107.049478.
[143] Y. Yamada, H. Nakatani, H. Yanaihara, M. Omote, Phase I clinical trial of 99mTc-etarfolatide, an imaging agent for folate receptor in healthy Japanese adults, Ann. Nucl. Med. 29 (2015) 792–798, https://doi.org/10.1007/s12149-015-1006-2.
[144] Endocyte, A Single-Center Phase I Clinical Study to Evaluate The Biodistribution and Safety of 99mTC-Etarfolatide (EC20) in Normal Volunteers, clinicaltrials.gov, 2014. https://clinicaltrials.gov/ct2/show/NCT01748864 (accessed August 26, 2021).
[145] Endocyte, CLINICAL STUDY OF A SINGLE-CENTER CLINICAL STUDY TO EVALUATE THE SAFETY AND BIODISTRIBUTION OF TECHNETIUM Tc 99m EC20 IN NORMAL VOLUNTEERS AND OVARIAN CANCER PATIENTS, clinicaltrials.gov, 2012. https://clinicaltrials.gov/ct2/show/NCT01689636 (accessed August 26, 2021).
[146] C.J. Mathias, D. Hubers, P.S. Low, M.A. Green, Synthesis of [99mTc]DTPA-Folate and Its Evaluation as a Folate-Receptor-Targeted Radiopharmaceutical, Bioconjug. Chem. 11 (2000) 253–257, https://doi.org/10.1021/bc9901447.
[147] A. Bettio, M. Honer, C. Müller, M. Brühlmeier, U. Müller, R. Schibli, V. Groehn, A.P. Schubiger, S.M. Ametamey, Synthesis and Preclinical Evaluation of a Folic Acid Derivative Labeled with 18F for PET Imaging of Folate Receptor-Positive Tumors, J. Nucl. Med. 47 (2006) 1153–1160.
[148] T.L. Ross, M. Honer, P.Y.H. Lam, T.L. Mindt, V. Groehn, R. Schibli, P.A. Schubiger, S.M. Ametamey, Fluorine-18 Click Radiosynthesis and Preclinical Evaluation of a New 18F-Labeled Folic Acid Derivative, Bioconjug. Chem. 19 (2008) 2462–2470, https://doi.org/10.1021/bc800356r.
[149] C.R. Fischer, C. Mueller, J. Reber, A. Mueller, S.D. Kraemer, S.M. Ametamey, R. Schibli, [F-18]Fluoro-Deoxy-Glucose Folate: A Novel PET Radiotracer with Improved in Vivo Properties for Folate Receptor Targeting, Bioconjug. Chem. 23 (2012) 805–813, https://doi.org/10.1021/bc200660z.
[150] H. Schieferstein, T. Betzel, C.R. Fischer, T.L. Ross, 18 F-click labeling and preclinical evaluation of a new 18 F-folate for PET imaging, EJNMMI Res. 3 (2013) 68, https://doi.org/10.1186/2191-219X-3-68.
[151] K. Kettenbach, L.M. Reffert, H. Schieferstein, S. Pektor, R. Eckert, M. Miederer, F. Rösch, T.L. Ross, Comparison Study of Two Differently Clicked 18F-Folates—Lipophilicity Plays a Key Role, Pharmaceuticals. 11 (2018) 30, https://doi.org/10.3390/ph11010030.
[152] K. Kettenbach, T.L. Ross, A 18F-labeled dibenzocyclooctyne (DBCO) derivative for copper-free click labeling of biomolecules, MedChemComm. 7 (2016) 654–657, https://doi.org/10.1039/C5MD00508F.
[153] S.D. Boss, C. Müller, K. Siwowska, J.I. Büchel, R.M. Schmid, V. Groehn, R. Schibli, S.M. Ametamey, Reduced 18F-Folate Conjugates as a New Class of PET Tracers for Folate Receptor Imaging, Bioconjug. Chem. 29 (2018) 1119–1130, https://doi.org/10.1021/acs.bioconjchem.7b00775.
[154] T.L. Ross, M. Honer, C. Müller, V. Groehn, R. Schibli, S.M. Ametamey, A New 18F-Labeled Folic Acid Derivative with Improved Properties for the PET Imaging of Folate Receptor-Positive Tumors, J. Nucl. Med. 51 (2010) 1756–1762, https://doi.org/10.2967/jnumed.110.079756.
[155] T. Betzel, C. Müller, V. Groehn, A. Müller, J. Reber, C.R. Fischer, S.D. Krämer, R. Schibli, S.M. Ametamey, Radiosynthesis and Preclinical Evaluation of 3′-Aza-2′-[18F]fluorofolic Acid: A Novel PET Radiotracer for Folate Receptor Targeting, Bioconjug. Chem. 24 (2013) 205–214, https://doi.org/10.1021/bc300483a.
[156] S.D. Boss, C. Mueller, K. Siwowska, R.M. Schmid, V. Groehn, R. Schibli, S.M. Ametamey, Diastereomerically Pure 6R- and 6S–3 '-Aza-2 '-F-18-Fluoro-5-Methyltetrahydrofolates Show Unprecedentedly High Uptake in Folate Receptor-Positive KB Tumors, J. Nucl. Med. 60 (2019) 135–141, https://doi.org/10.2967/jnumed.118.213314.
[157] P. Guzik, H.-Y. Fang, L.M. Deberle, M. Benešová, S. Cohrs, S.D. Boss, S.M. Ametamey, R. Schibli, C. Müller, Identification of a PET Radiotracer for Imaging of the Folate Receptor-α: A Potential Tool to Select Patients for Targeted Tumor Therapy, J. Nucl. Med. Off. Publ. Soc. Nucl. Med. 62 (2021) 1475–1481, https://doi.org/10.2967/jnumed.120.255760.
[158] Q. Chen, X. Meng, P. McQuade, D. Rubins, S.-A. Lin, Z. Zeng, H. Haley, P. Miller, D. González Trotter, P.S. Low, Synthesis and Preclinical Evaluation of Folate-NOTA-Al18F for PET Imaging of Folate-Receptor-Positive Tumors, Mol. Pharm. 13 (2016) 1520–1527, https://doi.org/10.1021/acs.molpharmaceut.5b00989.
[159] Q. Chen, X. Meng, P. McQuade, D. Rubins, S.-A. Lin, Z. Zeng, H. Haley, P. Miller, D. González Trotter, P.S. Low, Folate-PEG-NOTA-Al18F: A New Folate Based Radiotracer for PET Imaging of Folate Receptor-Positive Tumors, Mol. Pharm. 14 (2017) 4353–4361, https://doi.org/10.1021/acs.molpharmaceut.7b00415.
[160] M. Fani, X. Wang, G. Nicolas, C. Medina, I. Raynal, M. Port, H.R. Maecke, Development of new folate-based PET radiotracers: preclinical evaluation of 68 Ga-DOTA-folate conjugates, Eur. J. Nucl. Med. Mol. Imaging. 38 (2011) 108–119, https://doi.org/10.1007/s00259-010-1597-8.
[161] M. Fani, M.-L. Tamma, G.P. Nicolas, E. Lasri, C. Medina, I. Raynal, M. Port, W.A. Weber, H.R. Maecke, In Vivo Imaging of Folate Receptor Positive Tumor Xenografts Using Novel 68Ga-NODAGA-Folate Conjugates, Mol. Pharm. 9 (2012) 1136–1145, https://doi.org/10.1021/mp200418f.
[162] X. Zhang, Q. Yu, Y. He, C. Zhang, H. Zhu, Z. Yang, J. Lu, Synthesis and biological evaluation of 68Ga-labeled Pteroyl-Lys conjugates for folate receptor-targeted tumor imaging, J. Label. Compd. Radiopharm. 59 (2016) 346–353, https://doi.org/10.1002/jlcr.3410.
[163] S. Gnesin, J. Müller, I.A. Burger, A. Meisel, M. Siano, M. Früh, M. Choschzick, C. Müller, R. Schibli, S.M. Ametamey, P.A. Kaufmann, V. Treyer, J.O. Prior, N. Schaefer, Radiation dosimetry of 18F-AzaFol: A first in-human use of a folate receptor PET tracer, EJNMMI Res. 10 (2020) 32, https://doi.org/10.1186/s13550-020-00624-2.
[164] N. Schaefer, Biodistribution, Tumor Detection, and Radiation Dosimentry of [18F]-AZAFOL as POSITRON EMISSION TOMOGRAPHY (PET) Tracer in Folate Receptor Positive Cancer Imaging, clinicaltrials.gov, 2020. https://clinicaltrials.gov/ct2/show/NCT03242993 (accessed August 26, 2021).
[165] C. Müller, P. Guzik, K. Siwowska, S. Cohrs, R.M. Schmid, R. Schibli, Combining Albumin-Binding Properties and Interaction with Pemetrexed to Improve the Tissue Distribution of Radiofolates, Molecules. 23 (2018) 1465, https://doi.org/10.3390/molecules23061465.
[166] C. Müller, M. Brühlmeier, P.A. Schubiger, R. Schibli, Effects of Antifolate Drugs on the Cellular Uptake of Radiofolates In Vitro and In Vivo, J. Nucl. Med. 47 (2006) 2057–2064.
[167] C. Müller, R. Schibli, F. Forrer, E.P. Krenning, M. de Jong, Dose-dependent effects of (anti)folate preinjection on 99mTc-radiofolate uptake in tumors

and kidneys, Nucl. Med. Biol. 34 (2007) 603–608, https://doi.org/10.1016/j.nucmedbio.2007.06.001.
[168] C. Müller, J. Reber, C. Schlup, C.P. Leamon, R. Schibli, In Vitro and in Vivo Evaluation of an Innocuous Drug Cocktail To Improve the Quality of Folic Acid Targeted Nuclear Imaging in Preclinical Research, Mol. Pharm. 10 (2013) 967–974, https://doi.org/10.1021/mp300428p.
[169] J. Reber, S. Haller, C.P. Leamon, C. Müller, 177Lu-EC0800 Combined with the Antifolate Pemetrexed: Preclinical Pilot Study of Folate Receptor Targeted Radionuclide Tumor Therapy, Mol. Cancer Ther. 12 (2013) 2436–2445, https://doi.org/10.1158/1535-7163.MCT-13-0422-T.
[170] C. Müller, R. Schibli, Prospects in Folate Receptor-Targeted Radionuclide Therapy, Front. Oncol. 3 (2013) 249, https://doi.org/10.3389/fonc.2013.00249.
[171] Z. Liu, X. Chen, Simple bioconjugate chemistry serves great clinical advances: albumin as a versatile platform for diagnosis and precision therapy, Chem. Soc. Rev. 45 (2016) 1432–1456, https://doi.org/10.1039/C5CS00158G.
[172] M.S. Dennis, M. Zhang, Y.G. Meng, M. Kadkhodayan, D. Kirchhofer, D. Combs, L.A. Damico, Albumin Binding as a General Strategy for Improving the Pharmacokinetics of Proteins, J. Biol. Chem. 277 (2002) 35035–35043, https://doi.org/10.1074/jbc.M205854200.
[173] C.E. Dumelin, S. Trüssel, F. Buller, E. Trachsel, F. Bootz, Y. Zhang, L. Mannocci, S.C. Beck, M. Drumea-Mirancea, M.W. Seeliger, C. Baltes, T. Müggler, F. Kranz, M. Rudin, S. Melkko, J. Scheuermann, D. Neri, A Portable Albumin Binder from a DNA-Encoded Chemical Library, Angew. Chem. Int. Ed. 47 (2008) 3196–3201, https://doi.org/10.1002/anie.200704936.
[174] C.R. Fischer, V. Groehn, J. Reber, R. Schibli, S.M. Ametamey, C. Müller, Improved PET Imaging of Tumors in Mice Using a Novel 18 F-Folate Conjugate with an Albumin-Binding Entity, Mol. Imaging Biol. 15 (2013) 649–654, https://doi.org/10.1007/s11307-013-0651-x.
[175] C. Müller, E. Fischer, M. Behe, U. Köster, H. Dorrer, J. Reber, S. Haller, S. Cohrs, A. Blanc, J. Grünberg, M. Bunka, K. Zhernosekov, N. van der Meulen, K. Johnston, A. Türler, R. Schibli, Future prospects for SPECT imaging using the radiolanthanide terbium-155 — production and preclinical evaluation in tumor-bearing mice, Nucl. Med. Biol. 41 (2014) e58–e65, https://doi.org/10.1016/j.nucmedbio.2013.11.002.
[176] M. Ocak, A.G. Gillman, J. Bresee, L. Zhang, A.M. Vlad, C. Müller, R. Schibli, W.B. Edwards, C.J. Anderson, H.M. Gach, Folate Receptor-Targeted Multimodality Imaging of Ovarian Cancer in a Novel Syngeneic Mouse Model, Mol. Pharm. 12 (2015) 542–553, https://doi.org/10.1021/mp500628g.
[177] R. Farkas, K. Siwowska, S.M. Ametamey, R. Schibli, N.P. van der Meulen, C. Müller, 64Cu- and 68Ga-Based PET Imaging of Folate Receptor-Positive Tumors: Development and Evaluation of an Albumin-Binding NODAGA–Folate, Mol. Pharm. 13 (2016) 1979–1987, https://doi.org/10.1021/acs.molpharmaceut.6b00143.
[178] L.L. Radford, S. Fernandez, R. Beacham, R. El Sayed, R. Farkas, M. Benešová, C. Müller, S.E. Lapi, New 55Co-labeled Albumin-Binding Folate Derivatives as Potential PET Agents for Folate Receptor Imaging, Pharmaceuticals. 12 (2019) 166, https://doi.org/10.3390/ph12040166.
[179] M. Mirzaii, T. Kakavand, M. Talebi, S. Rajabifar, Electrodeposition iron target for the cyclotron production of 55Co in labeling proteins, J. Radioanal. Nucl. Chem. 292 (2012) 261–267, https://doi.org/10.1007/s10967-011-1399-x.
[180] A. Heppeler, J.P. André, I. Buschmann, X. Wang, J.-C. Reubi, M. Hennig, T.A. Kaden, H.R. Maecke, Metal-Ion-Dependent Biological Properties of a Chelator-Derived Somatostatin Analogue for Tumour Targeting, Chem. – Eur. J. 14 (2008) 3026–3034, https://doi.org/10.1002/chem.200701264.
[181] H. Thisgaard, M.L. Olesen, J.H. Dam, Radiosynthesis of 55Co- and 58mCo-labelled DOTATOC for positron emission tomography imaging and targeted radionuclide therapy, J. Label. Compd. Radiopharm. 54 (2011) 758–762, https://doi.org/10.1002/jlcr.1919.
[182] P. Goethals, A. Volkaert, C. Vandewielle, R. Dierckx, N. Lameire, 55Co-EDTA for renal imaging using positron emission tomography (PET): a feasibility study, Nucl. Med. Biol. 27 (2000) 77–81, https://doi.org/10.1016/S0969-8051(99)00077-3.
[183] G. Karanikas, J. Schmaljohann, M. Rodrigues, F. Chehne, S. Granegger, H. Sinzinger, Examination of Co-Complexes for Radiolabeling of Platelets in Positron Emission Tomographic Studies, Thromb. Res. 94 (1999) 111–115, https://doi.org/10.1016/S0049-3848(98)00204-7.
[184] C. Müller, M. Bunka, J. Reber, C. Fischer, K. Zhernosekov, A. Türler, R. Schibli, Promises of Cyclotron-Produced 44Sc as a Diagnostic Match for Trivalent β−-Emitters. In Vitro and In Vivo Study of a 44Sc-DOTA-Folate Conjugate, J. Nucl. Med. 54 (2013) 2168–2174, https://doi.org/10.2967/jnumed.113.123810.
[185] C. Müller, H. Struthers, C. Winiger, K. Zhernosekov, R. Schibli, DOTA Conjugate with an Albumin-Binding Entity Enables the First Folic Acid-Targeted 177Lu-Radionuclide Tumor Therapy in Mice, J. Nucl. Med. 54 (2013) 124–131, https://doi.org/10.2967/jnumed.112.107235.
[186] C. Müller, J. Reber, S. Haller, H. Dorrer, P. Bernhardt, K. Zhernosekov, A. Türler, R. Schibli, Direct in vitro and in vivo comparison of 161 Tb and 177 Lu using a tumour-targeting folate conjugate, Eur. J. Nucl. Med. Mol. Imaging. 41 (2014) 476–485, https://doi.org/10.1007/s00259-013-2563-z.
[187] A. Zacchetti, A. Coliva, E. Luison, E. Seregni, E. Bombardieri, A. Giussani, M. Figini, S. Canevari, 177Lu- labeled MOv18 as compared to 131I- or 90Y-labeled MOv18 has the better therapeutic effect in eradication of alpha folate receptor-expressing tumor xenografts, Nucl. Med. Biol. 36 (2009) 759–770, https://doi.org/10.1016/j.nucmedbio.2009.05.004.
[188] W.H. Kim, C.G. Kim, M.H. Kim, D.-W. Kim, C.R. Park, J.Y. Park, Y.-S. Lee, H. Youn, K.W. Kang, J.M. Jeong, J.-K. Chung, Preclinical evaluation of isostructural Tc-99m- and Re-188-folate-Gly-Gly-Cys-Glu for folate receptor-positive tumor targeting, Ann. Nucl. Med. 30 (2016) 369–379, https://doi.org/10.1007/s12149-016-1072-0.
[189] S. Haller, J. Reber, S. Brandt, P. Bernhardt, V. Groehn, R. Schibli, C. Müller, Folate receptor-targeted radionuclide therapy: preclinical investigation of anti-tumor effects and potential radionephropathy, Nucl. Med. Biol. 42 (2015) 770–779, https://doi.org/10.1016/j.nucmedbio.2015.06.006.
[190] K. Siwowska, S. Haller, F. Bortoli, M. Benešová, V. Groehn, P. Bernhardt, R. Schibli, C. Müller, Preclinical Comparison of Albumin-Binding Radiofolates: Impact of Linker Entities on the in Vitro and in Vivo Properties, Mol. Pharm. 14 (2017) 523–532, https://doi.org/10.1021/acs.molpharmaceut.6b01010.
[191] J. Svensson, J. Mölne, E. Forssell-Aronsson, M. Konijnenberg, P. Bernhardt, Nephrotoxicity profiles and threshold dose values for [177Lu]-DOTATATE in nude mice, Nucl. Med. Biol. 39 (2012) 756–762, https://doi.org/10.1016/j.nucmedbio.2012.02.003.
[192] C. Müller, J. Reber, S. Haller, H. Dorrer, U. Köster, K. Johnston, K. Zhernosekov, A. Türler, R. Schibli, Folate Receptor Targeted Alpha-Therapy Using Terbium-149, Pharmaceuticals. 7 (2014) 353–365, https://doi.org/10.3390/ph7030353.
[193] S. Haller, G. Pellegrini, C. Vermeulen, N.P. van der Meulen, U. Köster, P. Bernhardt, R. Schibli, C. Müller, Contribution of Auger/conversion electrons to renal side effects after radionuclide therapy: preclinical comparison of 161Tb-folate and 177Lu-folate, EJNMMI Res. 6 (2016) 13, https://doi.org/10.1186/s13550-016-0171-1.
[194] K. Siwowska, P. Guzik, K.A. Domnanich, J.M. Monné Rodríguez, P. Bernhardt, B. Ponsard, R. Hasler, F. Borgna, R. Schibli, U. Köster, N.P. van der Meulen, C. Müller, Therapeutic Potential of 47Sc in Comparison to 177Lu and 90Y: Preclinical Investigations, Pharmaceutics. 11 (2019) 424, https://doi.org/10.3390/pharmaceutics11080424.
[195] P. Guzik, M. Benešová, M. Ratz, J.M. Monné Rodríguez, L.M. Deberle, R. Schibli, C. Müller, Preclinical evaluation of 5-methyltetrahydrofolate-based radioconjugates—new perspectives for folate receptor–targeted radionuclide therapy, Eur. J. Nucl. Med. Mol. Imaging. 48 (2021) 972–983, https://doi.org/10.1007/s00259-020-04980-y.
[196] L.M. Deberle, M. Benešová, A.E. Becker, M. Ratz, P. Guzik, R. Schibli, C. Müller, Novel Synthetic Strategies Enable the Efficient Development of Folate Conjugates for Cancer Radiotheranostics, Bioconjug. Chem. 32 (2021) 1617–1628, https://doi.org/10.1021/acs.bioconjchem.1c00198.
[197] C. Catana, A.R. Guimaraes, B.R. Rosen, PET and MR Imaging: The Odd Couple or a Match Made in Heaven?, J Nucl. Med. 54 (2013) 815–824, https://doi.org/10.2967/jnumed.112.112771.
[198] E. Deshayes, R. Ladjohounlou, P.L. Fur, A. Pichard, C. Lozza, V. Boudousq, S. Sevestre, M. Jarlier, R. Kashani, J. Koch, J. Sosabowski, J. Foster, N. Chouin, F. Bruchertseifer, A. Morgenstern, P.-O. Kotzki, I. Navarro-Teulon, J.-P. Pouget, Radiolabeled Antibodies Against Müllerian-Inhibiting Substance Receptor, Type II: New Tools for a Theranostic Approach in Ovarian Cancer, J. Nucl. Med. 59 (2018) 1234–1242, https://doi.org/10.2967/jnumed.118.208611.
[199] GamaMabs Pharma, Open, Non Controlled, Multicenter, First-in-Human Study for the Evaluation of the Safety, Pharmacokinetics and Preliminary Antitumor Activity of GM102 in Patients With Advanced Pretreated Gynecological Cancer, clinicaltrials.gov, 2022. https://clinicaltrials.gov/ct2/show/NCT02978755 (accessed April 7, 2022).
[200] P. Estupina, A. Fontayne, J.-M. Barret, N. Kersual, O. Dubreuil, M.L. Blay, A. Pichard, M. Jarlier, M. Pugnière, M. Chauvin, T. Chardès, J.-P. Pouget, E. Deshayes, A. Rossignol, T. Abache, C. de Romeuf, A. Terrier, L. Verhaeghe, C. Gaucher, J.-F. Prost, A. Pèlegrin, I. Navarro-Teulon, The anti-tumor efficacy of 3C23K, a glyco-engineered humanized anti-MISRII antibody, in an ovarian cancer model is mainly mediated by engagement of immune effector cells, Oncotarget. 8 (2017) 37061–37079. 10.18632/oncotarget.15715.
[201] R.T. Morris, R.N. Joyrich, R.W. Naumann, N.P. Shah, A.H. Maurer, H.W. Strauss, J.M. Uszler, J.T. Symanowski, P.R. Ellis, W.A. Harb, Phase II study of treatment of advanced ovarian cancer with folate-receptor-targeted therapeutic (vintafolide) and companion SPECT-based imaging agent (99mTc-etarfolatide)†, Ann. Oncol. 25 (2014) 852–858, https://doi.org/10.1093/annonc/mdu024.